NASA Contractor Report 181851

Evaluation of Analysis Techniques for Low Frequency Interior Noise and Vibration of Commercial Aircraft

A. E. Landmann, H. F. Tillema, and S. E. Marshall

Boeing Commercial Airplanes
P.O. Box 3707
Seattle, Washington 98124-2207

Contract NAS1-18027

October 1989

National Aeronautics and
Space Administration

Langley Research Center
Hampton, Virginia 23665-5225

FOREWORD

This report contains comparisons of predicted and measured vibration and interior noise levels for an aircraft with aft mounted propeller engines. Based on these comparisons, recommendations are made for modeling and analysis techniques for evaluation of low-frequency engine noise and vibration in the passenger cabin. This work was conducted under NASA contract NAS1-18027 from January, 1987 through February, 1989. Work was managed by the Acoustics Division at the NASA Langley Research Center. During 1987 work, Mr. H. Morgan was the chief of the Acoustics Division and Mr. D. G. Stephens was the technical monitor for the contract. During the 1988 and early 1989 work, Mr. D. G. Stephens was chief of the Acoustics Division at NASA and Dr. K. Shepherd was the technical monitor for the contract.

All analytical work was performed under the direction of the Noise Research staff of the Boeing Commercial Airplanes. A number of engineering organizations and subcontractors contributed to the successful completion of the project as planned. Key contractor personnel responsible for this effort were—

Boeing

Noise Technology
- L. M. Butzel
- L. W. Craig
- C. G. Hodge
- A. E. Landmann
- S. E. Marshall
- G. K. Queitzsch
- P. M. Serati

Propulsion Technology
- M. A. Heidari
- R. L. Martin
- J. L. White
- T. F. Yantis

Structures Technology
- K. H. Dickenson
- R. L. Dreisbach
- R. R. Ensminger
- M. T. Hutchinson
- H. J. Jamshidiat
- E. E. Meyer
- H. F. Tillema

Weights Technology
- D. E. Cook
- D. J. Roberts

Subcontractors

- A. C. Aubert - Cambridge Collaborative, Inc.
- J. E. Manning - Cambridge Collaborative, Inc.
- L. D. Pope

TABLE OF CONTENTS

Page

FOREWORD i

TABLE OF CONTENTS iii

LIST OF TABLES v

LIST OF FIGURES vii

1.0 SUMMARY 1

2.0 INTRODUCTION 3

3.0 APPROACH 5
- 3.1 Noise and Vibration Tests 5
- 3.2 Analysis Model Development 7
  - 3.2.1 Finite Element Model 8
  - 3.2.2 Statistical Energy Analysis Model 9
  - 3.2.3 PAIN Model 13

4.0 RESULTS 15
- 4.1 Finite Element Analysis Results (FY 1987) 15
- 4.2 Finite Element Model Improvements (FY 1988) 20
- 4.3 Finite Element Analysis Results (FY 1988) 22
- 4.4 Statistical Energy Analysis Results (FY 1987) 33
- 4.5 Review of SEA Procedures for Low-Frequency Problems 38
  - 4.5.1 Acoustic Space Modal Density Estimate 38
  - 4.5.2 Structure Modal Density Estimates 39
  - 4.5.3 Use of Finite Element Models to Verify SEA Parameters 39
- 4.6 SEAM^{TM} Code Improvements 41
- 4.7 SEA Low-Frequency Model Improvements 43
  - 4.7.1 Input Power Estimate 43
  - 4.7.2 Modal Density Estimates 44
  - 4.7.3 Strut Connection Modeling 44
  - 4.7.4 Strut Loss Factor 46
- 4.8 Midfrequency Model Improvements 47
- 4.9 Statistical Energy Analysis Results (FY 1988) 49
- 4.10 PAIN Analysis Results (FY 1987) 55
- 4.11 PAIN Analysis Results (FY 1988) 57
- 4.12 PAIN Improvements and Feasibility Studies 62

Page

5.0 CONCLUSIONS AND RECOMMENDATIONS 65
5.1 Finite Element Analysis 65
5.2 Statistical Energy Analysis 66
5.3 PAIN Analysis 66

LIST OF TABLES

Table		Page
1	727 Demonstrator Airplane Ground Vibration Test (GVT) Shake Conditions	5
2	727 Demonstrator Airplane Flight Conditions	7
3	Modeling Time and Cost Comparison for 727 Demonstrator Airplane Finite Element Models	33

LIST OF FIGURES

Figure		Page
1	Prediction Program Comparisons and Comments	1
2	727 Demonstrator Airplane—General Arrangement	6
3	BS 1010 Microphone and Accelerometer Locations	7
4	727 Demonstrator Airplane—Finite Element Model Finite Element Method	8
5	GE36 Demonstrator Engine Finite Element Model	10
6	25-Element Low-Frequency SEAM™ Model (20- to 100-Hz Range)	11
7	100-Element Midfrequency SEAM™ Model (100- to 400-Hz Range)	12
8	Propeller Aircraft Interior Noise Model	14
9	727 Demonstrator Airplane Predicted Versus Measured Frame Mode Shape at BS 1010—21.5 Hz	15
10	727 Demonstrator Airplane GVT—Roving Microphone Data	16
11	727 Demonstrator Airplane GVT Accelerometer Data Frame Versus Ceiling Panel Response at Stringer 4	17
12	Finite Element Prediction Versus 727/GE36 Demonstrator Test; GVT—Front Mount Vertical Shake	18
13	Finite Element Prediction Versus 727/GE36 Demonstrator Test; GVT—Aft Lower Mount Lateral Shake	20
14	Original and Revised Ceiling Panel Weight Distribution	21
15	Original and Revised Hat Rack Weight Distribution	21
16	Acoustic Mesh Typical Cross Section	23
17	727 Demonstrator Airplane—Reduced Finite Element Models	24
18	Finite Element Prediction Versus 727/GE36 Demonstrator Test; Ground Vibration Test—Front Mount Vertical Shake	25
19	Longitudinal Variations Around BS 1010—GE Side Window Seat Microphone Prediction	26
20	Finite Element Prediction Versus 727/GE36 Demonstrator Test; Ground Vibration Test—Aft Lower Mount Lateral Shake	27
21	Finite Element Predictions Versus 727/GE36 Demonstrator Test; Ground Vibration Test—Front Mount Vertical Shake	28
22	Finite Element Predictions Versus 727/GE36 Demonstrator Test; Ground Vibration Test—Aft Lower Mount Fore-Aft Shake	29
23	Finite Element Predictions Versus 727/GE36 Demonstrator Test; Ground Vibration Test—Aft Lower Mount Vertical Shake	30
24	Finite Element Predictions Versus 727/GE36 Demonstrator Test; Ground Vibration Test—Aft Lower Mount Lateral Shake	32
25	SEAM™ Predicted Levels Versus 727 Demonstrator Test Data: GVT—Forward Mount Lateral Shake	34

Figure		Page
26	Low-Frequency SEAM™ Model Predicted Levels Versus 727 Demonstrator Test Data; GVT—Forward Mount Vertical Shake	35
27	Midfrequency SEAM™ Model Predicted Levels Versus 727 Demonstrator Test Data; GVT—Forward Mount Vertical Shake	37
28	Asymptotic Modal Densities for the Low-Frequency SEA Model	40
29	Input Power Comparisons	42
30	Response Predictions for the Low-Frequency Baseline Model Using Measured Input Power—Vertical Shake	43
31	Composite Strut Modal Density Based on Spacing Between Peaks in the Measured Vertical Shake Input Power	45
32	Instantaneous Modal Density for the Cabin Acoustic Space	46
33	Comparison of Modal Density Prediction Procedures—Interior Acoustic Space	47
34	Midfrequency SEAM Model Variable Panel Density	48
35	Response Predictions for the Low-Frequency Improved Model—Vertical Shake	50
36	Response Predictions for the Low-Frequency Improved Model Using Measured Input Power Vertical Shake	51
37	Response Predictions for the Low-Frequency Improved Model—Fore-Aft Shake	52
38	Response Predictions for the Low-Frequency Improved Model Using Measured Input Power Fore-Aft Shake	53
39	Response Predictions, Midfrequency Model Side-of-Body Shake, Improved Model	54
40	Measured Minus Predicted SPL Using Improved Midfrequency Model	55
41	Power Flow Diagram for Elements of PAINUDF Model	56
42	Measured Versus PAINUDF Predicted Levels	57
43	Average of Seat Measurements Versus PAINUDF Space Average Prediction	58
44	Propeller Wavefronts for Blade Downsweep (Forward Rotor) and Blade Upsweep (Aft Rotor) at Ø = 105°	59
45	Propeller Wavefronts for Blade Downsweep (Forward Rotor) and Blade Upsweep (Aft Rotor) at Ø = 80°	59
46	Measured and PAINUDF Predicted Levels for Open Panel and Conical Empennage Models	60
47	Measured and PAINUDF Predicted Levels Phase Sensitivity Study	60
48	Comparison of Propeller Field Phase Contours ANOPP Phase Versus Dummy Phase	61
49	Measured and PAINUDF Predicted Levels PAINUDF Sensitivity Study to Excitation Models (Mach = 0.80 at 35 000 ft)	62
50	Example of Sidewall Layer Configurations	63

1.0 SUMMARY

This document summarizes a 2-year effort to evaluate the application of selected analysis techniques to low-frequency cabin noise associated with advanced propeller engine installations. Work was funded by a NASA contract, NAS1-18027.

Three design analysis techniques were chosen for evaluation including finite element analysis, statistical energy analysis (SEA), and a power flow method using elements of SEA (computer program Propeller Aircraft Interior Noise (PAIN)). An overview of the three procedures is provided in figure 1. Data from tests of a 727 airplane (modified to accept a propeller engine) were used to compare with predictions.

Comparisons of predicted and measured levels at the end of the first year's effort showed reasonable agreement leading to the conclusion that each technique had value for propeller engine noise predictions on large commercial transports. However, variations in agreement were large enough to remain cautious and led to recommendations for further work with each technique. This recommended work was accomplished in the second year's effort.

Assessment of the second year's results leads to the conclusion that the selected techniques can accurately predict trends and can be useful to a designer, but that absolute level predictions remain unreliable due to complexity of the aircraft structure and low modal densities. The extremely complex nature of the modified 727 demonstrator airplane may be largely responsible for this conclusion. It would be worthwhile to apply these techniques to more conventional aircraft structure cases.

	FEM	SEAM		PAIN
		Low-frequency model	High-frequency model	
Frequency range (this study)	Rotor	Rotor and rotor harmonics (<100 Hz)	Rotor harmonics and BPF	BPF
Calculations	Modes, display, SPL versus position and frequency	Power, modal densities coupling loss factors, space average display and SPL		Power structural modes space average SPL
Advantages	Good detail versus frequency, position	Inexpensive/quick model changes/power flow analysis/ variance estimates		Moderate exp Good trim definition
Disadvantages	Expensive, hard to change model	Lack of spatial details/high estimate variance for low modal density cases		Lack of spatial details, excitation field complexity
Use	Detailed predictions design work for existing or new airplanes	Power flow analysis for existing airplanes Preliminary design		Preliminary design

Figure 1. Prediction Program Comparisons and Comments

U90196RI-4

2.0 INTRODUCTION

The primary sources of cabin noise on advanced propeller-powered aircraft are low- to mid-frequency (i.e., below 500 Hz) structure borne noise (caused by engine unbalances) and engine-radiated propeller tones. Conventional sound proofing treatments, such as damping tapes or fiberglass blankets, are not very effective in this frequency range. Also, most low- to mid-frequency design tools tend to be based on idealized cylindrical models of the aircraft fuselage, which ignore effects of tapered empennage sections, pressure bulkheads, floors, etc. Effective reduction of low- to mid-frequency noise requires the development of improved design analysis tools. These improved tools will lead to a better understanding of the mechanisms involved and provide guidance for developing new suppression concepts.

The objective of the FY 1987 task under contract NAS1-18027 was to evaluate the ability of three analysis techniques (contained in existing computer programs) to predict cabin noise and vibration. Specific steps of this effort were as follows:

1. Predict cabin noise, together with vibration levels of the floor, cabin sidewall, pressure bulkhead, empennage, and strut at rotor (once per revolution) and propeller-blade-passage frequencies.

2. Compare predicted levels with measured levels from a 727 demonstrator aircraft modified to accept a GE36 counter-rotating propeller engine. Make predictions and comparisons for ground vibration test and inflight conditions.

3. Determine strengths and shortcomings of prediction program procedures and/or modeling techniques and identify potential means for improvements.

The objectives of the FY 1988 task were to incorporate recommended improvements, repredict noise and vibration levels, compare the new predictions to measured levels, assess results, and make recommendations for future use of these procedures.

3.0 APPROACH

While the NASA contract focused on predictions and comparisons with test data, preliminary work including 727 test descriptions and analysis model development is also included in this report.

3.1 NOISE AND VIBRATION TESTS

Noise and vibration testing on a 727 aircraft, modified for installation of a GE36 counter-rotating propeller engine, provided the database with which to compare predictions. During ground vibration tests, before engine installation, the strut was excited by a shaker to determine airframe and cabin response to engine mount vibration. Response to shaker inputs at each engine mount location was recorded. In addition, side-of-body shake testing was performed on the fin, empennage, and aft passenger cabin to simulate high-level acoustic loading from the propellers. Ground vibration test conditions are given in table 1. The 727 was configured with an acoustic test arena aft of body station 890. Standard 727 interior trim and four passenger seat rows were installed in this area. General layout of the aircraft is shown in figure 2.

Instrumentation locations were reviewed to ensure adequate data for comparison with predicted levels. Cabin microphones were placed in the acoustic arena to monitor noise at passenger seated and standing locations as well as next to interior vibration sensors (fig. 3). Also shown are accelerometers positioned in the passenger cabin to monitor fuselage sidewall, floor, and cabin interior trim response. Accelerometers were placed on the pressure bulkhead, empennage, and strut to evaluate the transmission path to the passenger cabin. A total of 128 response channels were measured for each ground vibration test condition.

Due to data channel limitations during flight testing, fuselage and cabin accelerometer numbers were reduced. Further reductions were required to add flush mounted exterior microphones for the purpose of measuring propeller noise excitation levels. Different cruise and low-power flight conditions were completed (table 2).

Table 1. 727 Demonstrator Airplane Ground Vibration Test (GVT) Shake Conditions

Side-of-body shakes, 10 to 400 Hz	Engine mount shakes, 2 to 200 Hz
BS 1160 WL 320	Front mount vertical
BS 1270 WL 190	Front mount lateral
BS 1300 WL 250	Aft upper mount vertical
BS 1310 WL 340	Aft upper mount lateral
BS 1400 WL 400	Aft upper mount fore to aft
BS 1050 WL 230	Aft lower mount vertical
	Aft lower mount lateral
	Aft lower mount fore to aft

U100196R1-1

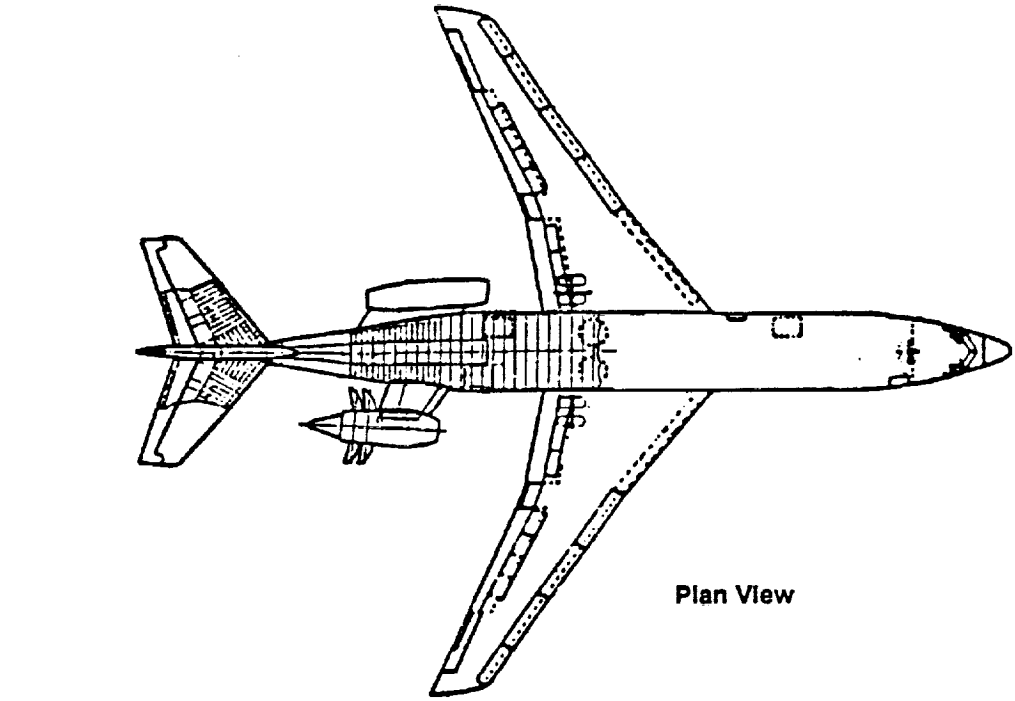

Plan View

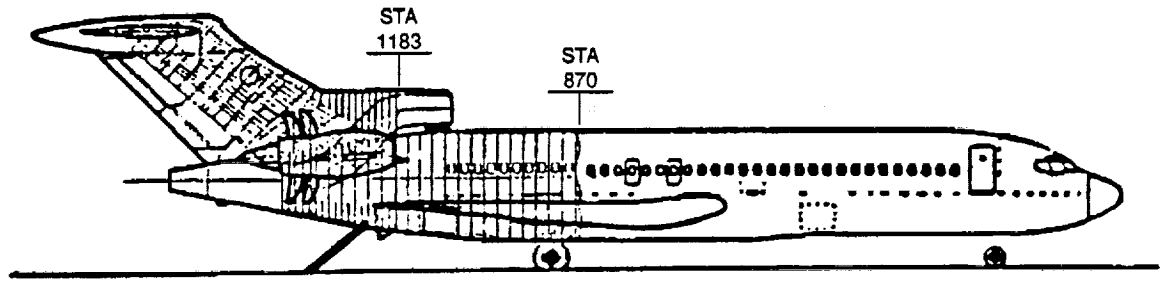

Right Side View

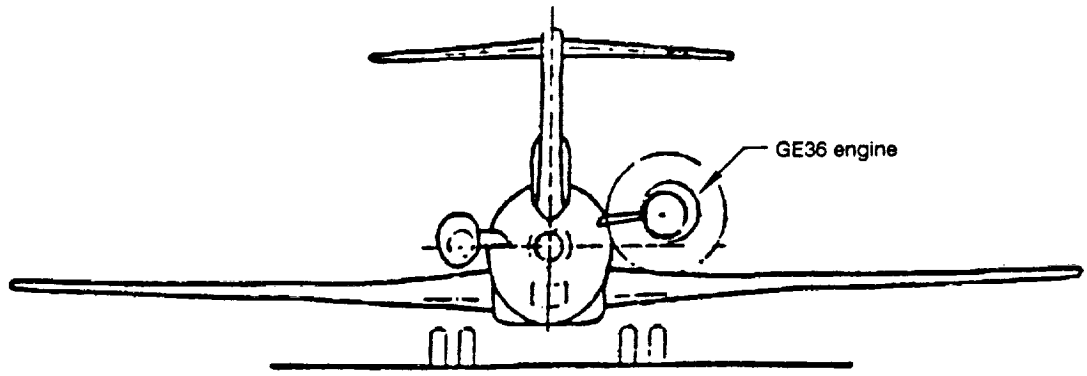

Rear View

Figure 2. 727 Demonstrator Airplane – General Arrangement

U90196RI-5

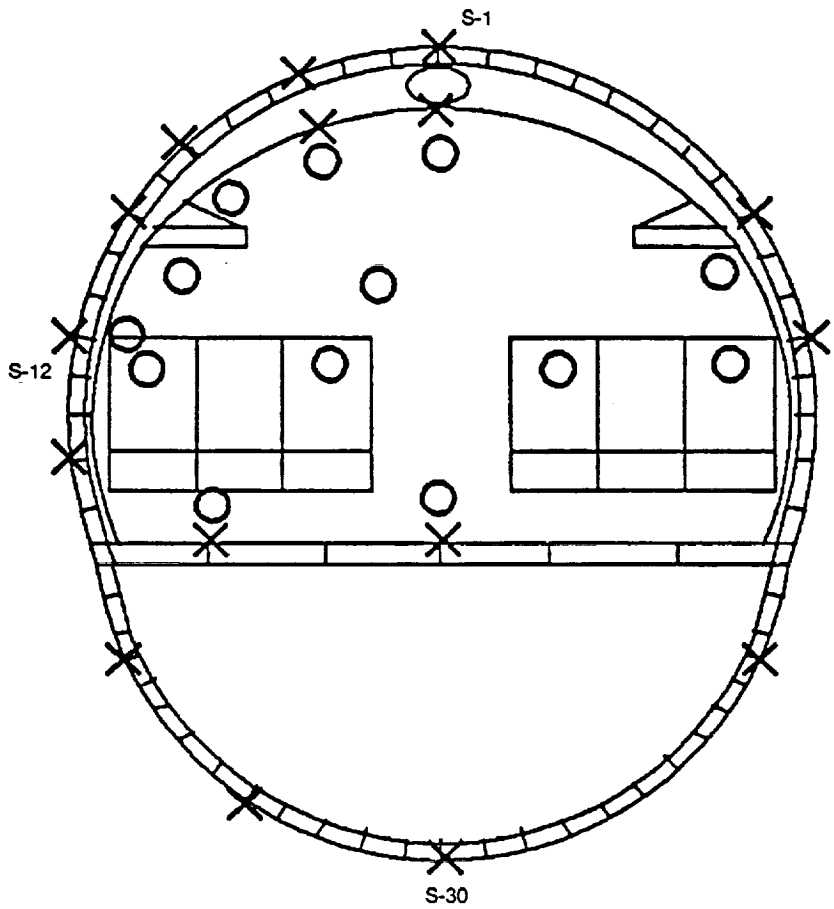

Figure 3. BS 1010 Microphone and Accelerometer Locations

9-U90196-6

Table 2. 727 Demonstrator Airplane Flight Conditions

Mach No.	Altitude, ft	Blade-passage frequency, Hz
0.80	35 000	169
0.72	35 000	170
0.42	10 000	180
0.25	4200	180

U90196R1-2

3.2 ANALYSIS MODEL DEVELOPMENT

Three design analysis techniques were chosen for evaluation including finite element analysis, statistical energy analysis (SEA), and a power flow method using elements of SEA (computer program PAIN). An existing general application SEA computer program, SEAM^{TM}, was chosen for evaluation based in part on past successful applications to helicopter, ship, and automobile problems. The developer of SEAM^{TM}, Cambridge Collaborative, Inc., was retained as a subcontractor for this effort. Computer

program PAIN was specifically developed for propeller interior noise predictions. L. D. Pope, a co-author of PAIN was also retained as a subcontractor.

3.2.1 FINITE ELEMENT MODEL

As a starting point for finite element analysis, an existing 727 aircraft finite element model suitable for loads analysis was selected. Changes to model the modified structure (to accommodate the propeller engine), the mass of the interior trim and systems, and an interior cabin acoustic volume were then incorporated. The model is shown in figure 4. Detailed finite element models of the fuselage containing the acoustic arena and structural elements along the transmission path, such as the pressure bulkhead, empennage, vertical fin, and strut, were used. In the fuselage section, body frames, floor beams, stringers, and skin were all individually modeled. Body frames and floor beams were represented as beams, stringers as rods, and skin as membrane plates. In the test arena section, nodes were located at each frame and

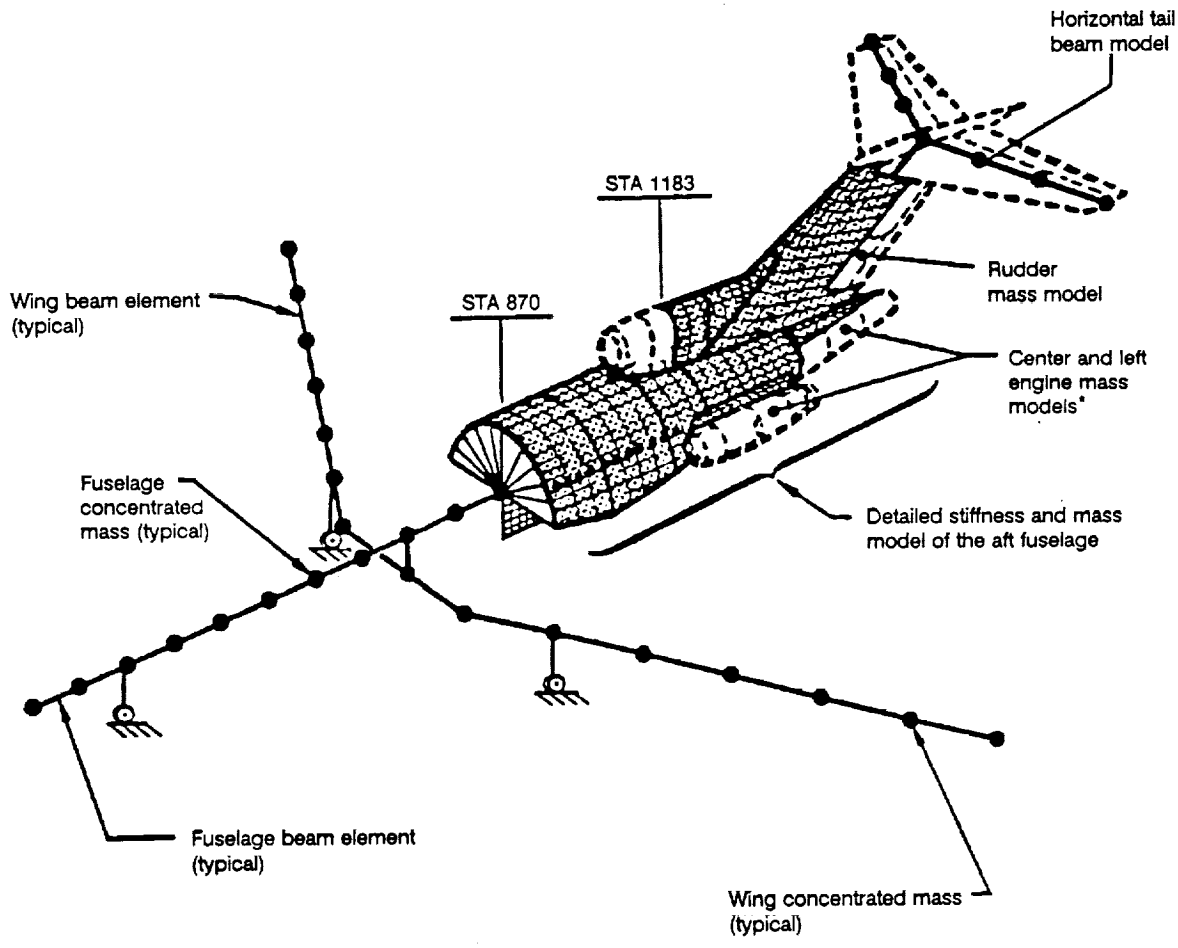

* Right engine was not included in the ground vibration test (GVT) configuration.

Figure 4. 727 Demonstrator Airplane – Finite Element Model Finite Element Method

9-U90196RI-7

stringer intersection. Nodes of the cabin acoustic model interfaced with existing sidewall, floor, and bulkhead structural nodes.

The model was completed by including beam models of the forward fuselage, wings, and horizontal tail. The complete aircraft model was generated because the contribution of gross airplane modes to transmission of low-frequency rotor noise was unknown, but potentially important.

Due to model size and existing node spacing, it was decided to limit predictions to the rotor frequency range. The fuselage nodes were at each frame and stringer intersection, which would have been too coarse a grid to predict skin panel modes that occur in the propeller-blade-passage frequency range (~200 Hz). Because no dynamic nodes of the interior trim were expected below 30 Hz, the interior trim was modeled by lumped mass only. Seat absorption was expected to be minimal below 30 Hz; therefore, seats were also represented by lumped mass only. Additional tap tests of interior trim surfaces and roving microphone measurements were made around seats to validate these assumptions.

For inflight calculations, an engine model was also developed consisting of a beam element representation of the core engine and a shell model of the propulsion section (fig. 5).

Predictions using this model were made for unit force inputs and compared to measured ground vibration test (GVT) and flight transfer functions.

3.2.2 STATISTICAL ENERGY ANALYSIS MODEL

The primary task within the SEA procedure is to formulate power balance expressions for the substructures (energy storing mode groups) of the model. The substructures are typically simple representations (e.g., plates, beams, and acoustic volumes) for sections of the modeled system. Physical information describing the system is used to define the substructure properties such as modal density (the average number of resonances per unit frequency), characteristic wave number (a quantity directly related to the average wavelength of a mode), characteristic impedance (the ratio of the maximum force to the maximum velocity for a mode of vibration), and coupling loss factor (a parameter controlling the average flow of energy between two groups of modes). The power expressions are then solved for the modal energies within the substructures. From the modal energies, the response variables of interest for the specified substructures are determined. The input excitation for a SEA model is applied as the power input to a subsystem of modes.

Because of the smaller model size requirements for SEA, it was decided to use this technique to predict levels for both the rotor and propeller-blade-passage frequency ranges. The first model developed as part of the SEA effort was intended to predict the structural and acoustic response near the propeller tone frequency (100- to 400-Hz frequency range). This model consisted of approximately 400 SEAM^{TM} type subsystems and more than 2000 junctions, which, up to this point, was the largest SEAM^{TM} model developed by Cambridge Collaborative. This model contained elements representing the composite bending and inplane activity of frame and stringer stiffened structure, elements that represented skin panels without stiffeners (bending and inplane), trim elements, cabin acoustic space elements, and

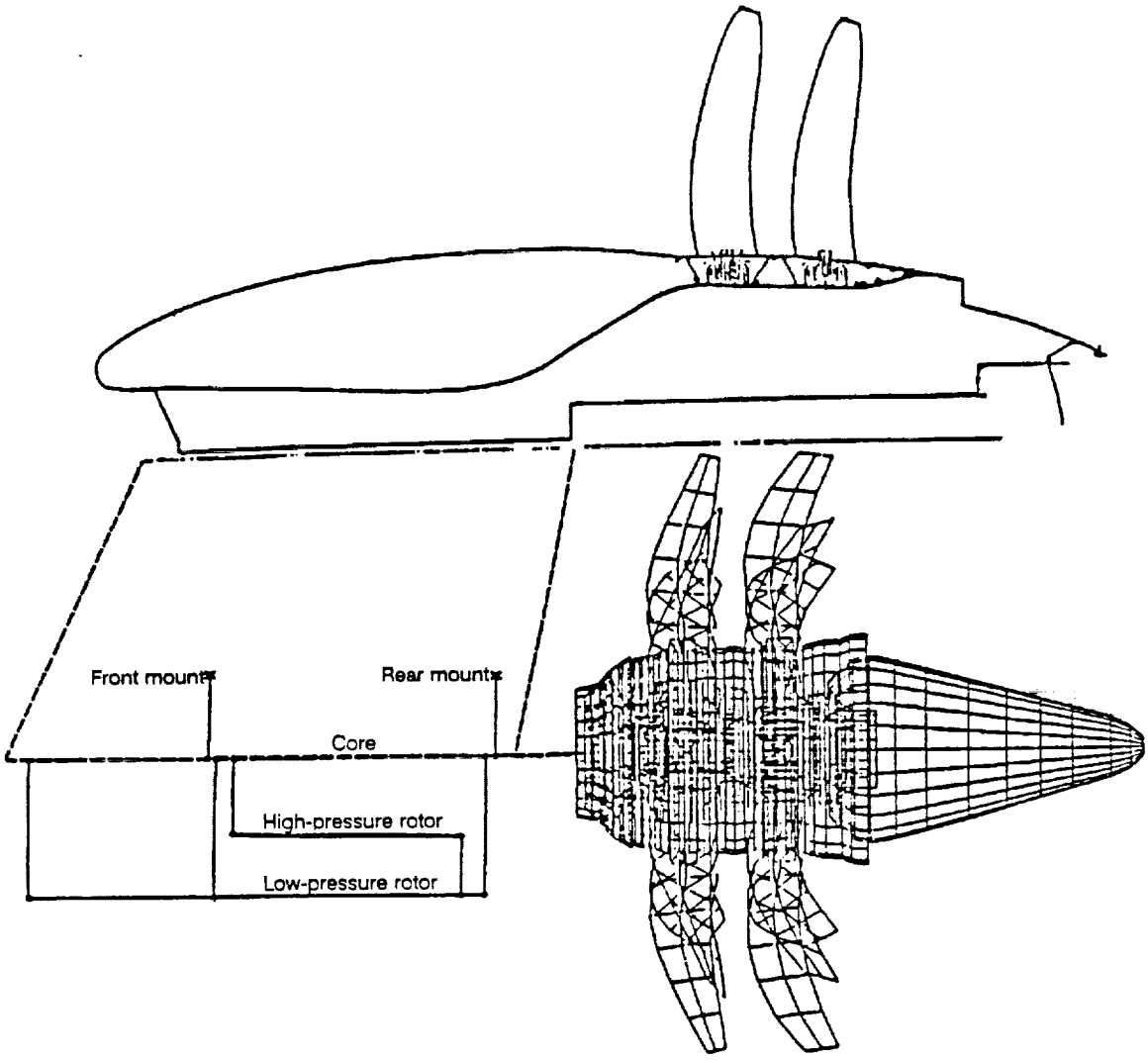

Figure 5. GE36 Demonstrator Engine Finite Element Model

9-U90196R1-9

acoustic elements that represented the space between the fuselage sidewall and trim panel. Initial predictions with this model indicated good agreement at the drive point, but overprediction at points away from the drive point. Cambridge Collaborative concluded that the inability of the model to predict the measured rolloff in response was due to the inclusion of inplane subsystems in the model, which lead to overcoupling between subsystems.

In addition, it was found that the small element sizes resulted in modal densities that were too low based on Cambridge Collaborative's past experience. As a result of these efforts, new models for rotor and propeller tone predictions were generated (figs. 6 and 7) using larger substructure elements and eliminating inplane activity. Data from manufacturing drawings were used to generate separate models in each frequency range using basic pipe, plate beam, and airspace elements available in SEAM^{TM}.

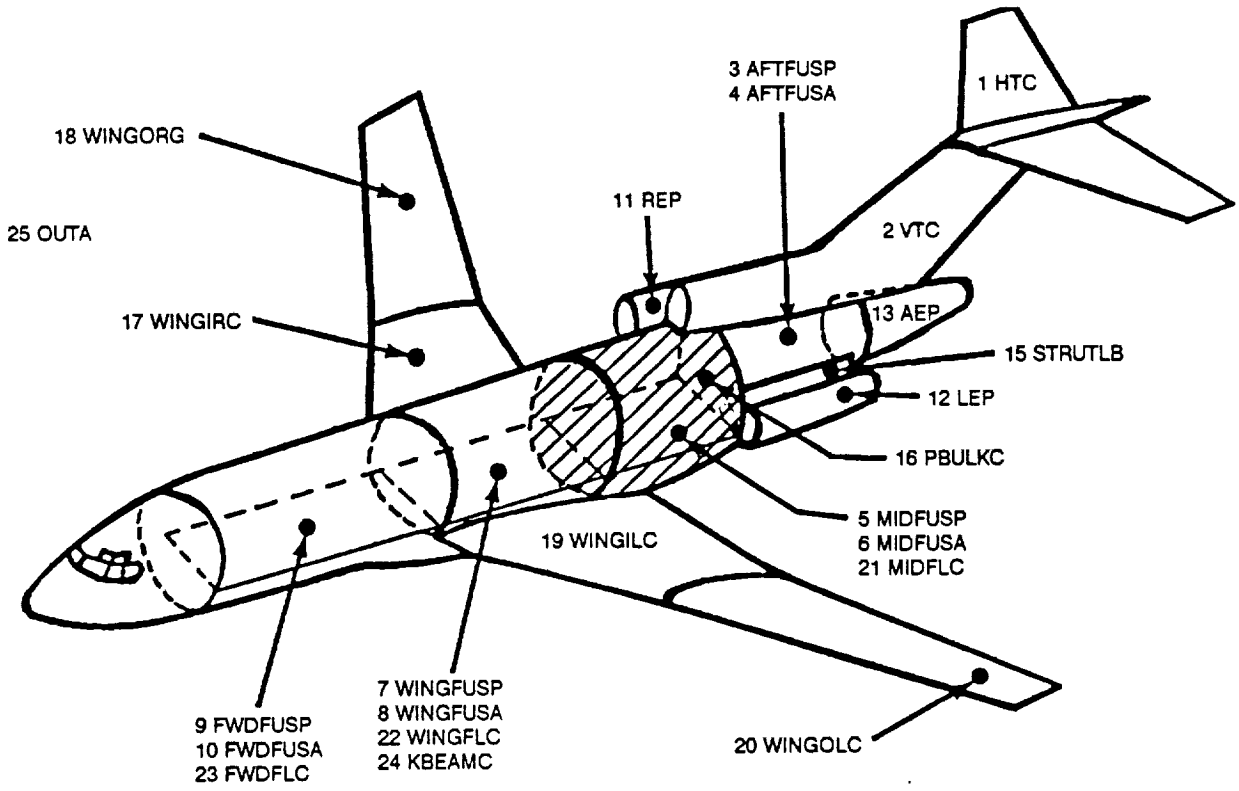

Elements:
25 pipes, plates, and acoustic cavities
21 structural
4 acoustic

Figure 6. 25-Element Low-Frequency SEAM™ Model (20- to 100-Hz Range)

9-U90196RI-10

The low-frequency model was developed to predict the interior acoustic response to mechanical excitation of the engine strut. The transmission of vibration from the unducted fan (UDF) engine caused by fan rotor imbalance was expected to dominate cabin noise within the low-frequency range (20 to 100 Hz). As with the finite element model, the low-frequency SEA model (for rotor frequencies) did not account for cabin trim or seats (other than mass). The substructure elements shown in figure 6 were selected based on natural boundaries between areas of different structural properties or construction. Rather than the detailed finite element modeling of skin, stringers, and frames, composite bending stiffnesses of the plate or pipe elements were calculated to include the effects of the aircraft structural elements as described below.

The material properties required for the SEA model are density, longitudinal wavespeed, shear wavespeed, and damping loss factor. The substructures used in the low-frequency model consist of composite bending modes. Effective material properties for these substructures were obtained from a composite bending calculation that includes the mass and stiffness of frames and stringers and the mass of fuselage sidewall trim panels. The properties and thickness of a homogeneous structure were set to obtain the same bending wavespeed and surface density. Two approaches can be used: (1) an equivalent material density approach (or stiffness thickness approach) in which the thickness of the structure is

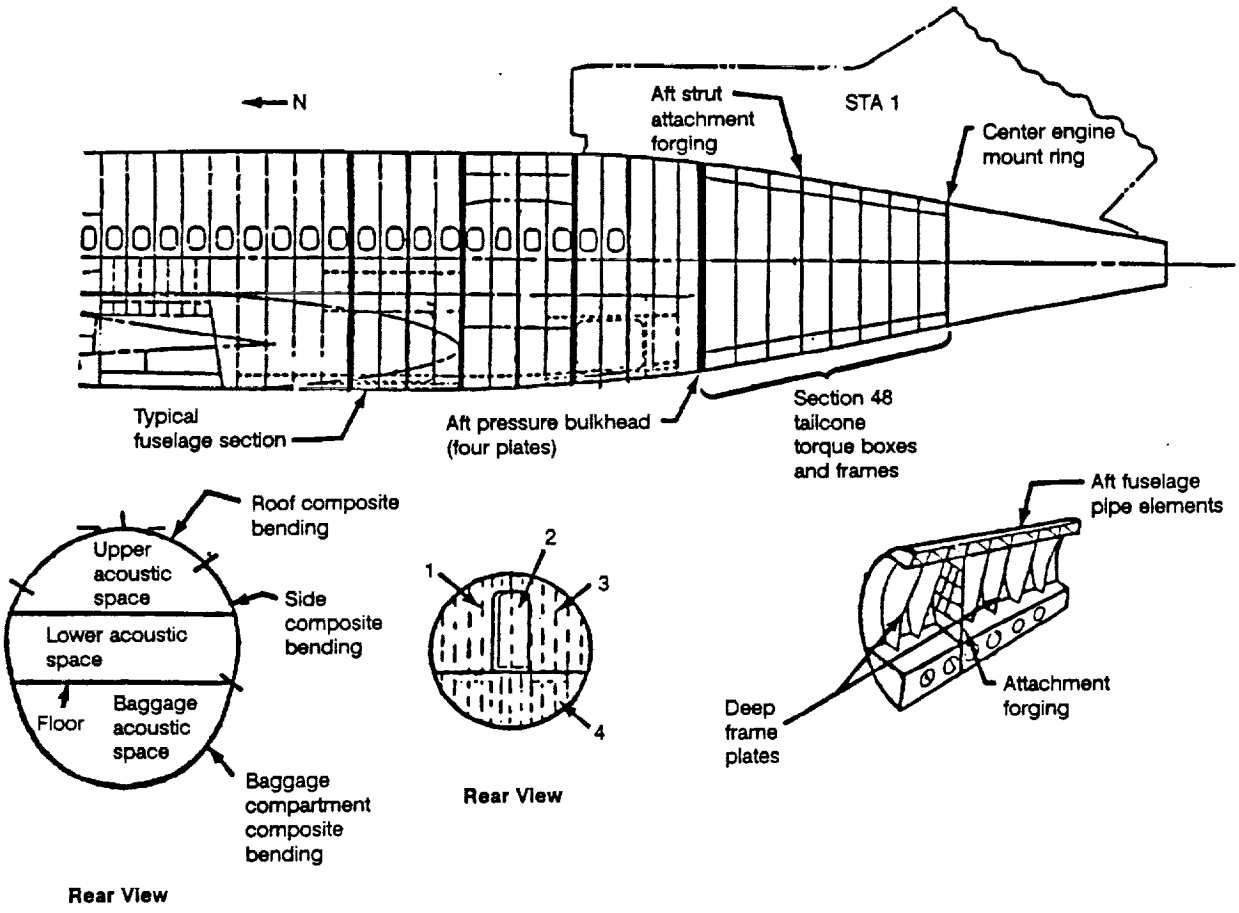

Figure 7. 100-Element Midfrequency SEAM™ Model (100- to 400-Hz Range)

9-U90196R1-11

modified to give the correct bending wavespeed and the density is modified to give the correct density per unit area and (2) an equivalent material density approach (or mass thickness approach) in which the thickness of the structure is modified to give the correct density per unit area and the longitudinal wavespeed is modified to give the correct bending wavespeed. For the low-frequency model the equivalent material density approach was used for all shell or pipe substructures and the equivalent wavespeed approach was used for plate structures. Use of the equivalent material density approach for shell or pipe substructures allowed the longitudinal wavespeed to be held constant so that the ring frequency of the substructure was unchanged.

The mid-frequency SEA model (for propeller frequencies-fig. 7) differed from the low-frequency model in substructure element size, composition, and handling of the trim and seats. The substructure element boundaries were chosen to reflect finer variations in construction (both axially and circumferentially) that were felt might effect response in this frequency range. Composite bending stiffnesses as well as skin membrane stiffnesses were included in the fuselage plate elements. Because independent dynamic modes of the interior trim were expected in this frequency range, the trim was modeled separately as plates. Acoustic spaces between the skin and trim panels were also included. The effect of seats was

included by separately modeling acoustic volumes above and below seatback levels. Coupling between acoustic volumes below seatback level was adjusted to account for seat blockage. Material properties were generated in the same fashion as for the low-frequency model.

Model predictions for both cases were again made for unit force inputs and compared to measured GVT and flight transfer functions.

3.2.3 PAIN MODEL

The Propeller Aircraft Interior Noise (PAIN) prediction method (theory and computer implementation) was previously developed by L. D. Pope, et al., under the auspices of NASA. The PAIN model estimates the space average sound level in an airplane cabin resulting from an excitation field incident on the exterior fuselage (fig. 8A). The excitation field consists of the pressure time history for a wing-mounted rotating propeller as defined by a grid of points on the fuselage surface.

The computer program PAIN was used to predict inflight cabin noise levels at the propeller-blade-passage frequency. As mentioned above, PAIN was originally developed for general aviation aircraft with wing-mounted propeller engines. In this form, only one uniform fuselage structural description was allowed. In contrast, the 727 demonstrator aircraft had an aft fuselage-mounted propeller engine, and most of the propeller tone noise fell on the empennage rather than the passenger cabin fuselage. Therefore, before PAIN could be used, a significant modification for 727 predictions was completed by reformulating the problem to allow representation of both the passenger cabin fuselage and empennage structures (fig. 8B). The 727 demonstrator airplane empennage consists of a very stiff sidewall supported by torque boxes at the top and bottom. To model this behavior, the empennage was represented by open, curved panels.

The capability to model both fuselage and empennage structures is contained in computer program Propeller Aircraft Interior Noise Unducted Fan (PAINUDF). The empennage element allows for the region on which the excitation field acts to differ in both construction and location from the fuselage region inside which cabin noise estimates are desired. Additionally, a junction between the two regions is defined by a structurally significant (but nonacoustically radiating) bulkhead.

With PAIN, the fuselage sidewall is modeled in a simpler manner than with finite element modeling. The sidewall was represented as a cylinder with an equivalent skin thickness based on skin dimensions and smeared frame and stringer properties. The floor was modeled in a similar manner. The interior trim was modeled as an airgap with absorption and a limp mass trim. The interior airspace was modeled as one uniform volume. Data from manufacturing drawings were used to determine equivalent skin and floor panel thicknesses, insulation properties, and trim mass.

Data from flush-mounted microphones were then used to describe excitation forces, allowing inflight aft cabin noise level predictions to be made. Changes to the computer code as well as predictions and comparisons were made under the NASA contract.

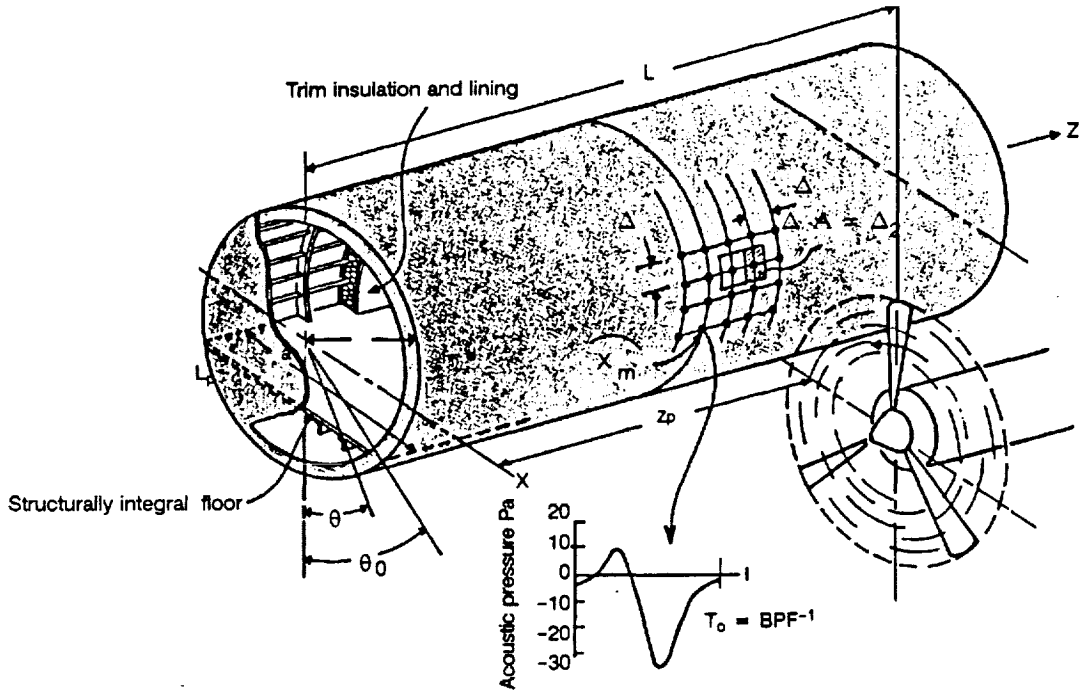

(a) PAIN Model for Wing–Mounted Engine

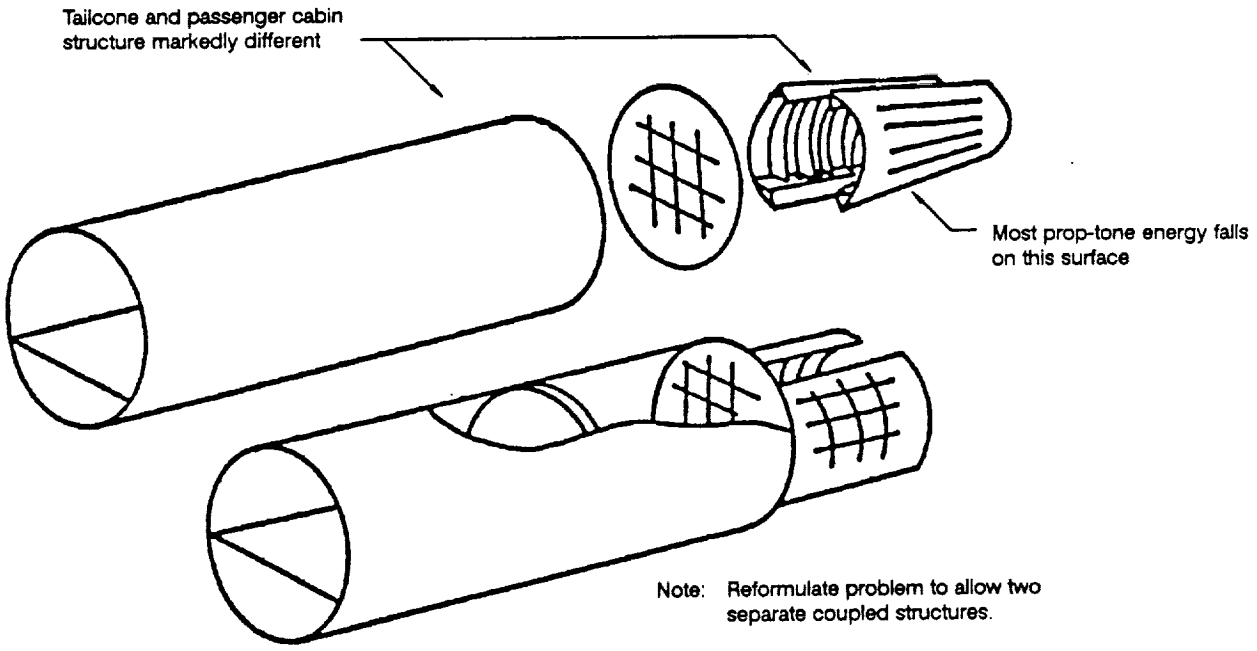

(b) 727/GE36 Demonstrator Airplane PAIN Model

Figure 8. Propeller Aircraft Interior Noise Model

U90196R1-12

4.0 RESULTS

4.1 FINITE ELEMENT ANALYSIS RESULTS (FY 1987)

Predictions were made to encompass the rotor frequency range (< 30 Hz) and were compared to GVT and flight test conditions. A modal solution was used, meaning a limited number of structural and acoustic modes were computed and used to generate forced response predictions. In this case, 150 structural modes (0 to 73 Hz) and 100 acoustic modes (0 to 230 Hz) were used.

Inspection of predicted mode shapes showed gross airplane modes involving the wings, tail, and fuselage from 0 to 30 Hz; local frame and floor bending modes occurred above 20 Hz. Comparison with test data showed good agreement. Below 20 Hz, predicted gross airplane mode shapes matched results from measured data, with predicted resonant frequencies typically within 5% of those measured. From 20 to 30 Hz, fuselage modes occur in which the frame exhibits a maximum of three half-waves around the passenger cabin and the floor one half-wave across the cabin. Measured data showed similar response characteristics (fig. 9). The measured data in figure 9 includes both frame and floor bending plus rigid body translation associated with gross airframe bending. Since only radial accelerometers were used during testing, the local bending and rigid translation responses could not be separated. It was recommended that future rotor frequency shake tests use biaxial accelerometers. A few modes related to strut response

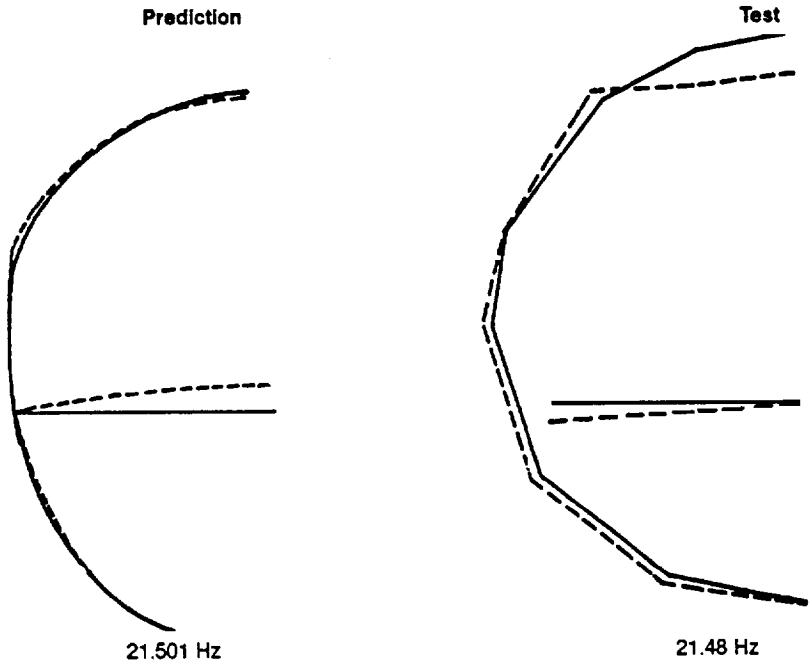

Figure 9. 727 Demonstrator Airplane Predicted Versus Measured Frame Mode Shape at BS 1010—21.5 Hz

U90196R1-14

were also identified, but either did not appear in measured data or were shifted in frequency by a significant amount. The cause of these modes was investigated as part of the FY 1988 task.

One cabin acoustic mode was predicted in the frequency range below 30 Hz. At 23 Hz a longitudinal mode was predicted and represented by a standing half-wave between the pressure bulkhead and a partition at body station 890 used to separate the test arena from the rest of the airplane. Cross-cabin modes occurred at more than 50 Hz.

As stated in the Approach section, additional tests were performed to validate seat and trim modeling assumptions for the rotor frequency range. Noise measurements made at several locations around one seat during a body shake condition showed only small variations at less than 50 Hz (fig. 10). Trim and ceiling panel tap tests showed no modes in the rotor frequency range. Shake test data showed that the ceiling panel followed the primary structure response to slightly more than 30 Hz (fig. 11).

Example comparisons of test with analysis for the strut, pressure bulkhead, fuselage sidewall, floor, and acoustic space are given in figures 12A through 12F for one GVT condition. Predicted peak levels fell

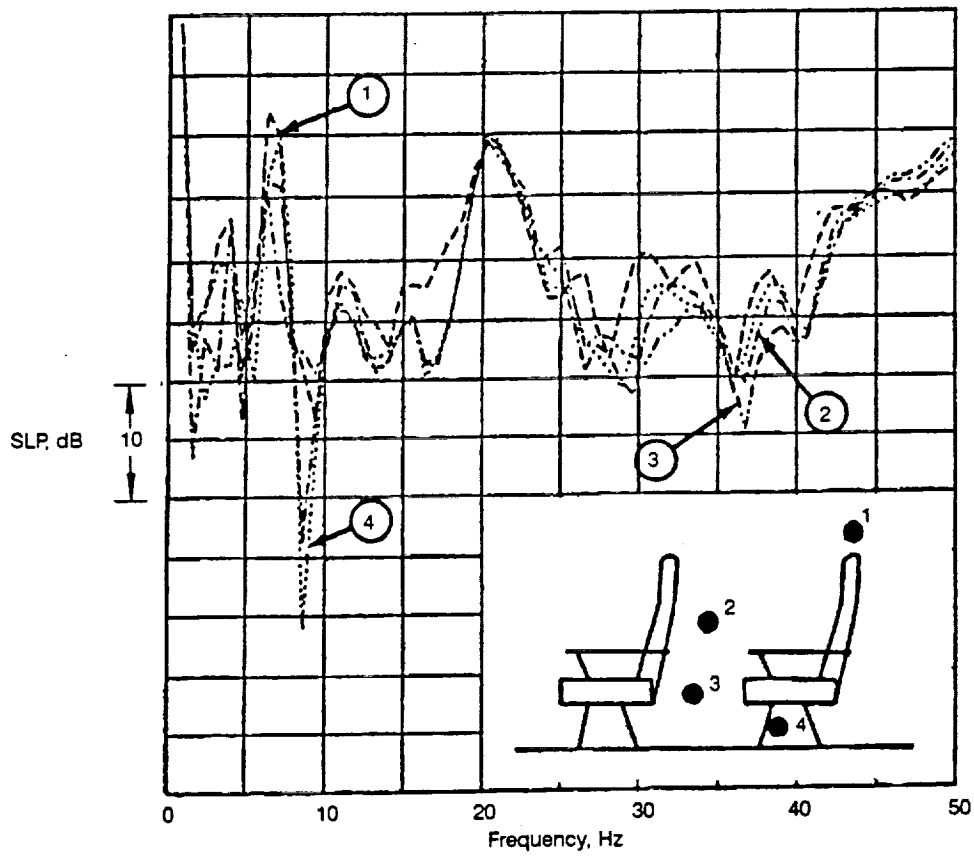

Figure 10. 727 Demonstrator Airplane GVT—Roving Microphone Data

9-U90196R1-15

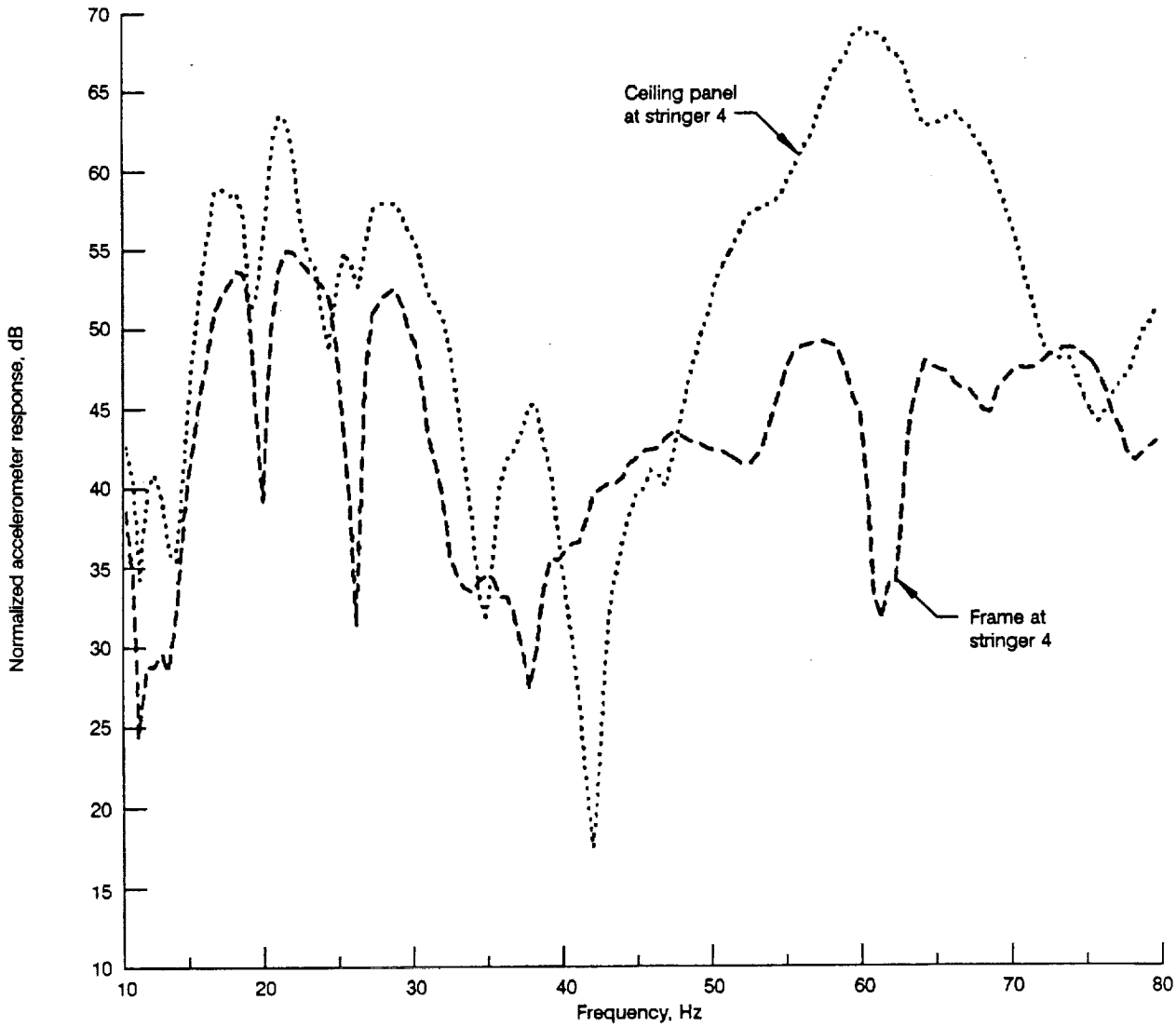

Figure 11. 727 Demonstrator Airplane GVT Accelerometer Data Frame Versus Ceiling Panel Response at Stringer 4

9-U90196R1-16

within 10 dB of the measured levels with frequency shifts up to 1.5 Hz. It was felt that agreement could be improved with the additional modeling studies and recommendations discussed below.

Figure 12A compares measured and predicted strut response for the vertical strut shake condition. Generally, levels were overpredicted at less than 19 Hz and underpredicted at more than 19 Hz. The mode predicted at 14.5 Hz and shown shifted in the test data to near 16 Hz illustrates some of the questions about strut modeling that were recommended for investigation.

Figure 12B shows radial response of a stringer at the intersection of the forward strut spar and the pressure bulkhead. Agreement was very good although the trend of overprediction at low frequencies and

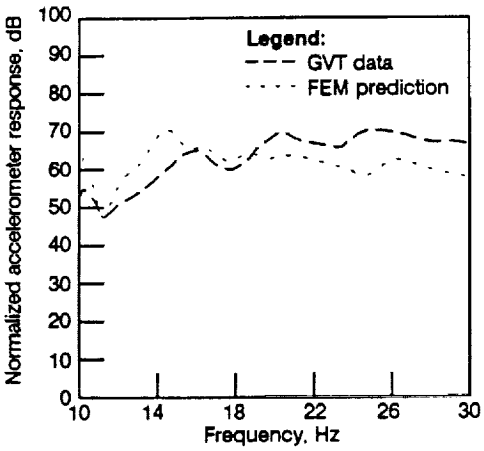

(a) Front Mount Vertical Drive Point

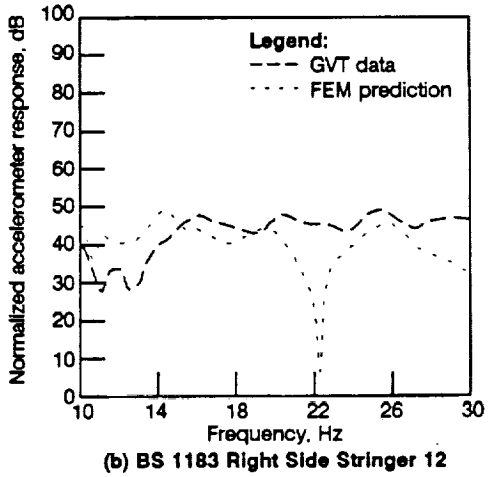

(b) BS 1183 Right Side Stringer 12 Radial Frame Response

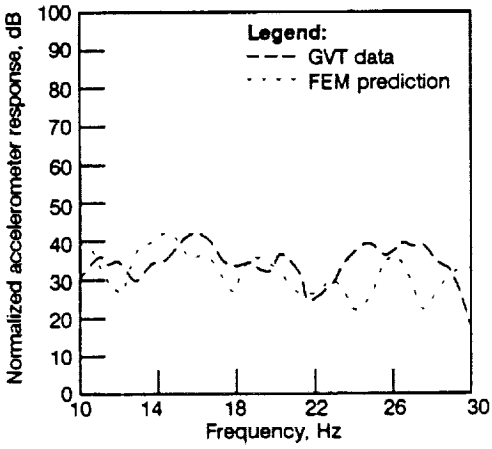

(c) BS 1183 Aft Pressure Bulkhead Right Side Fore-Aft Response

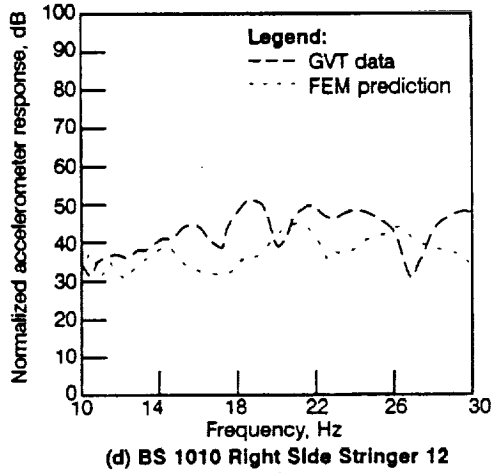

(d) BS 1010 Right Side Stringer 12 Radial Frame Response

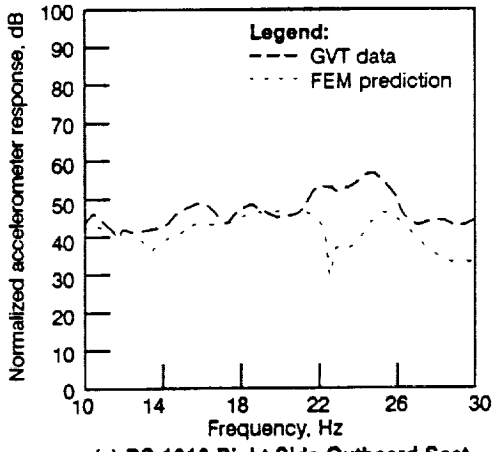

(e) BS 1010 Right Side Outboard Seat Track Vertical Floor Response

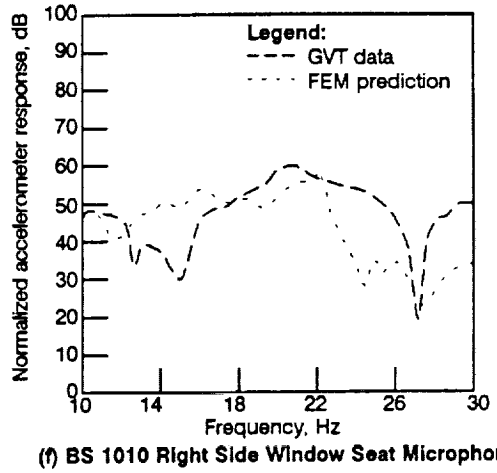

(f) BS 1010 Right Side Window Seat Microphone

Figure 12. Finite Element Prediction Versus 727/GE36 Demonstrator Test; GVT – Front Mount Vertical Shake

9-U90196R1-17

underprediction at higher frequencies seen in the strut response was repeated. The drop out at 22.5 Hz appeared to be related to a spurious strut mode.

Figure 12C compares predicted and measured pressure bulkhead response. Predicted levels were very close to test with a 1.5-Hz shift in frequency believed to be related to the above noted strut modes.

Figures 12D, E, and F show body frame, floor, and acoustic response comparisons at body station 1010, approximately the middle of the test arena. While comparisons are reasonable, some of the largest variations between prediction and test were noted at floor and frame locations. Also, the differences varied considerably between individual measurement points. It was believed that inappropriate lumping of interior masses might have shifted the predicted locations of modal node points, which could have a substantial effect when comparing individual points. At the beginning of the modeling effort, it was assumed that the interior trim mass could be uniformly spread. From these results, it appeared that this assumption was not valid. Interior trim and seats are in fact mounted at discrete locations with the baggage racks and seats being cantilevered from the frames and floor beams. It was recommended that sensitivity studies of mass representation and distribution be completed using the 727 demonstrator airplane model to define mass loading representation requirements.

Figure 12F compares predicted and measured noise levels at a passenger seat. The major trends were predicted and good agreement at the peak response point (for the half-wave axial mode) was observed. It was noted, however, that the predicted response peak was sharper and shifted to a higher frequency than the data. A partition located at body station 890 to separate the test arena from the rest of the airplane was assumed to be rigid for modeling purposes. Inspection of the data suggested that the partition was providing some low-frequency absorption in the form of mechanical vibration. This tended to broaden peak response and shift it to a lower frequency as seen in the test data.

In the initial finite element model, only the cabin airspace was represented. Previous analysis on simplified fuselage section models indicated that the cargo compartment airspace could have a significant effect on passenger cabin acoustic response, particularly at acoustic resonances. It was recommended that this be included in the full 727 demonstrator airplane model.

Comparisons of predicted and measured levels for other shake conditions generally led to the same conclusions as the vertical shake condition with the following one exception. For shake directions in the plane of the strut, a predicted strut mode at 23 Hz coupled with the cabin acoustic mode at the same frequency resulted in an overprediction of interior noise levels. Measured data showed a similar strut mode with lower response near 28 Hz (fig. 13A). The resulting overprediction in noise is shown in figure 13B. Another factor possibly contributing to the overprediction at the acoustic resonance was the rigid boundary condition assumed for the acoustic curtain.

Flight data predictions did not match well with measured levels. The model showed a great deal of sensitivity to both input unbalance levels and phase between propellers. Unfortunately, measured response data did not include phase information referenced to the propellers that made assessment of flight

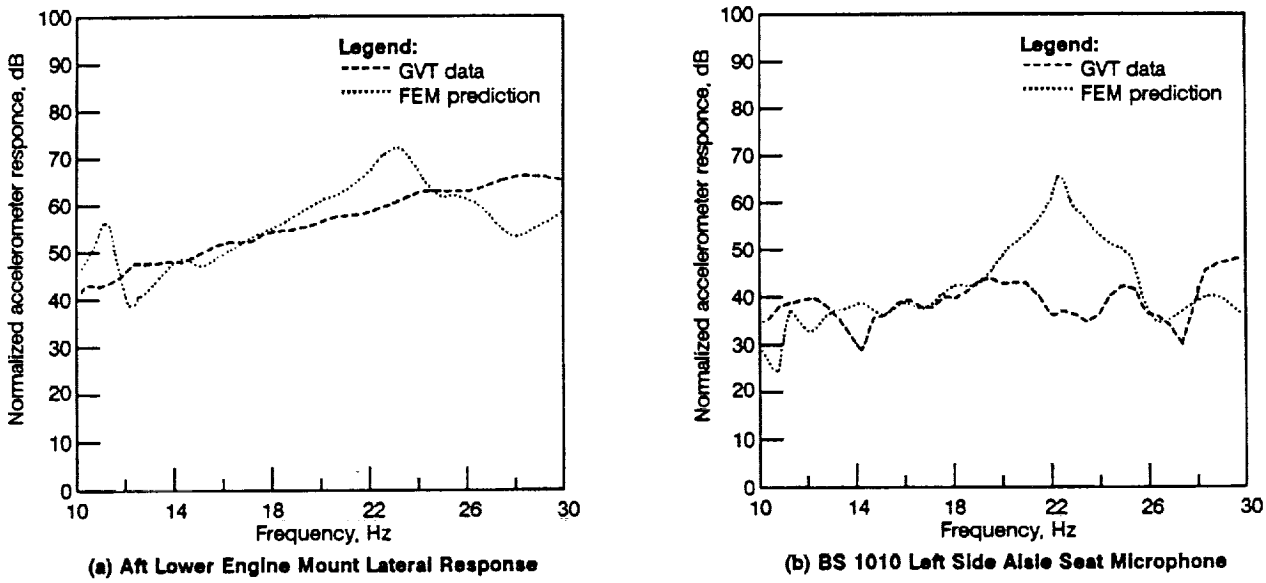

Figure 13. Finite Element Prediction Versus 727/GE36 Demonstrator Test; GVT – Aft Lower Mount Lateral Shake

9-U90196R1-18

predictions difficult. Phase measurements referenced to propellers were recommended for any future testing.

Agreement between predicted and GVT data showed the finite element modeling procedure to be a valid tool for predicting low-frequency structural-acoustic behavior. Based on the above results, it was recommended that studies of strut and acoustic curtain modeling and trim mass distribution be completed.

Use of the finite element model was found to be time consuming and expensive. The sheer size of the model made assembly and checkout a very lengthy process. Turnaround of results was also slow. It was also recommended to systematically reduce the size and simplify the model to define the minimum model size requirements versus frequency. As stated previously, the entire aircraft was modeled because the effect of gross airplane modes was not known.

4.2 FINITE ELEMENT MODEL IMPROVEMENTS (FY 1988)

The existing finite element model was refined by improving the mass distribution of interior nonstructural elements and improving the acoustic curtain representation. The propeller engine strut model was checked for modeling errors due to spurious modes identified during 1987 work. Some errors were found and corrected. Details are given below.

The initial finite element modeling procedure simply smeared the mass of interior trim and seats evenly as shown for a ceiling panel example in figure 14A. In fact, this panel is supported only at discrete points along its edges. The mass of the ceiling panel was redefined as concentrated masses at the attachment points only (fig. 14B). The hat rack and seats were originally defined as lumped masses at the fuselage

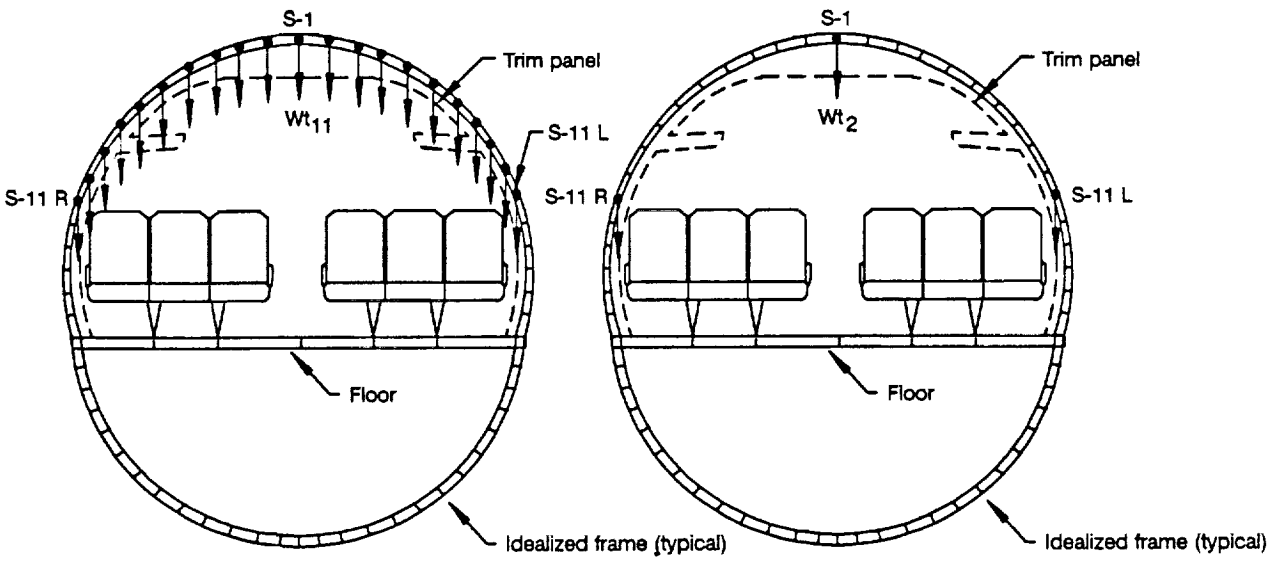

(a) Original Ceiling Panel Weight Distribution **(b) Revised Ceiling Panel Weight Distribution**

Figure 14. Original and Revised Ceiling Panel Weight Distribution

U90196R1-19

mold line and in the plane of the floor, respectively. Their masses were redefined as concentrated masses located at the center of gravity. The hat rack change is portrayed in figure 15.

The test airplane configuration included a partition to separate the forward portion of the aircraft, which was filled with test equipment from the aft acoustic test arena. This partition was constructed from a honeycomb board with fiberglass and lead vinyl installed on both sides. Original modeling assumed this

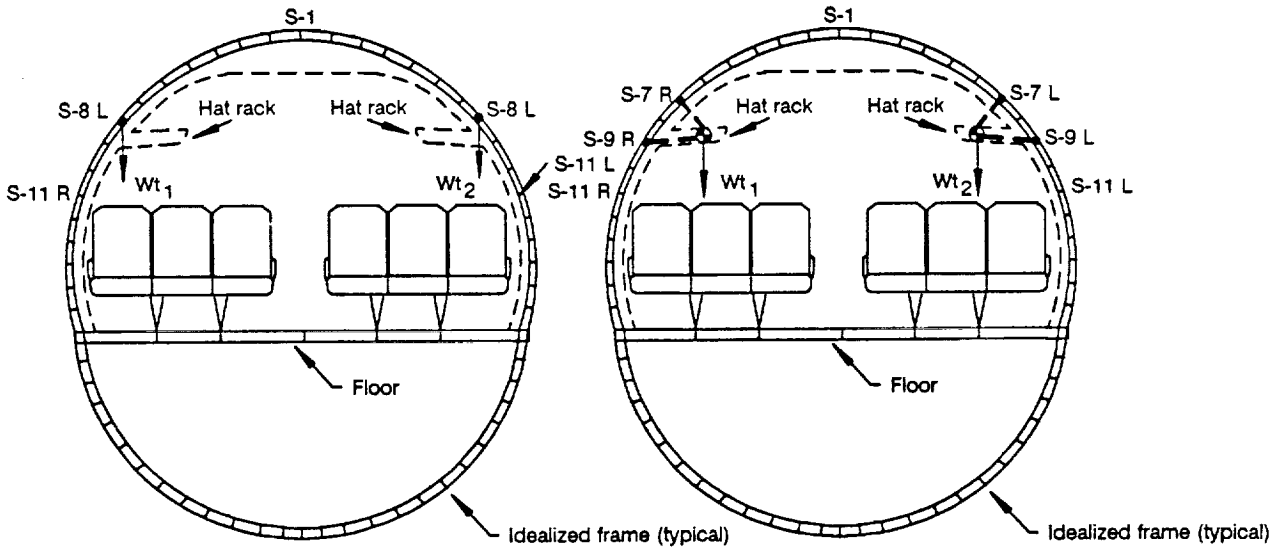

(a) Original Hat Rack Weight Distribution **(b) Revised Hat Rack Weight Distribution**

Figure 15. Original and Revised Hat Rack Weight Distribution

U90196R1-20

partition to be rigid. Predicted acoustic response showed the acoustic resonance to be 1 to 2 Hz more than seen in the test. This may be the result of ignoring the effects of mechanical vibration in the initial model. Therefore, the acoustic partition model was changed to a flexible partition using brick elements to represent the mass and stiffness of the fiberglass and lead vinyl septum on the test arena side.

It was noted previously that strut modes were predicted that either did not occur in the measured results or were at significantly different frequencies. It was suspected that the strut and empennage connection, very complex for the modified demonstrator aircraft, might be in error. The model was compared to drawings and a few changes were made with the net effect of increasing strut stiffness.

The above changes constituted the improved finite element model that was used to repredict ground vibration test conditions. In addition, further studies were conducted by representing the cargo compartment airspace and by systematically reducing the size of the improved model. A finite element mesh of the cargo compartment airspace was generated that interfaced with the lower sidewall and floor structural nodes. The cabin acoustic model interfaced with the same floor nodes allowing coupling between the acoustic spaces (fig. 16).

As was noted previously, the size of the finite element model made its use time consuming and expensive. Figure 17 shows model representations that were studied to define minimum model size requirements. In the first case, the stiffness and mass substructures aft of BS 1183 were dynamically reduced to the retained degrees of freedom at the aft pressure bulkhead and the engine attach points. In the second case, the empennage and tail section aft of the strut rear spar were replaced by a beam model. Finally, a representation that ignored structure aft of the strut rear spar and forward of the acoustic test arena was considered.

4.3 FINITE ELEMENT ANALYSIS RESULTS (FY 1988)

Predictions made using the refined baseline model are given in figures 18 through 24. Figures 18 and 20 compare 1987 and 1988 predictions to GVT data. In this case, results are plotted up to 40 Hz in order to better understand response characteristics around 30 Hz. Overall, the refined finite element model yields reasonable predictions of the GVT response. The most notable improvement in predictions associated with this model is the acoustic response at the acoustic resonance for lateral and axial shake conditions.

Figure 18 compares predictions to test for a front mount vertical shake condition at several of the positions discussed previously. At the drive point (fig. 18A) the new prediction follows the trends seen in the GVT. As a direct result of the improved strut and bulkhead modeling, a closer match of prediction and test is obtained at less than 24 Hz. At more than 24 Hz, the model still underpredicts the data.

Figures 18B, C, and D show body frame, floor, and acoustic response comparisons at approximately the middle of the test arena (BS 1010). It was this area that was noted to have some of the largest variations between prediction and test when evaluating 1987 results. This led to the review and improvement of the interior trim mass distribution in the refined model. Although the refined model yields reasonable

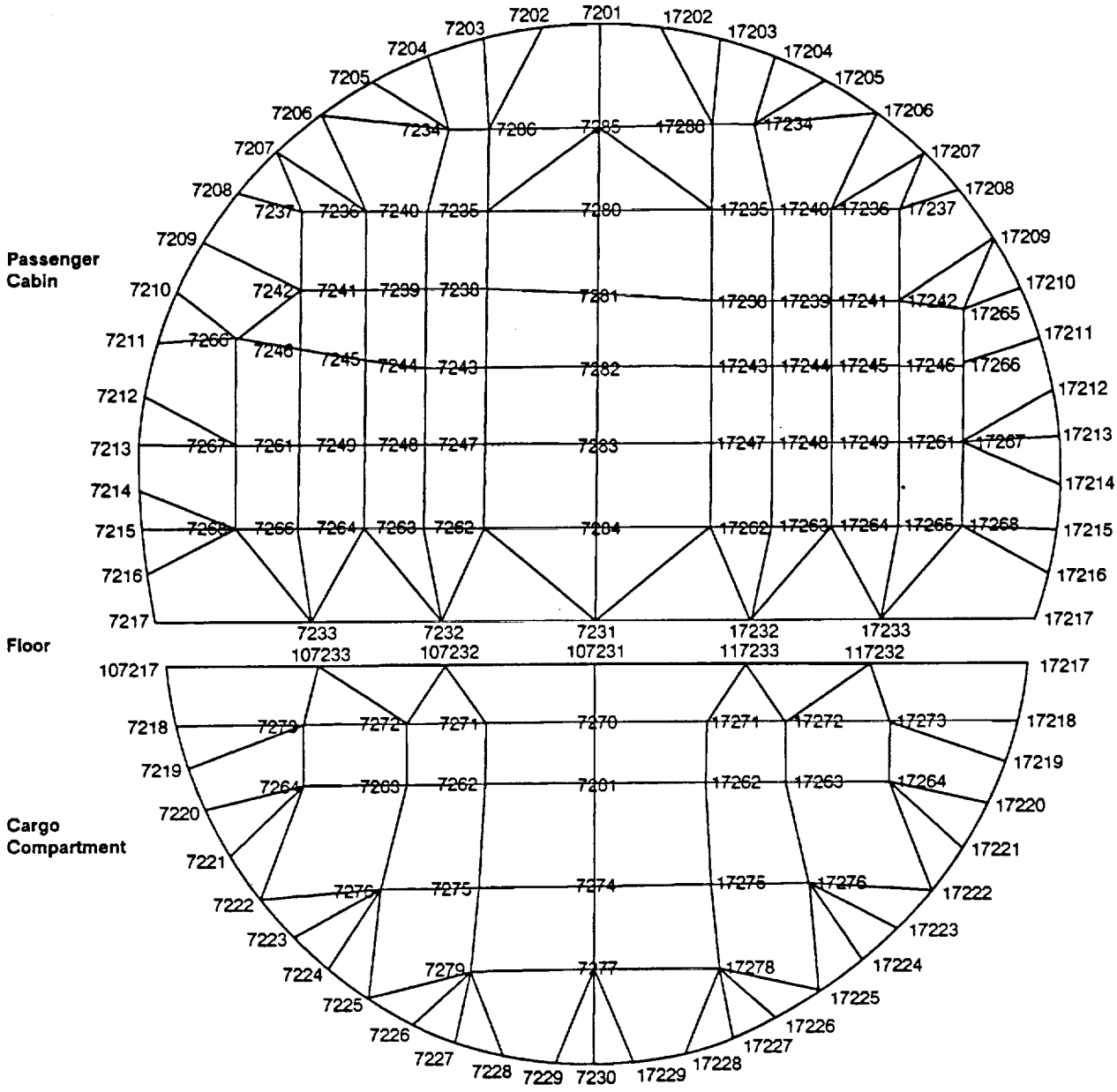

Figure 16. Acoustic Mesh Typical Cross Section

9-U90196R1-21

predictions of trends and levels, there is no clear improvement over 1987 results. In fact, the response prediction for the window seat microphone appears worse. However, at this frequency the model is very sensitive to axial position because of the node line of the first acoustic mode. Changing the acoustic partition properties has moved the predicted response node position slightly. Figure 19 compares the predicted noise levels at three sequential axial positions near the GVT measurement point. As can be seen, there is a 20 dB difference at approximately 22 Hz in the three predictions with the prediction for BS 990 closely matching the data at BS 1010. This illustrates one of the difficulties in comparing the test data to prediction on a point-to-point basis.

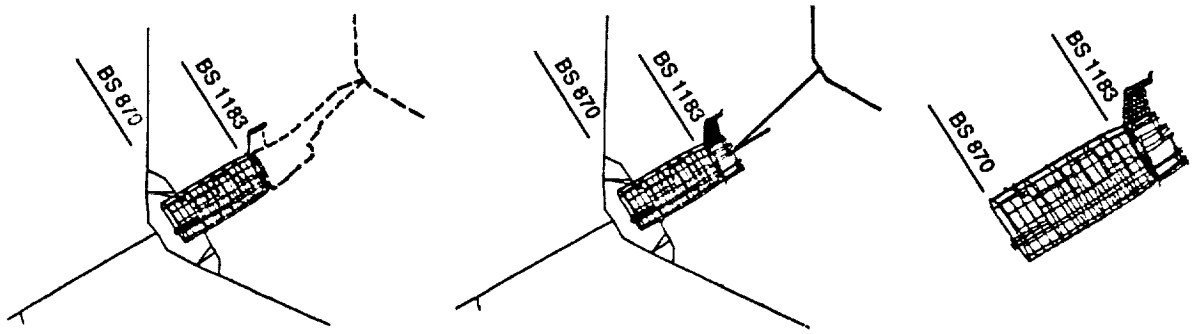

Reduced model A – dynamic reduction of aft-end shell structure

Reduced model B – aft-end beam model

Reduced model C – passenger cabin and strut model

Figure 17. 727 Demonstrator Airplane – Reduced Finite Element Models

9-U90106R1-22

For the lateral shake condition, the refined model did a better job than the original model based on improvements to the strut and acoustic curtain models. At the drive point, the predicted response follows the measured response trend at less than 24 Hz (fig. 20A). The refined model now predicts a mode at 24.5 Hz (versus 23 Hz originally) that corresponds to a 28-Hz peak in the measured data. Similarly, a 37-Hz peak in the measured data is also underpredicted by approximately 3 Hz. This improvement in strut response prediction coupled with the more accurate representation of the acoustic curtain led to a much improved prediction for the interior noise level (fig. 20B).

As stated earlier, point-to-point comparisons of test data and prediction can be difficult due to uncertainties associated with exact location of test instrumentation and small differences in location between predicted and measured modal node lines. An alternate way to assess the finite element model predictions is to compare the range of response for all individual measurements of a common set of instrumentation with the corresponding predicted levels. Figures 21 and 22 compare measured ranges of test data to predictions for the front mount vertical shake and aft lower mount fore-aft shake conditions, respectively. The areas shown for comparison are the bulkhead, the floor, the body frame at BS 1010, and the cabin interior.

For the front mount vertical shake condition, the majority of predictions for the individual locations fall within the range of measured data with the exception of the floor response. Predictions are particularly good at more than 20 Hz. For comparison, data and predictions for an aft mount fore-aft shake condition are presented in figure 22. The same general comments for the front mount vertical shake condition apply here as well. Note that the model accurately predicts the changing sensitivity of the cabin sidewall and airspace to force inputs in the vertical and axial directions. That is, for the vertical shake condition measured and predicted response remains fairly constant while for the fore-aft shake condition, both clearly rise with increasing frequency.

Using the refined model, the effect of modeling the cargo compartment acoustic space was evaluated. A finite element mesh of the cargo compartment was generated that interfaced with lower sidewall and floor structural nodes. The cabin acoustic model interfaced with the same floor nodes (fig. 16) allowing coupling between the two compartments. Predictions show small differences to the cabin acoustic response most notably at the cabin acoustic resonance and at a cargo compartment acoustic resonance,

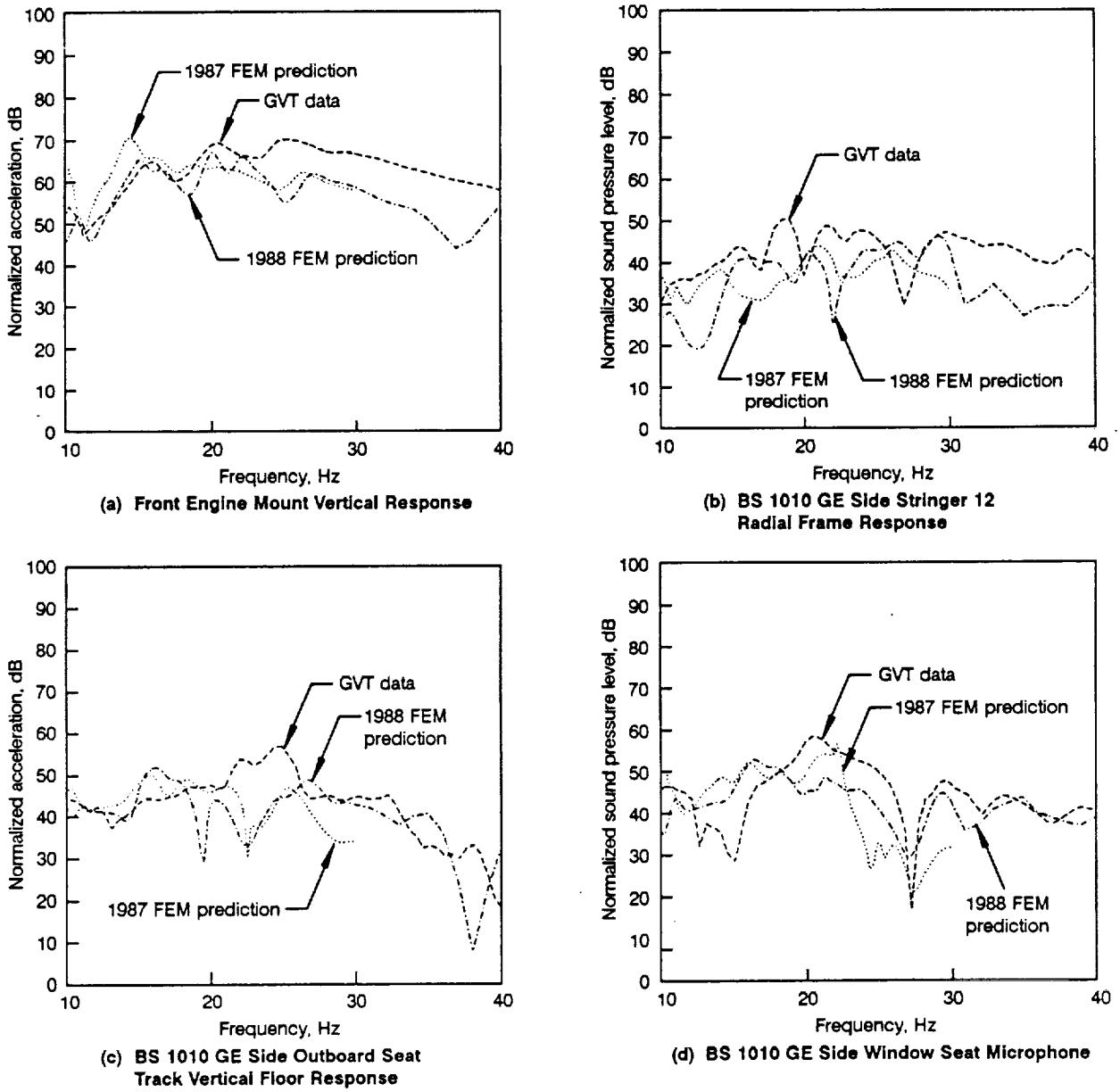

Figure 18. Finite Element Prediction Versus 727/GE36 Demonstrator Test; Ground Vibration Test – Front Mount Vertical Shake

9-U90198-23

which occurs at 32 Hz. However, the general characteristics of the response are not changed and further studies were completed without the cargo compartment model.

A study was also completed to help define minimum modeling size requirements. It was noted that the tremendous size of the finite element model made model checkout and predictions time consuming and expensive. A series of model size reductions were previously described (fig. 17). These models were used to predict response to several shake conditions in order to assess prediction costs and associated accuracy. Table 3 gives cost and model size comparisons for each model as referenced to the baseline (refined)

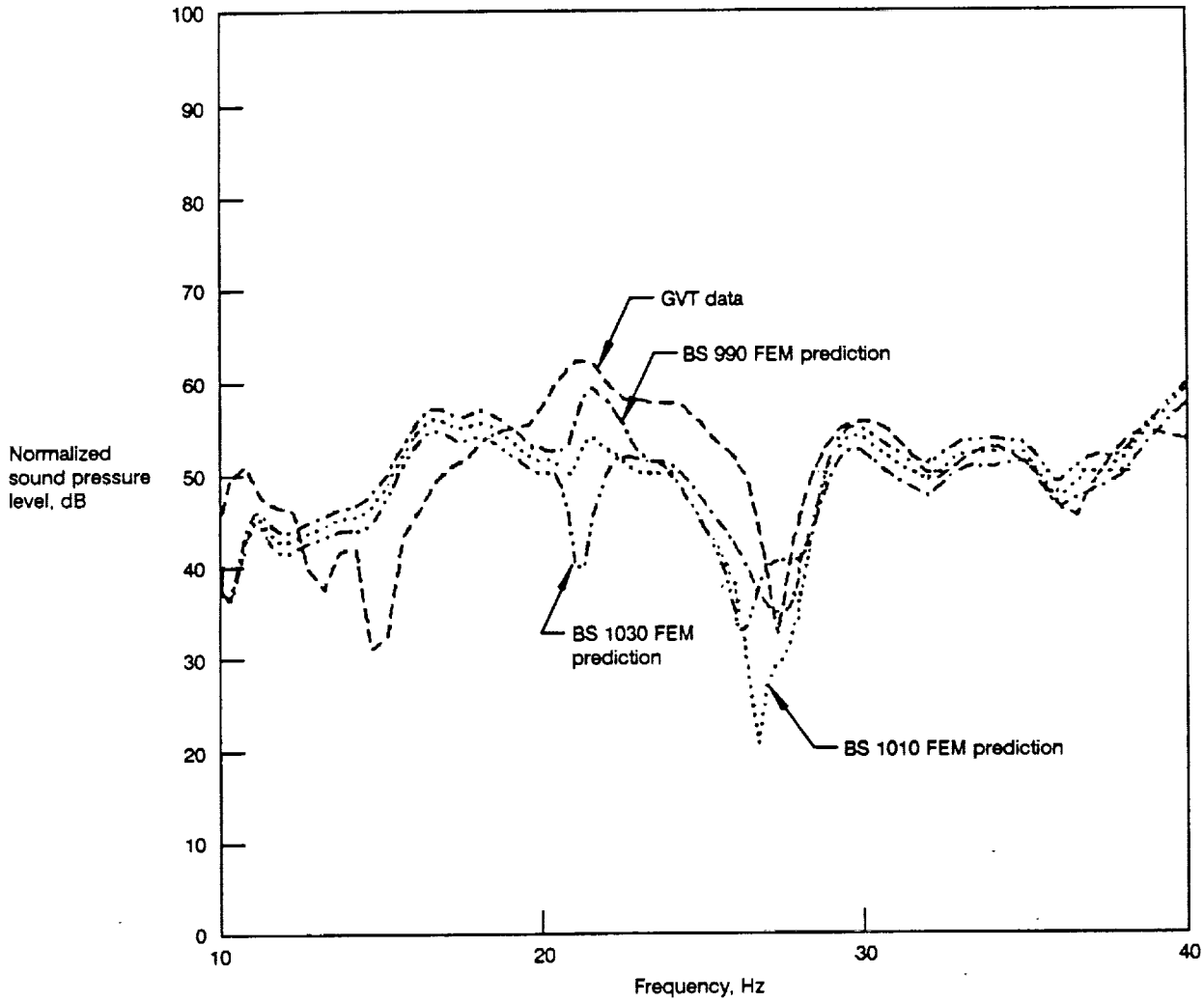

Figure 19. Longitudinal Variations Around BS 1010—GE Side Window Seat Microphone Prediction

9-U90196-24

model. As can be seen, 40% to 60% reductions in computing costs were achieved as well as up to 40% reductions in model size. Figures 23A and 23B compare the baseline model to the reduced models for passenger cabin sidewall and acoustic response, respectively, for an aft lower mount vertical shake condition. The results shown in figure 23 are typical for all the shake conditions. It was felt that reduced models A and B still gave reasonable results, but that complete elimination of the tail, wing, and forward body structure (reduced model C) degrade predictions to unacceptable levels within the frequency range studied. A further comparison that more clearly illustrates this conclusion is contained in figure 24. The importance of gross airplane modes in prediction transmission and radiation of engine vibration noise within this frequency range has been noted previously.

The refined model reflects a valid representation of the 727 demonstrator airplane per production drawings. Inclusion of trim structural and seat absorption models might offer some improvement although tap tests and noise surveys completed during ground tests indicate the main effects would occur at more

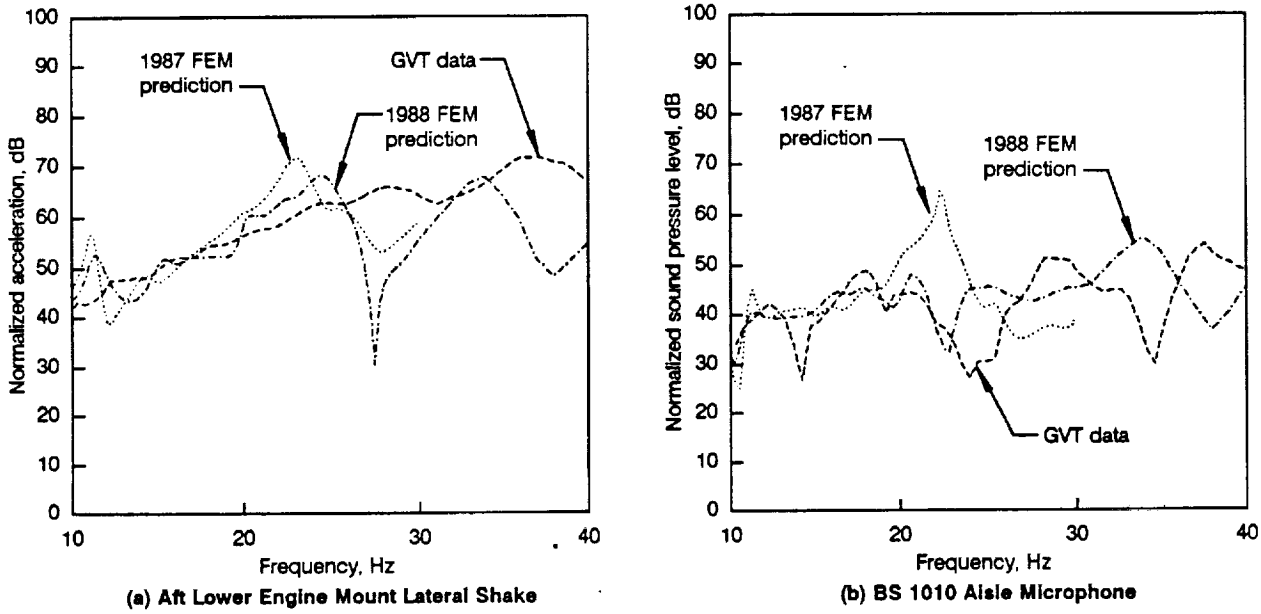

Figure 20. Finite Element Prediction Versus 727/GE36 Demonstrator Test; Ground Vibration Test—Aft Lower Mount Lateral Shake

9-U90196-25

than 40 Hz. The extremely complex empennage and strut structure, modified for the GE36 engine, make modeling difficult and may lead to some problems that would not be encountered in more conventional structure. Given the above comments and the results presented in this section, it is concluded that finite element models can be used to predict differences in cabin noise and vibration sensitivity to engine unbalance forces for different force levels and directions and for different aircraft configurations. However, the ability to predict absolute levels at discrete frequencies, with accuracy typically required to make cabin noise guarantees, has not been demonstrated.

Other studies with the model for flight predictions have shown that the phase relationships between multiple input forces can shift predicted cabin noise levels 20 dB or more. This result has been validated independently on flight tests of conventional turbofan aircraft. Thus, the analyst also needs a good understanding of engine response characteristics in order to assess cabin noise at engine rotor frequencies.

Model reduction studies indicate that within the frequency range studied in this effort, some representation of the entire aircraft is required. That is, low-frequency whole body and wing modes can contribute to transmission and radiation of engine rotor noise. This effect diminishes with increasing frequency. Therefore, the analyst should have some understanding of the aircraft response modes versus the frequency range of his interest in order to determine model size requirements.

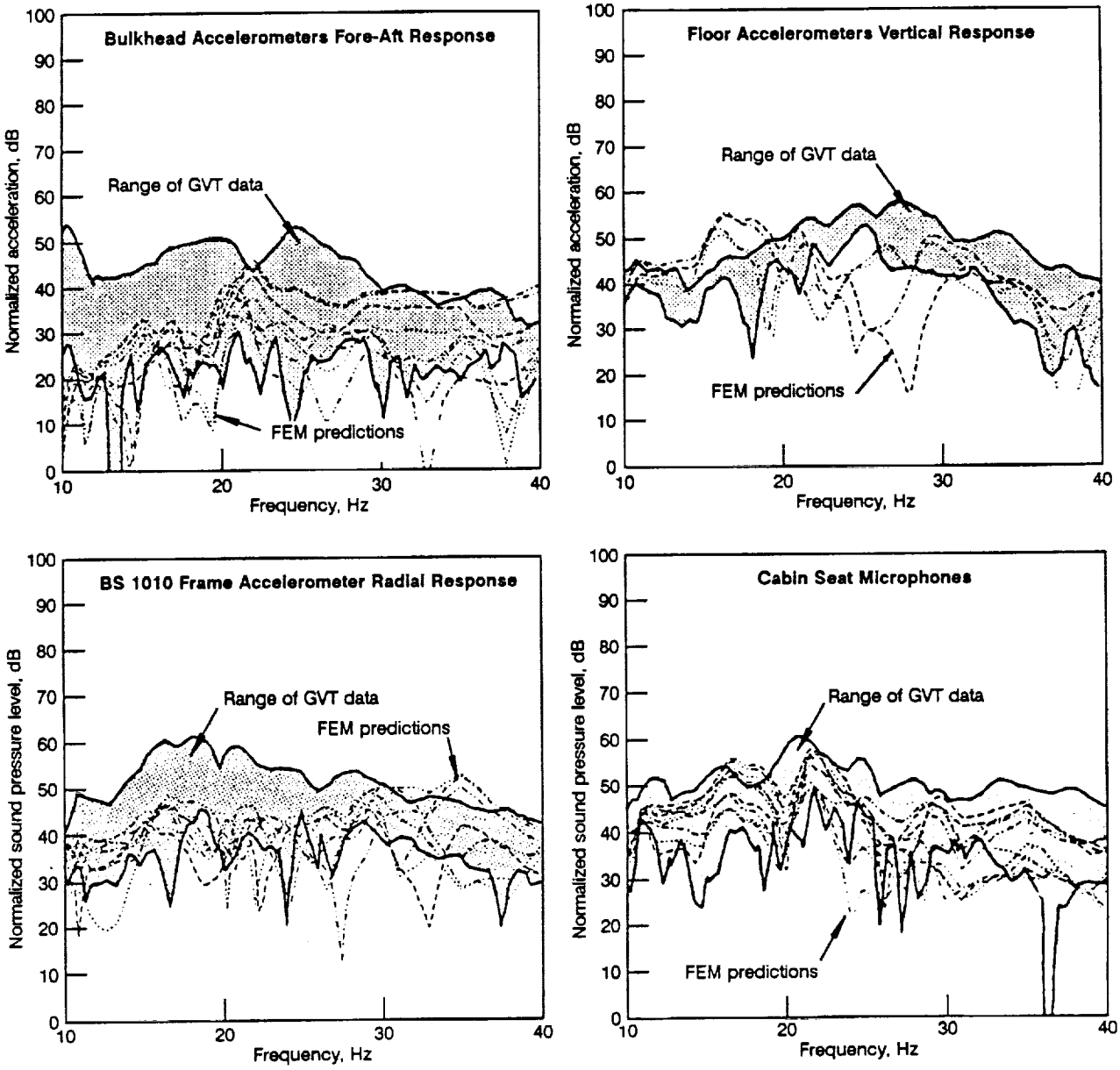

Figure 21. Finite Element Predictions Versus 727/GE36 Demonstrator Test; Ground Vibration Test—Front Mount Vertical Shake

9-U90196-26

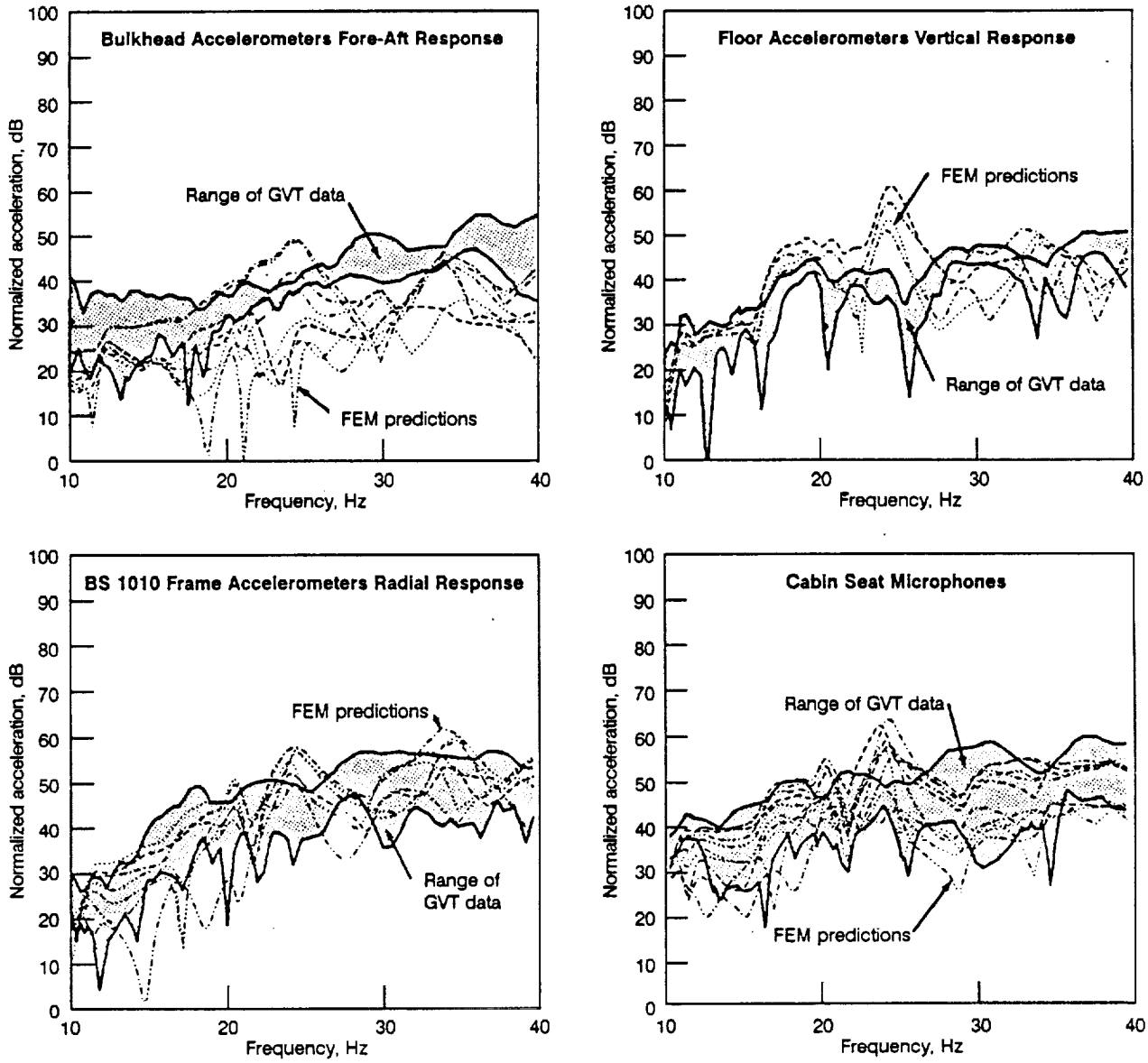

Figure 22. Finite Element Predictions Versus 727/GE36 Demonstrator Test; Ground Vibration Test—Aft Lower Mount Fore-Aft Shake

9-U90196-27

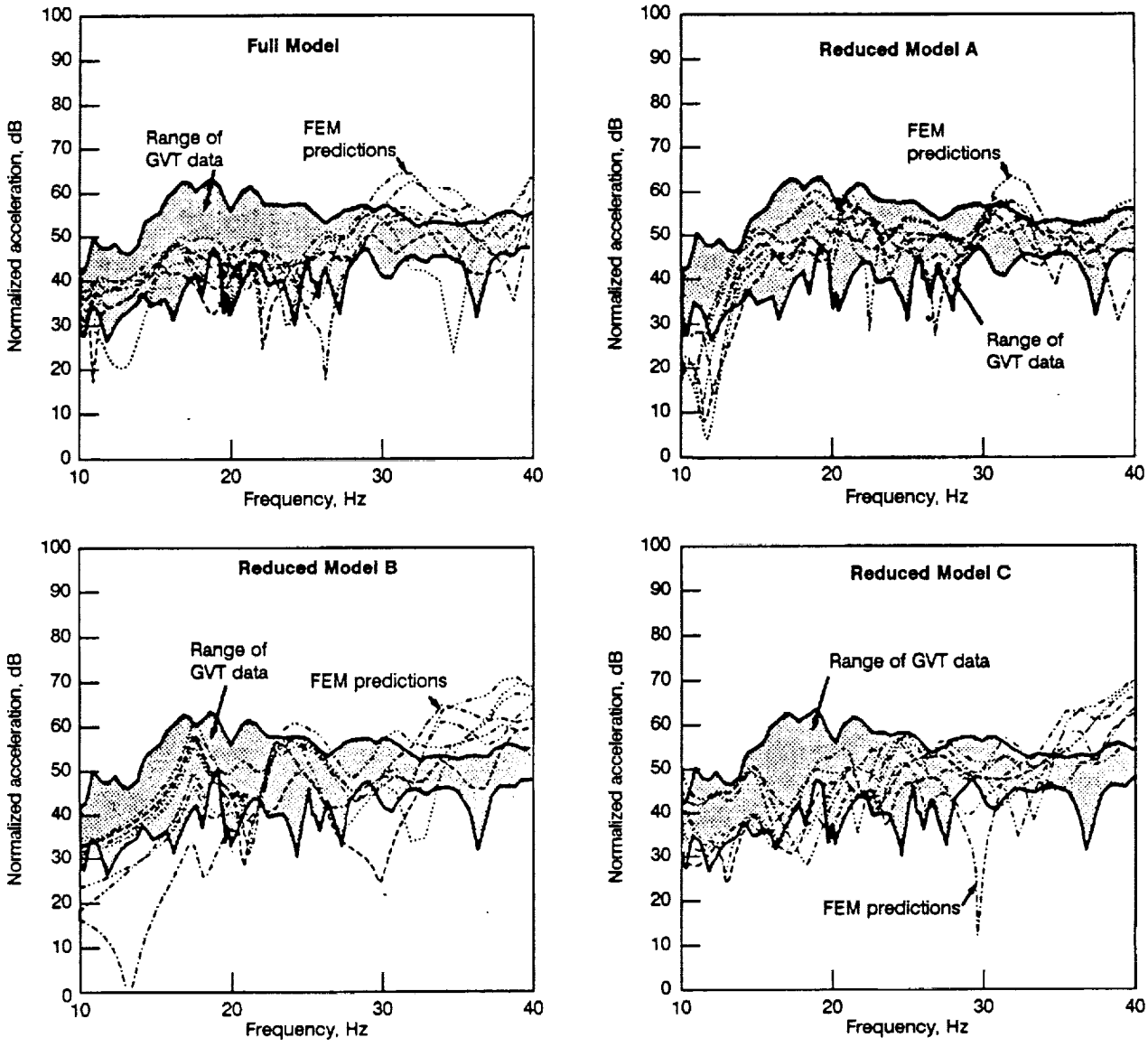

(a) BS 1010 Frame Accelerometers Radial Response

Figure 23. Finite Element Predictions Versus 727/GE36 Demonstrator Test; Ground Vibration Test—Aft Lower Mount Vertical Shake

9-U90196-28

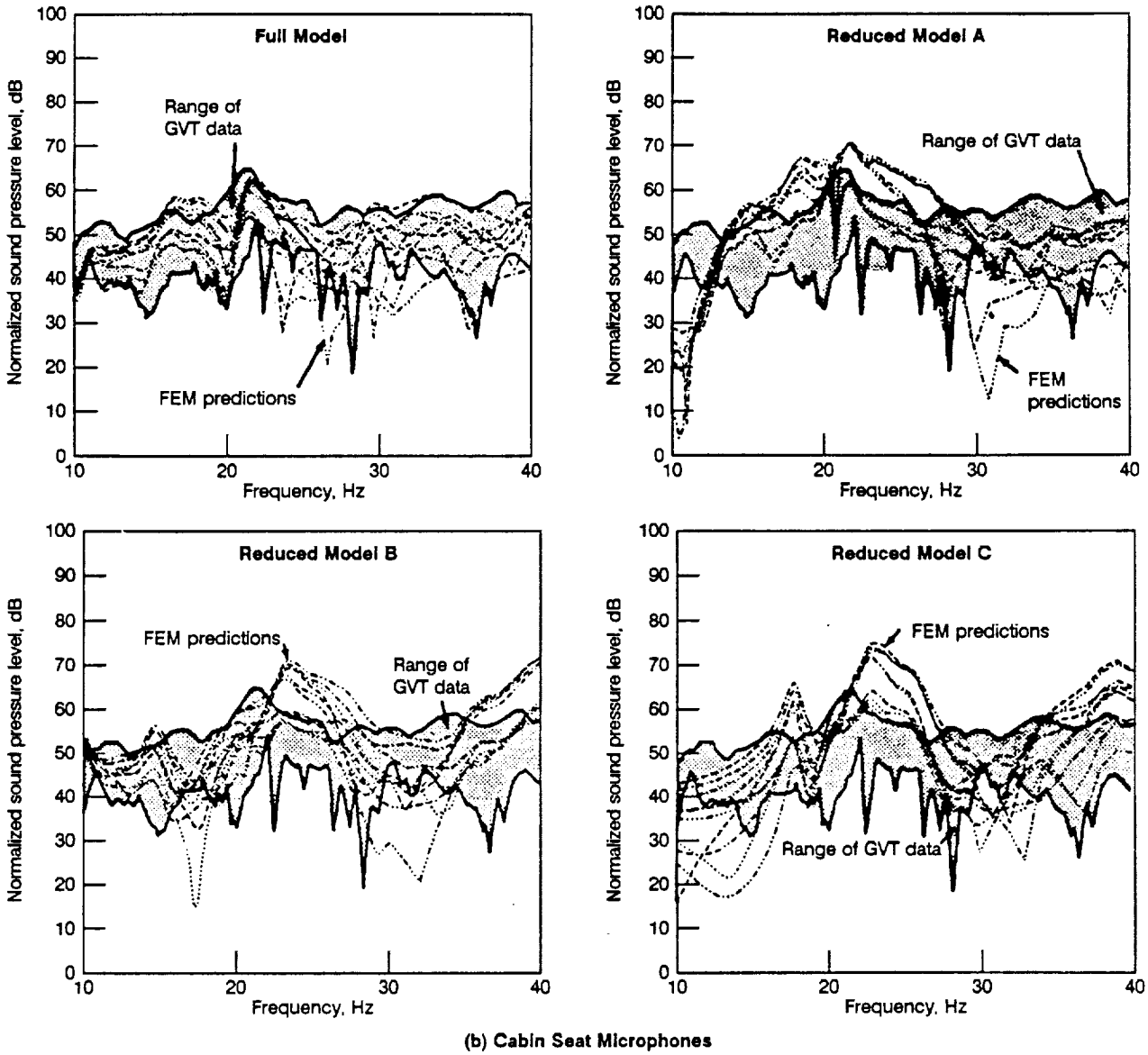

Figure 23. Finite Element Predictions Versus 727/GE36 Demonstrator Test; Ground Vibration Test – Aft Lower Mount Vertical Shake

9-U90196-28a

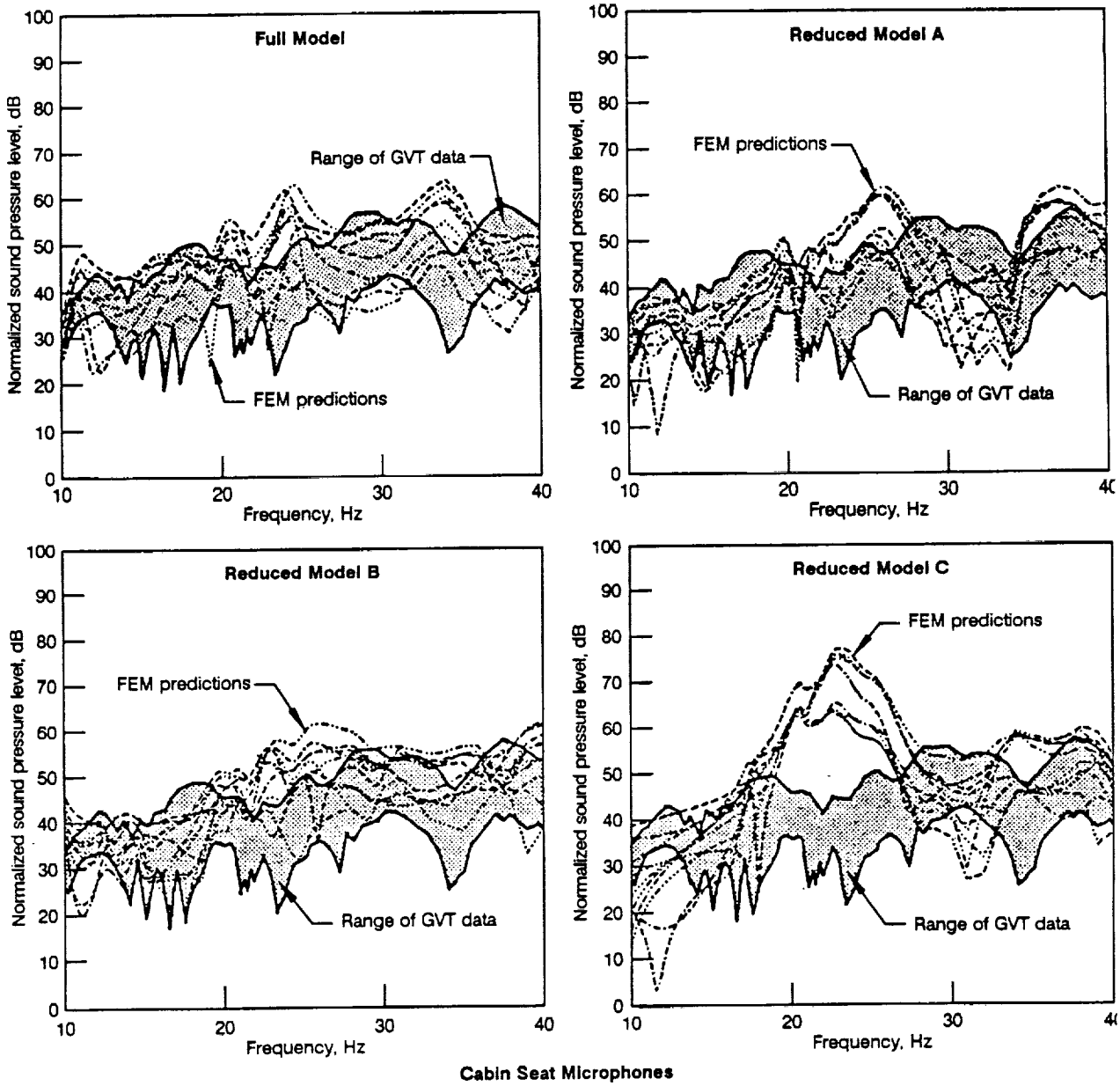

Figure 24. Finite Element Predictions Versus 727/GE36 Demonstrator Test; Ground Vibration Test—Aft Lower Mount Lateral Shake

9-U90196-2

Table 3. Modeling Time and Cost Comparison for 727 Demonstrator Airplane Finite Element Models

Model	Scaled number of structural nodes	Scaled number of structural elements	Scaled cost of modal calculation	Scaled cost of one forced response calculation	Scaled cost of modal plus one forced response calculation
Baseline	1.00	1.00	0.64	0.36	1.00
Reduced model A	1.00	1.00	0.44	0.15	0.59
Reduced model B	0.67	0.71	0.33	0.29	0.62
Reduced model C	0.65	0.61	0.28	0.16	0.44

U90196R1-3

4.4 STATISTICAL ENERGY ANALYSIS RESULTS (FY 1987)

Statistical energy analysis models were developed to predict response for the rotor frequency range and the propeller frequency range. Predictions were compared to engine strut shake, side-of-body shake, and flight test conditions.

Unlike the finite element analysis, which used specific structural and acoustic modes, the SEA models relied on predicted modal densities within each substructure to calculate power transfer to the passenger cabin structure and airspace. Specific mode shapes for frequencies were not calculated, rather a statistical description of modes and interaction of modes with adjacent substructures was used. Thus, predictions for structures with higher modal densities tend to be better. As part of this effort, it was found that the dimensions and physical properties of aircraft structures tend to give low modal densities for the frequency ranges studied.

Low-Frequency Model

Low-frequency (rotor) model predictions were made up to 100 Hz for eight strut shakes, one side-of-body shake, and one flight test condition. The model was felt to be valid over this frequency range despite lumped mass representation of the interior trim. Results from the midfrequency (propeller) model showed energy transfer from the trim to be small compared to that from sidewall structure modes.

Example comparisons of ground test data with low-frequency model predictions for lateral and vertical strut shake condition are given in figures 25A through 25D and 26A through 26C for the strut, fuselage sidewall, floor, and acoustic space. The predicted average represents the space average response for the subsystem. The 95% confidence intervals represent the range or variance predicted for response at individual locations on or within the substructure (up to 95% confidence). All of the available measured data on or within the subsystem were compared to the prediction.

The following general observations were made:

1. For the most part, the data fell within the predicted confidence interval, although the interval appeared to be somewhat greater than the corresponding ranges of measured data for the lateral shake condition and somewhat less for the vertical condition.

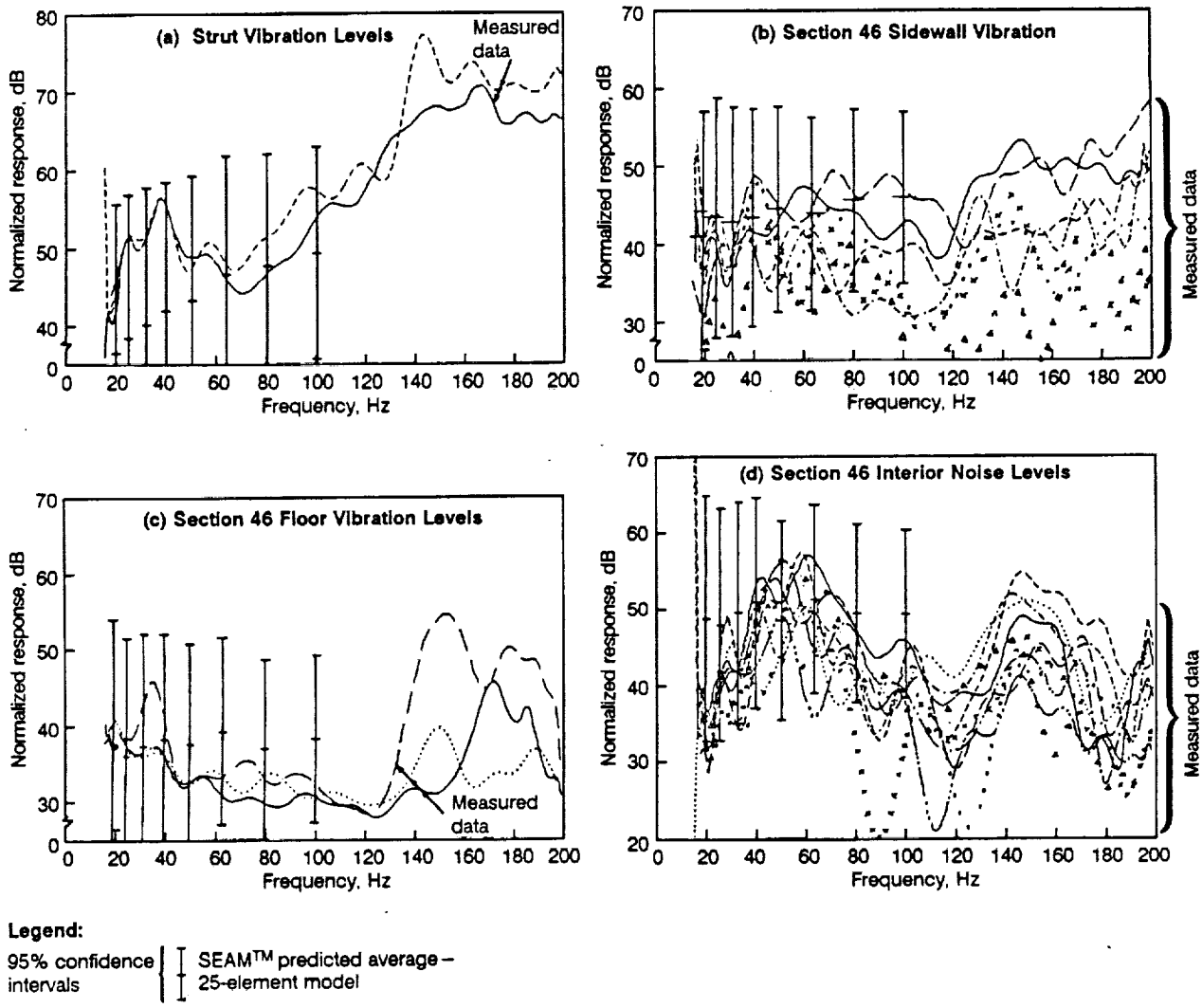

Figure 25. SEAM™ Predicted Levels Versus 727 Demonstrator Test Data; GVT – Forward Mount Lateral Shake

9-U90196-30

2. The data peaks were in generally good agreement with the upper limit of the confidence interval, but the predicted average exceeded the data average at many frequencies.

3. The rise and fall of the data mean with frequency was not predicted by the model, particularly for strut and acoustic response.

For the lateral strut shake condition, the large confidence interval was due to uncertainty in predicted power input to the strut inplane subsystem. This uncertainty results from the low modal density of the strut inplane subsystem. For any structure, the range between maximum and minimum levels will increase as the modal density is decreased.

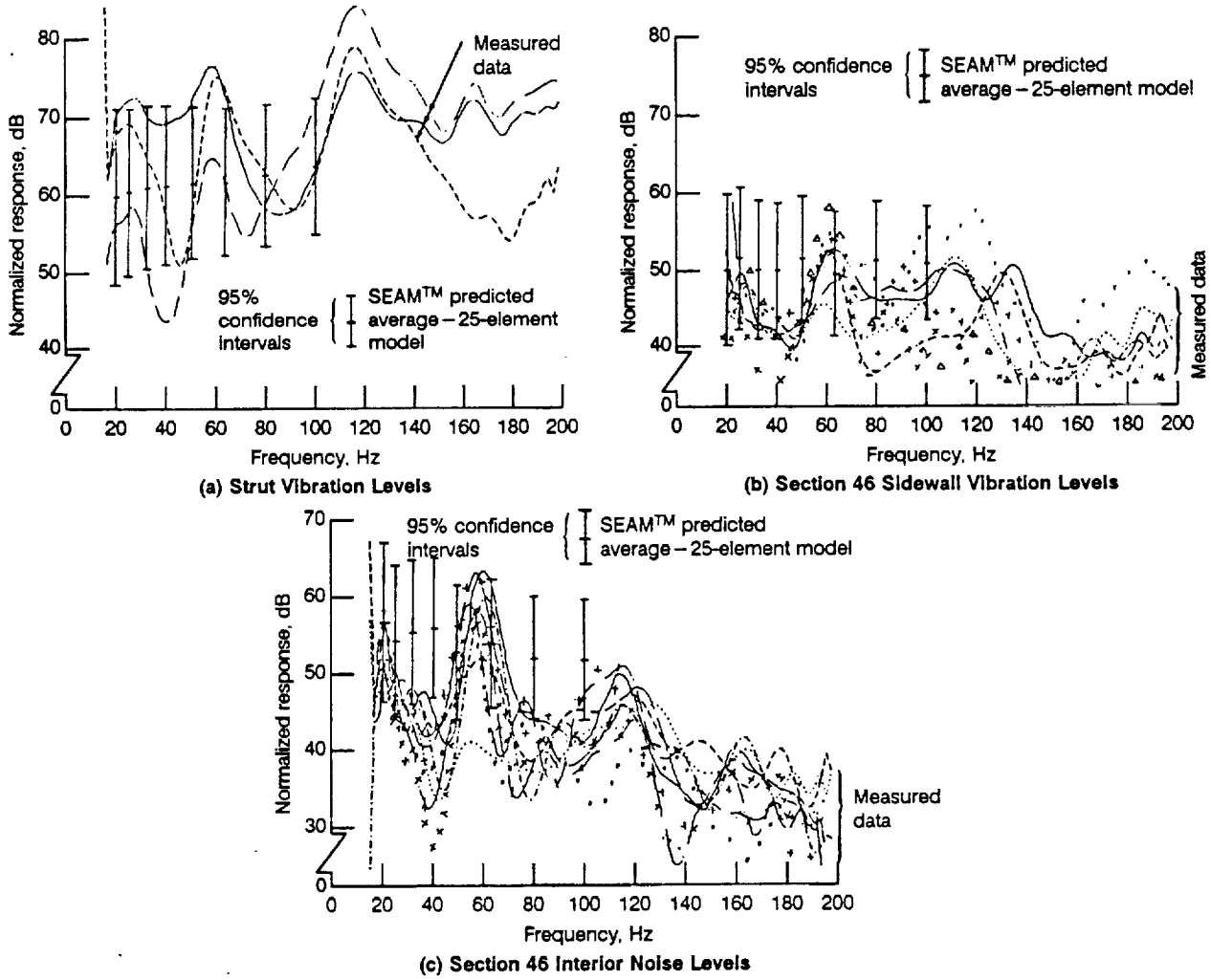

Figure 26. Low-Frequency SEAM™ Model Predicted Levels Versus 727 Demonstrator Test Data; GVT – Forward Mount Vertical Shake

9-U80196-31

It was found that for this and other test conditions, the response at locations away from the drive point were overpredicted by a biased amount. This indicted that predicted power inputs, corresponding to the measured input force, were too high although the transmission modeling is correct. (This may seem at odds with the underprediction of strut response shown in figure 25A. However, the measured data are at the end of the strut near the drive point and does not accurately represent average strut response or power.) The overprediction of power input was related to modeling the drive point structure as an unbounded system.

Finally, the failure of the model to predict variations of the mean was attributed to low modal densities in the actual aircraft structure in this frequency range. This led to the possibility of individual modes dominating response. In this case high strut response near 40 Hz and a cross-cabin acoustic mode near 50 Hz appeared to combine to give the broad peak in acoustic levels.

By comparing figures 25 and 26, it was noted that the model predicted the very large measured difference in strut response for the lateral and vertical drive conditions, as well as the much lower interior noise. This again indicated the transmission modeling was correct and that SEA is capable of predicting aircraft response trends at low frequencies.

Midfrequency Model

Midfrequency model predictions were made for two strut shake, three side-of-body shake, and one flight test condition. Originally, it was planned to make predictions for more GVT conditions. However, the additional time and budget expended on the initial modeling effort (400-element model) and subsequent revisions precluded this.

Evaluation of the model concluded that composite-bending stiffness modes of the sidewall dominated energy transfer to the passenger cabin when compared to trim-panel-bending and skin-membrane-bending modes. The same observations made for the low-frequency model generally held for comparisons of mid-frequency model predictions to test. Predictions tended to be somewhat better and the influence of individual modes was minimized in this frequency range. The test arena acoustic space was represented by three space subsystems rather than one (in the low-frequency model) and falloff in level versus body station was accurately predicted. Figure 27A presents sample midfrequency model predictions for a GVT strut shake condition. Again, the strut response appears underpredicted, but note that all the measurement points are at the end of the strut. Figure 27B shows predictions for sidewall vibration levels, and figure 27C shows predictions for aft interior noise levels.

Flight test predictions were hampered again by the inability to estimate input power, a situation also noted when using PAIN as described later. In this case, measured accelerations were used to develop input forces. Predicted responses downstream of the strut showed consistent bias levels (overprediction) with respect to the measured data. This indicated that estimated power was again overpredicted but that energy flow was accurately modeled.

Based on the results presented, it was concluded that SEA shows promise in providing relatively simple models for evaluation of low-frequency noise and vibration transmission. The mean and variance estimates provided by SEAM^{TM} are useful to the designer in that the upper bound of predicted response can be compared to requirements for maximum allowable noise and vibration. The power flow analysis feature can be useful in guiding design type and application of suppression hardware.

Two areas of study were recommended including investigation of power input estimation techniques and improved modal density estimates for low-frequency problems.

In this effort, excitation loading (input power) was developed from input forces and conductance of the strut (or body) derived from the SEA model. Results showed the response to be consistently overpredicted, while the rate of response falloff (with distance from the drive point) was accurately predicted. This suggested that the input power was overpredicted. In the model, the input power was predicted in terms of the average conductance of the subsystem (associated with the drive point), with the

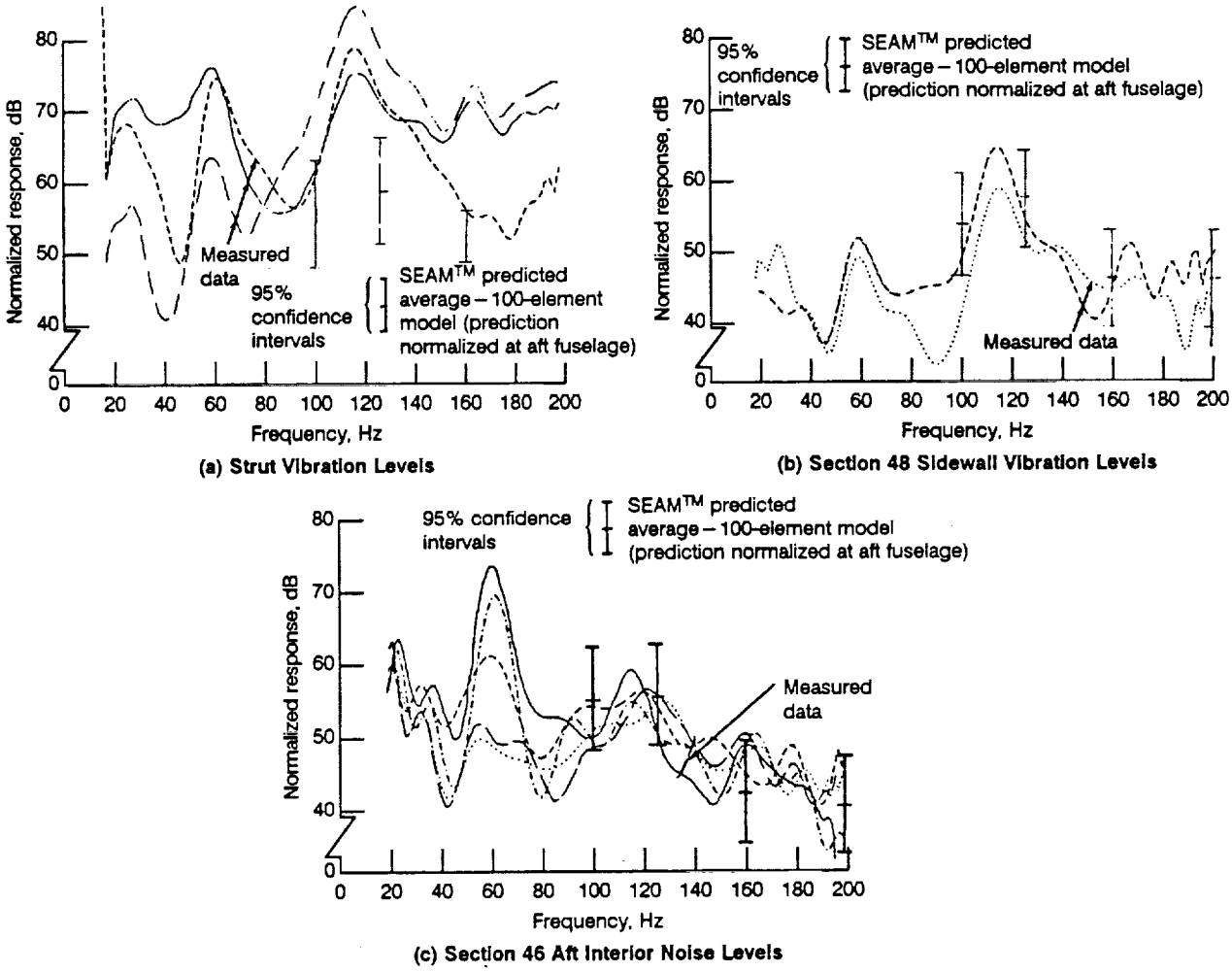

Figure 27. Midfrequency SEAM™ Model Predicted Levels Versus 727 Demonstrator Test Data; GVT – Forward Mount Vertical Shake

9-U90196-32

average encompassing at least one resonance frequency of the subsystem. At frequencies below the first subsystem resonance, the input power will be incorrectly predicted. Some method for handling these cases must be developed.

It was noted that the SEA predictions do not follow variations with frequency of the measured mean response. A review of data indicated that low modal density in the aircraft structure may result in response that can be dominated by a few individual modes. Because SEA does not calculate specific modes, it will not tend to predict this behavior. For example, a cross-cabin acoustic mode near 50 Hz seemed to influence measured noise levels, but the SEA model only predicted modal densities based on volume of the acoustic space. In this low-frequency range, it was recommended to study how SEA could be augmented by modal density estimates from simple models of selected subsystems. These models would represent closed form or finite element solutions that could predict specific modes.

4.5 REVIEW OF SEA PROCEDURES FOR LOW-FREQUENCY PROBLEMS

Before modifying the SEA models to improve predictions, a number of studies regarding SEA procedures and potential enhancements for low-frequency problems were undertaken. Tasks were defined for evaluating methods to improve modal density estimates (including the use of finite element modeling), to improve input power estimates, and to improve variance predictions.

The modal density is an important element in the calculation of statistical energy analysis parameters. For continuous systems, the number of modes with resonance frequencies in a given band (the mode count) is determined from the modal density. The mode count relates the modal energy to the mean-square response. Impedance functions, which, along with prescribed mechanical or acoustical sources, determine input power to SEA subsystems, are calculated from the modal densities. The modal density also enters directly into the relationship between coupling loss factor and the coupling parameter use in the matrix formulations of the SEA power balance equations. Finally, the modal density forms the basis for a statistical description of the resonance frequencies. In such a description, the resonance frequencies are assumed to be random "events." The modal density specifies the mean rate of occurrence for these events per unit frequency. Methods to improve modal density estimates are described below.

At high frequencies, the modal density of a continuous dynamic system can be shown to approach an asymptotic limit that depends on the dimensions of the system. These asymptotic limits are written as—

$$n^{1\text{-}D}(\omega) = \frac{L}{\pi c_g} \tag{1a}$$

$$n^{2\text{-}D}(\omega) = \frac{kA}{2\pi c_g} \tag{1b}$$

$$n^{3\text{-}D}(\omega) = \frac{k^2 V}{2\pi^2 c_g} \tag{1c}$$

where c_g is the group speed for the system, k is the wavenumber, and the geometric parameters L, A, and V refer to the length, area, and volume of the system, respectively. The asymptotic forms for the modal density are valid at high frequencies regardless of the boundary conditions and can be applied to both structural and acoustic systems as long as the correct wavenumber and group speed are used.

4.5.1 ACOUSTIC SPACE MODAL DENSITY ESTIMATE

The modal density for acoustic spaces can be determined quite simply from the asymptotic forms for the modal densities because the wavenumber and group speed are related to the radian frequency and the speed of sound in the acoustic media. The asymptotic forms for the modal densities are useful for acoustic spaces that can be idealized as one, two, or three dimensional. Most spaces, however, can be idealized in this way only over limited ranges of frequency. In general, the modal density of acoustic spaces can be described as the sum of one-, two-, and three-dimensional asymptotic modal densities,

$$n(\omega) = \frac{L}{\pi c_a} + \frac{\omega A}{2\pi c_a^2} + \frac{\omega^2 V}{2\pi^2 c_a^3} \qquad (2)$$

where the parameters are selected to provide the best representation of the modal density for the acoustic space over the entire frequency range of interest. This form of the modal density provides three geometric parameters that can be adjusted according to modeling rules for specific types of acoustic spaces. Generally, the first term is selected to obtain the desired modal density at low frequencies, where one-dimensional modes dominate. The second term is selected to obtain the desired modal density at midfrequencies where two-dimensional modes dominate, and the third term is selected to obtain the desired modal density at high frequencies where three-dimensional modes dominate. In some cases only two of the three terms in the general expression will be needed. Example calculations for the 727 demonstrator airplane are given in section 4.7.2.

4.5.2 STRUCTURE MODAL DENSITY ESTIMATES

The modal density of a structural subsystem can also be obtained from the asymptotic forms for the modal density given by equations 1. In general, a structural subsystem may have different types of modes, e.g., bending, inplane compression, inplane shear, and torsional vibration modes. The different types of modes are usually placed in separate SEA subsystems. As part of this study, general modal density expressions were developed for each type of mode. To use these expressions requires that a wavenumber and group speed be determined for each type of mode. However, the calculation of wavenumber and group speed is more complex than for acoustic spaces. For the 727 demonstrator airplane model, further studies were limited to the use of finite element models or measured data.

4.5.3 USE OF FINITE ELEMENT MODELS TO VERIFY SEA PARAMETERS

Statistical energy analysis is an effective technique for modeling complex dynamic systems having many modes of vibration. SEA is generally perceived to complement finite element modeling by providing a prediction procedure at high frequencies where the great number of degrees of freedom required for finite element modeling is prohibitive. Finite element models can also complement SEA modeling by providing data to determine parameters such as modal density, power input, and coupling loss factors for complex structures.

As discussed previously, the modal density is used in the calculation of several SEA parameters. Thus, an immediate use for finite element modeling is to determine the subsystem modal densities. A finite element model of an SEA substructure can be used to calculate the substructure resonance frequencies.

The asymptotic values of the modal densities for the substructures of the 727/GE36 demonstrator airplane as computed for the low-frequency SEA model are shown in figure 28 over the frequency range 20 to 100 Hz. The modal densities of the cabin acoustic space (subsystem 6), the fuselage sidewall (subsystem 5), and the cabin floor (subsystem 21) show an average resonance frequency spacing (inverse modal density) of approximately 8 Hz. The modal densities for these subsystems are sufficiently large that the use of the asymptotic form of the modal density should be valid.

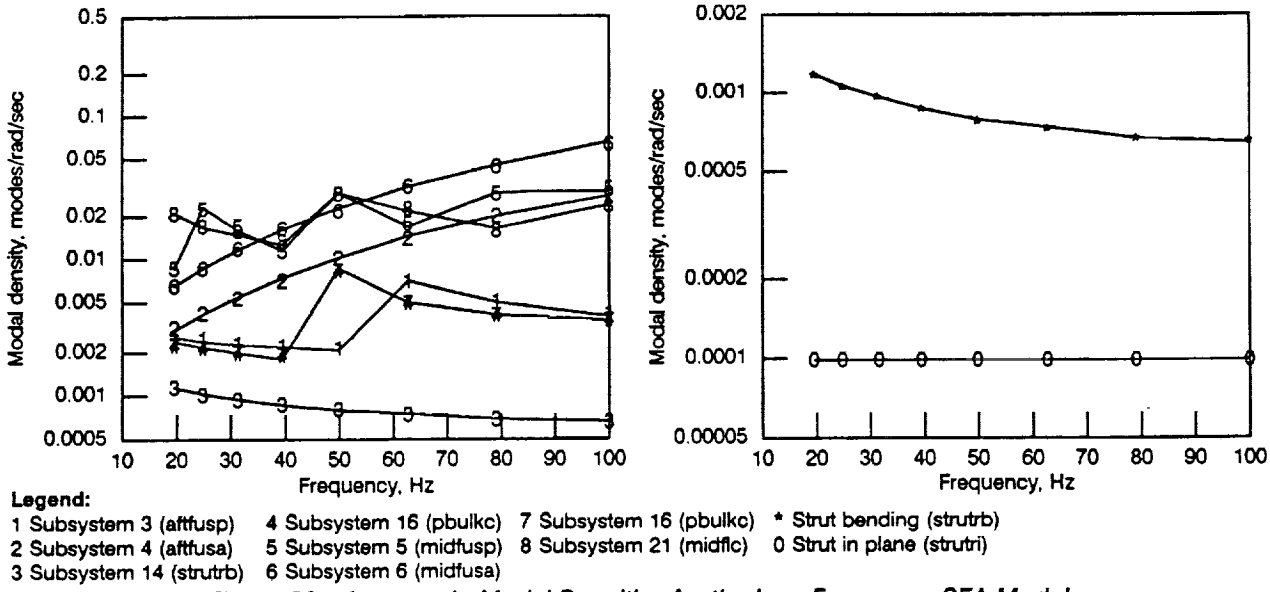

Figure 28. Asymptotic Modal Densities for the Low-Frequency SEA Model

9-U90196-33

The predicted modal densities for the pressure bulkhead (subsystem 16), the aft fuselage empennage structure (subsystem 3), and the empennage acoustic space (subsystem 4) show an average resonance frequency spacing of approximately 50 Hz. The complexity of the structures and the empennage acoustic space is sufficiently great that the predicted modal densities should be checked using a finite element model to obtain a modal density. Because of the fairly large frequency spacing, the use of the asymptotic forms to predict the modal densities for these subsystems is questionable.

Predicted modal densities for the strut are even smaller. The obvious solution to the SEA modeling problem for a small modal density is to increase the size of the subsystem. In the case of the strut, a subsystem could be created that includes the strut, a major section (perhaps all) of the aft fuselage empennage, and the pressure bulkhead. Although the problem could potentially be alleviated in this manner, the procedure of calculating SEA parameters for such a subsystem have yet to be developed. However, the use of a finite element model would appear to be a reasonable approach to obtaining the modal density for such subsystem.

As part of this task, a procedure for using finite element data to calculate a modal density was established. Briefly, a single substructure is selected to be modeled. Simple boundary conditions are chosen to approximate bordering subsystems. Eigenvalues are then calculated to a frequency somewhat more than the upper frequency of interest. At each eigenvalue the frequency spacing to the next eigenvalue is calculated. The frequency spacings are then inverted to find an "instantaneous modal density," which is plotted to compare with the asymptotic modal density.

An example of this procedure using the cabin acoustic space is given in section 4.7.2. A new strut modal density is also calculated in section 4.7.2, but rather than using the FEM predicted frequencies,

measured modal densities of the composite system were used in a like fashion. Obviously, it is desirable that the complexity of subsystem finite element models be kept to a minimum otherwise the advantages of SEA, such as small model size and quick result turnaround, are lost.

A second use for finite element modeling is to determine the input power from prescribed excitations. In SEA the input power is obtained from a statistical impedance analysis. Finite element models can also be employed to compute power input and, thereby, provide a means to check the validity of the SEA calculations.

A third use for finite element modeling is to provide data for calculating the coupling loss factor. Because coupling loss factors are formulated in terms of modal densities and impedances, improved estimates for the modal densities and impedances will lead to improved coupling loss factor predictions.

4.6 SEAM^{TM} CODE IMPROVEMENTS

In the baseline low-frequency model, the power input to the strut is calculated assuming that the strut subsystem has infinite boundary conditions. Based on studies completed, the finiteness of the subsystem and "loading" effects caused by other subsystems connected to the strut should be accounted for.

The input power calculation in the SEAM code has been improved. The input power at a given frequency or in a band of frequencies is the product of the mean-square force applied to the system and the drive point conductance (real part of the mobility). When a mass is added to the structure at the point of excitation, the impedance (inverse of mobility) of the combined system is the sum of the structure impedance plus the mass impedance. In general, the structure impedance is a complex number with real and imaginary parts, while the mass impedance has only an imaginary part. In earlier versions of SEAM the mass impedance was improperly set to be real. This resulted in incorrect power input calculations, although the error was not great. The current SEAM code properly calculates the power input using the correct imaginary value for the mass impedance.

In SEA the predicted variance depends on the inverse of the product of the modal density and the loss factor. At low frequencies, where the modal densities are small, the variance can be quite large. Again, considering the effect of bordering subsystems on the subsystem in question, an "effective loss factor" has been defined that includes both energy dissipation to damping within the subsystem as well as energy transmitted to connected subsystems.

In order to evaluate the improvements to the SEAM computational procedure, the original and new input power estimates are shown in figure 29 along with the measured input power for the vertical and lateral drives, respectively. The SEA mean for the vertical drive condition is 1 to 2 dB more than the lateral drive condition and in somewhat better agreement with the measured power input. The SEA mean for the lateral drive conditions is not significantly changed.

The SEAM code provides a prediction for the variance (standard deviation squared) of the power input. In SEA it is generally assumed that the power input is a log normal distribution, i.e., the variable 10

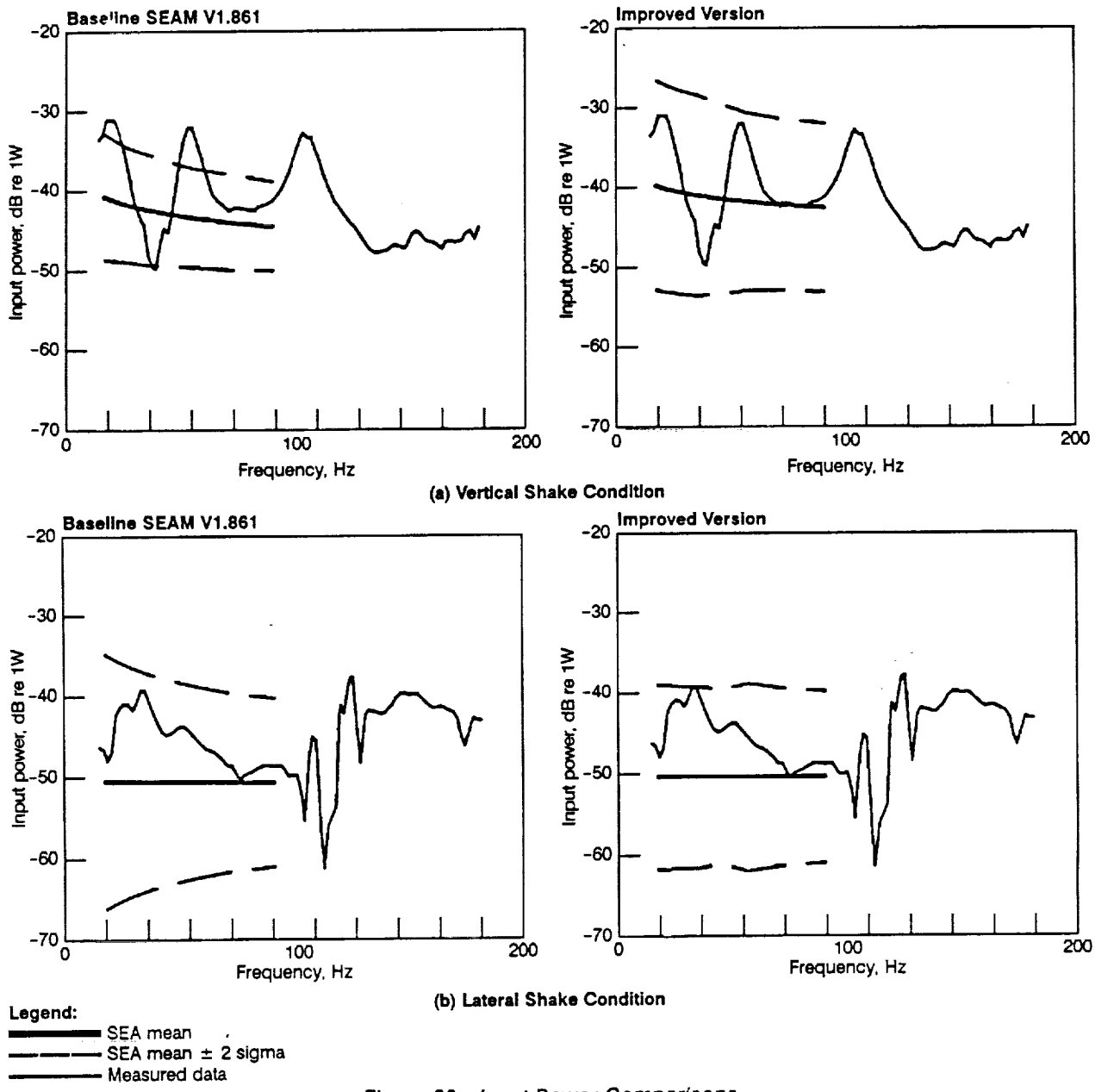

Figure 29. Input Power Comparisons

LOG_{10} [power input] is normally distributed. Given this assumption, 95% of the power input data in decibels should fall within a range defined by the mean ±2 times the standard deviation. Thus, this range can be used as a 95% confidence interval. In figure 29, the confidence interval has increased approximately 5 dB to encompass the data for the vertical drive and has decreased up to 5 dB at less than 60 Hz as desired for the lateral drive, so that the standard deviation is now essentially constant with frequency. The same trend is true of the response prediction standard deviations.

4.7 SEA LOW-FREQUENCY MODEL IMPROVEMENTS

A number of improvements to the low-frequency model were made including the input power estimation, new modal density estimates for the cabin acoustic space and the strut, a new estimate for the strut loss factor, and an improvement to the modeling of the strut connection. Details are given below.

4.7.1 INPUT POWER ESTIMATE

During the ground test measurements, impedances were measured at the drive points. It was therefore possible to use conductance, the real part of the mobility (inverse impedance), to obtain a measured value for the power input. The variance in the SEA predictions includes a variance in the input power. By specifying directly the measured input power in the SEA model, the overall prediction variance can be reduced thereby improving the prediction accuracy.

The predictions obtained when measured input powers are used directly are given in figure 30 for the vertical shake condition. The SEA mean is plotted with the mean of the measured data for clarity of presentation. The predicted results are too high, which indicates that the coupling between the strut and the empennage is too high. Clearly, simply changing the input power level without correcting the low strut modal density is not satisfactory.

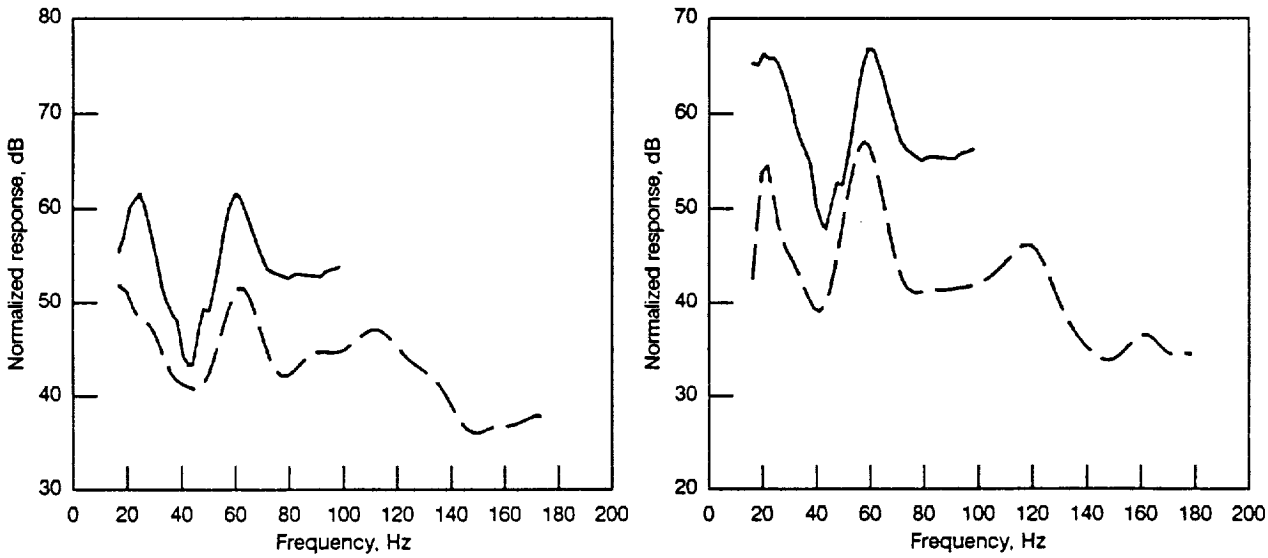

(a) Section 46 Sidewall Vibration (midfusp)

(b) Section 46 Interior Noise Levels (midfusa)

Legend:
SEAM
Average of measured data

Figure 30. Response Predictions for the Low-Frequency Baseline Model Using Measured Input Power – Vertical Shake

9-U90196-35

4.7.2 MODAL DENSITY ESTIMATES

The modal densities for the strut do not include the effect of boundary conditions or connected structures. A composite modal density, which lumps together both the strut and sections of the empennage, was determined from the spacing between peaks in the measured input power. These frequency spacings were inverted to calculate modal density in the same way that spacing between eigenvalues predicted from a finite element model would be used (fig. 31A). Because modal density cannot be input directly in the SEAM program, it was necessary to modify the strut properties to simulate the modal density derived from the measured data. This was accomplished by increasing the strut length by a factor of four while decreasing the strut density by the same factor to maintain a constant strut mass. The comparison of the SEAM calculated modal density with that calculated from the measured input power peak spacings is shown in figure 31B.

The use of a finite element model to validate a modal density estimate is illustrated for the cabin acoustic space. A method for determining the modal densities from finite element models has been discussed. To demonstrate the procedure, the first 100 modes for the acoustic interior of the Boeing 727/GE36 demonstrator aircraft were computed from a finite element model with 1525 three-dimensional elements. The resonance frequencies were sorted in ascending order, adjacent frequencies subtracted to compute the interval between resonance frequencies, and the intervals inverted to obtain an "instantaneous" modal density. The result of the calculation is shown in figure 32. When presented in this manner the resonance frequency data appear to be random.

Figure 33 presents the modal density data smoothed over a 10-Hz bandwidth. The data in this plot have been obtained by counting the number of resonance frequencies in each 10-Hz-wide band and dividing by bandwidth. The result is a series of data points with a 10-Hz spacing, which can now be compared with predicted modal densities.

In order to more accurately represent the demonstrator airplane test environment, the dimensions of the interior acoustic space were re-evaluated and modified from those used in the 1987 SEA model predictions. The modal density prediction using the cabin acoustic space volume ($52m^3$) in equation 1c is shown in figure 33. The estimate is seen to underpredict the modal density obtained from the finite element data. The second procedure is to use the general form of the modal density given by equation 2. The volume was selected to equal the volume of the cabin ($52m^3$), the area to equal the area of the floor ($22.3m^2$), and the length to equal the length from the lavatory walls to the acoustic barrier (6.1m). The resulting modal density is also shown in figure 33. The use of the area and length terms improve the agreement between the finite element data and the prediction. This estimate was used in all further studies.

4.7.3 STRUT CONNECTION MODELING

It was noted that in the lateral drive model, the strut inplane subsystem is connected to both the empennage and pressure bulkhead bending mode groups. In fact, the strut should only be connected to the inplane modes of the pressure bulkhead. However, there are no inplane modes of the pressure bulkhead

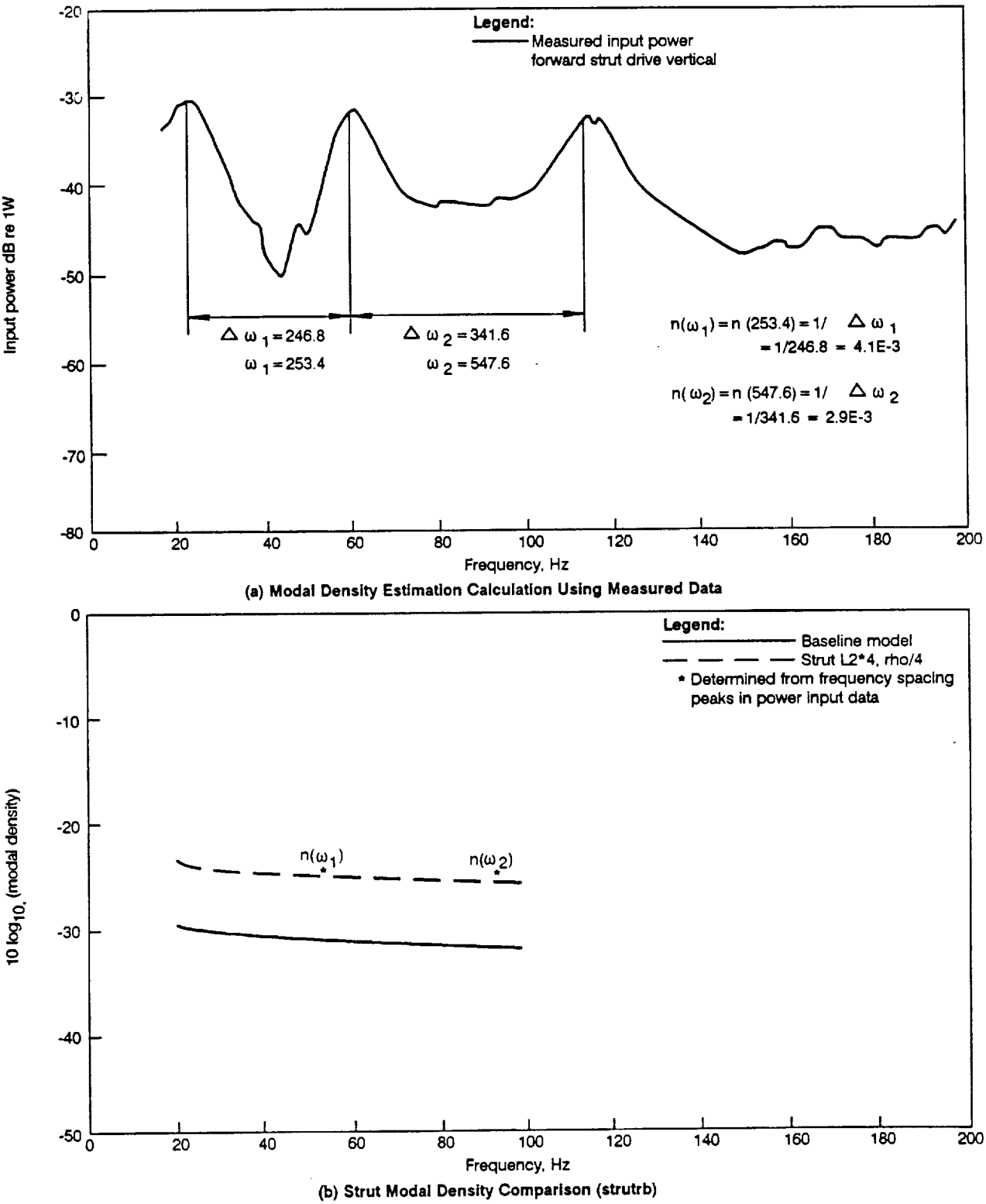

Figure 31. Composite Strut Modal Density Based on Spacing Between Peaks in the Measured Vertical Shake Input Power

U90169-36

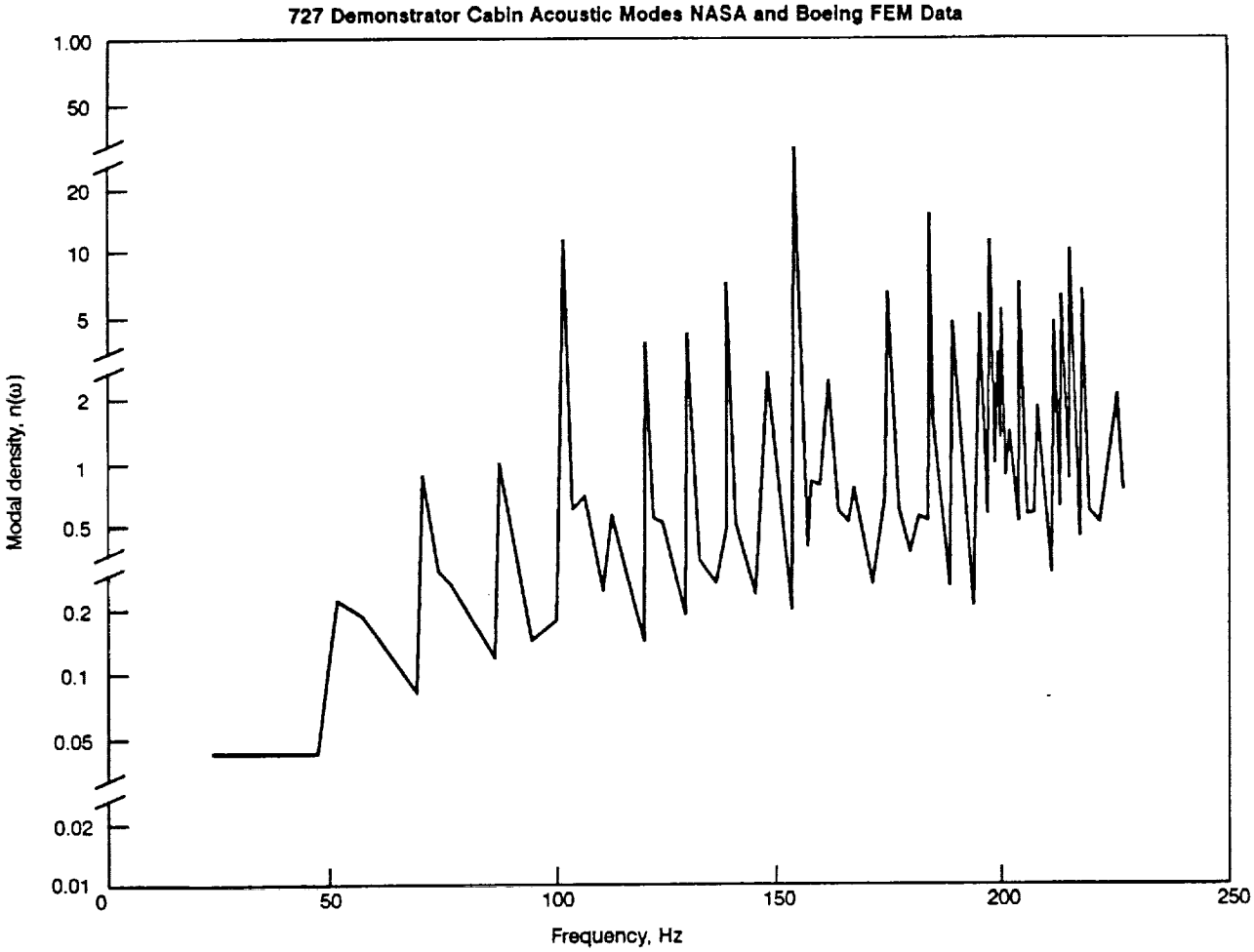

Figure 32. Instantaneous Modal Density for the Cabin Acoustic Space

9-U90196-37

to excite at the frequencies involved. A better model of the strut connection to the fuselage is a junction with the strut inplane and the empennage through the mass of the bulkhead, so that the nonresonant impedance of the bulkhead is taken into account.

4.7.4 STRUT LOSS FACTOR

At this point, predictions were made to determine the effect of the above described changes. It was noted that predictions were all about 5 dB high including the strut vibration level. Because most of the strut energy is lost to damping (approximately 80% of the power input to the strut is damped internally), the high predictions can be lowered by increasing strut damping. This will allow a better comparison of the power flow prediction capabilities of the model. The damping was increased to a value of 0.24 (12% of critical), which while arbitrary is not unreasonable considering the strut is a highly bolted structure filled with hydraulic system components. Results are given in section 4.9.

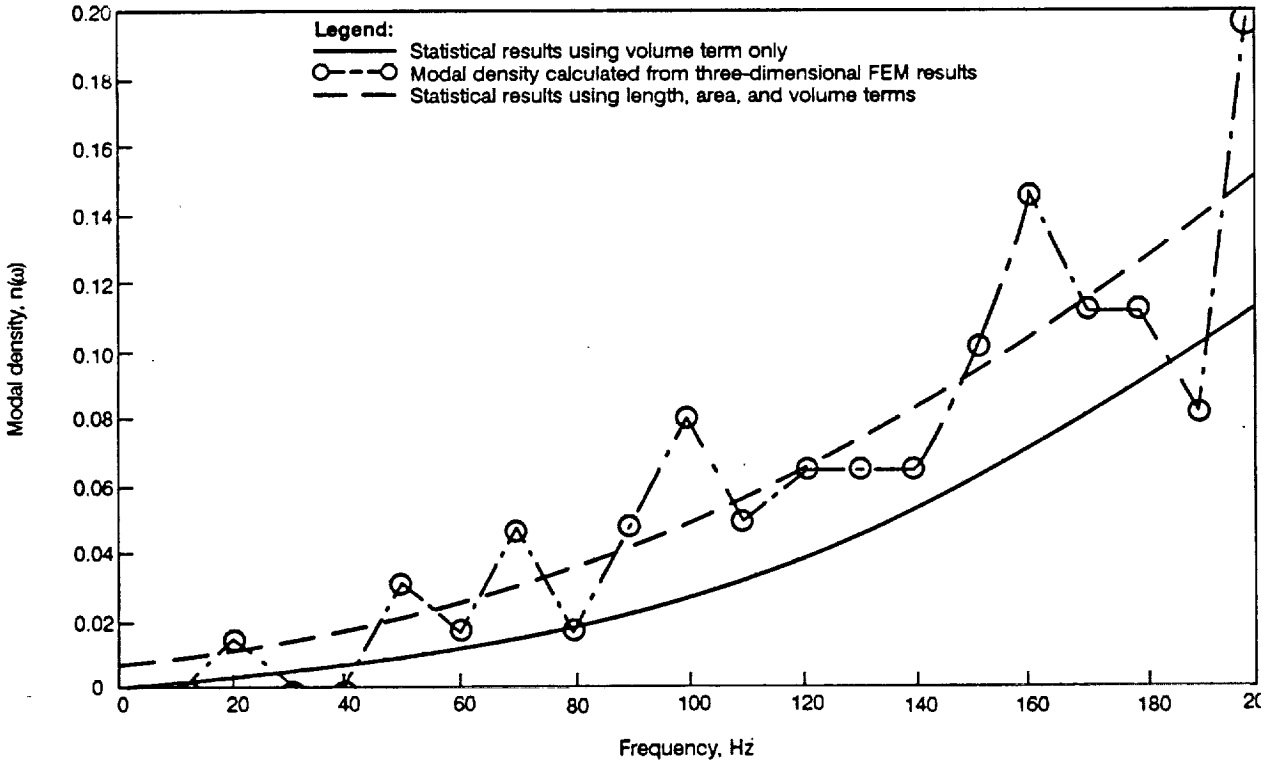

Figure 33. Comparison of Modal Density Prediction Procedures—Interior Acoustic Space

9-U90196-3

4.8 MIDFREQUENCY MODEL IMPROVEMENTS

The midfrequency model was originally developed to predict cabin noise from 100 to 400 Hz for both strut vibration and empennage acoustic excitation. However, during the effort to improve the low-frequency model, it was found that this model could be used up to 200 Hz for strut vibration conditions. Thus, efforts to improve the midfrequency model have focused on side-of-body shaker and inflight acoustic excitation.

The first attempt to improve the accuracy of the midfrequency model was to use the measured power input. As with the low-frequency model, some improvement was observed although further work on improving modeling accuracy was felt to be needed.

In setting up the midfrequency model, the empennage was modeled using the properties of the skin panels, stringers, and added honeycomb panels. The frames and torsion boxes were not included in deriving equivalent homogeneous cross-section properties. Above the frequency of the first subpanel resonance, the modeling assumption is correct. However, at low frequencies the properties must be changed to include the stiffening effect of the frames and torsion box structure. The complexity of the empennage structure precludes development of a modeling procedure without use of measured data. The approach,

NASA
National Aeronautics and Space Administration

Report Documentation Page

1. Report No.	2. Government Accession No.	3. Recipient's Catalog No.
NASA CR-181851		

4. Title and Subtitle

Evaluation of Analysis Techniques for Low Frequency Interior Noise and Vibration of Commercial Aircraft

5. Report Date

October 1989

6. Performing Organization Code

7. Author(s)

A. E. Landmann, H. F. Tillema, and S. E. Marshall

8. Performing Organization Report No.

D6-54871

10. Work Unit No.

9. Performing Organization Name and Address

Boeing Commercial Airplanes
P. O. Box 3707
Seattle, WA 98124-2207

11. Contract or Grant No.

NAS1-18027

13. Type of Report and Period Covered

Contractor Report

12. Sponsoring Agency Name and Address

National Aeronautics and Space Administration
Langley Research Center
Hampton, VA 23665-5225

14. Sponsoring Agency Code

15. Supplementary Notes

Langley Technical Writer: Kevin P. Shepherd
Final Report

16. Abstract

This report documents the application and evaluation of selected analysis techniques for the prediction of low-frequency cabin noise and vibration associated with propeller engine installations. Three analysis techniques were chosen for evaluation including finite element analysis, statistical energy analysis (SEA), and a power flow method using elements of SEA (computer program PAIN). Data from ground and flight tests of a 727 airplane modified to accept a GE36 counter-rotating propeller engine were used to compare with the predictions. Generally, the comparisons show reasonable agreement, leading to the conclusion that each technique has value for estimating potential impact of candidate noise suppression features. However, variations were large enough to remain cautious about prediction of absolute levels for new aircraft. Recommended improvements for each procedure are made.

17. Key Words (Suggested by Author(s))

1. Advanced Propeller Engines
2. Analytical Techniques
3. Cabin Vibration
4. Interior Noise

18. Distribution Statement

Unclassified - Unlimited

19. Security Classif. (of this report)	20. Security Classif. (of this page)	21. No. of pages	22. Price
Unclassified	Unclassified	76	

therefore, was to change the properties of the empennage structure so that the predictions of input power and empennage response would match the data.

Using this procedure the drive point impedance was modified by constructing a model with a frequency dependent empennage density (fig. 34). Note the very large and abrupt shift that was required to match data. This seems to validate the above comments regarding modeling accuracy of the empennage, as the break in density occurs where the first subpanel resonances would be expected to occur. This would result in a dramatic shift in input power impedance reflected by the large change in density. Comparisons with data are presented in section 4.9.

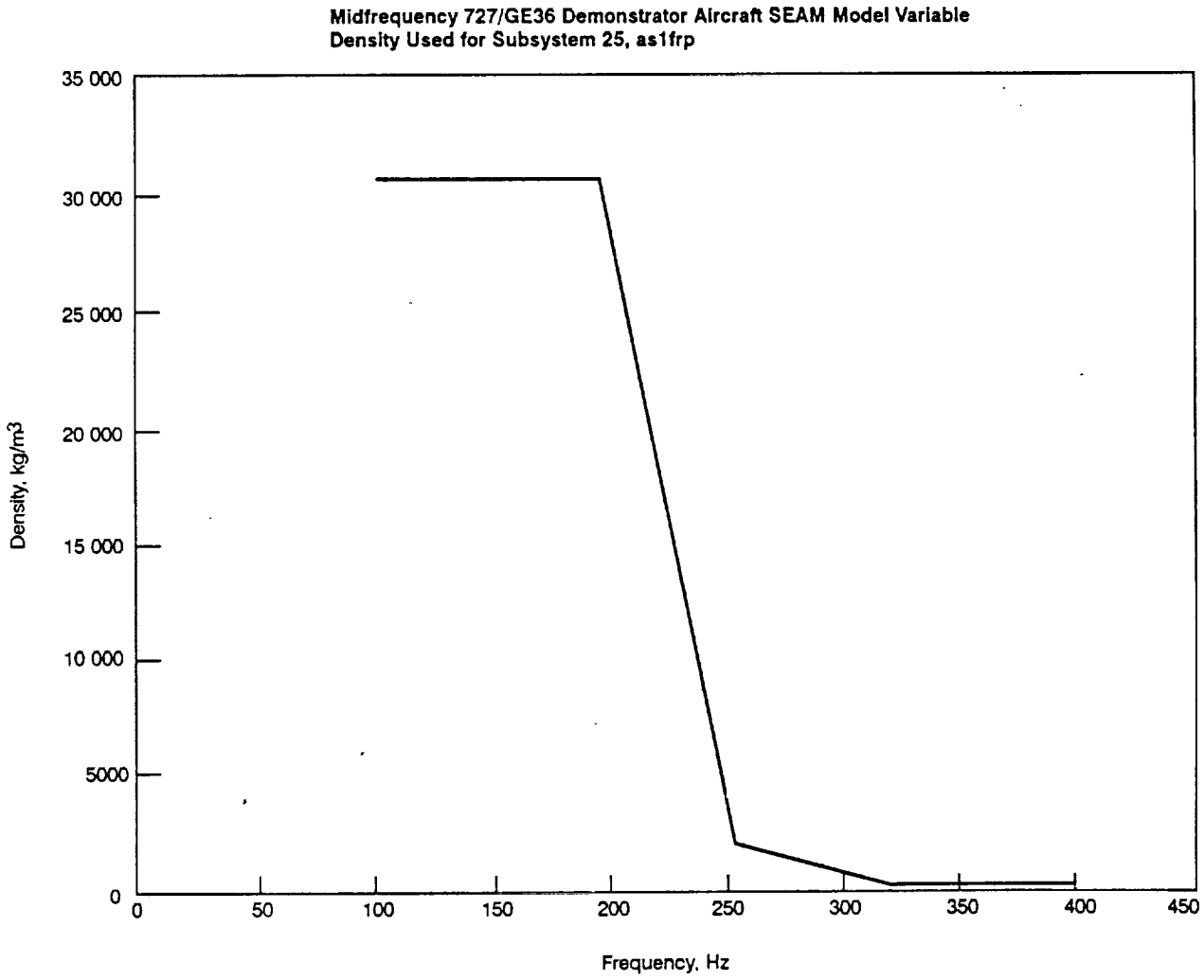

Figure 34. Midfrequency SEAM Model Variable Panel Density

9-U90196-39

4.9 STATISTICAL ENERGY ANALYSIS RESULTS (FY 1988)

The low-frequency model incorporates the new airspace modal density estimate, the composite strut modal density, revised strut damping, and the improved strut connection model. Results obtained using this model are described below.

Response predictions for the vertical shake condition are given in figure 35. Note that predictions have been extended to 200 Hz. Comparisons with measured data show very good agreement with some overprediction of acoustic levels at high frequencies. The data falls within the predicted confidence interval, the data peaks are in good agreement with the upper limit of the confidence interval, and in most cases the predicted average matches the measured average. As was noted earlier, these results were obtained by increasing strut damping to an arbitrary but not unreasonable level. An almost exact match of the data is obtained when measured input powers are used (fig. 36). Comparisons for fore-aft (figs. 37 and 38) and lateral strut shake conditions are similar to the vertical shake condition.

Because data from the vertical and lateral shake conditions were used in determining parameters for the improved model, good agreement with data for these conditions is not unexpected. However, the comparison of the prediction and data for the fore-aft shake condition also shows good agreement, thereby supporting the general validity of the improvements.

Flight predictions at the rotor frequency fundamental and harmonics were also made. Predictions using measured GVT transfer functions as the "best" possible prediction were compared with predictions using SEA estimated transfer functions. In both cases, measured inflight vibration levels were combined with measured GVT strut impedances to infer forces acting on the strut. Both predictions overestimated flight levels (by approximately 4 and 6 dB, respectively), but it is noteworthy that the SEA prediction was within 2 dB of the "best" possible prediction using GVT measured transfer functions.

Comparison of predicted (using the midfrequency model) and measured results for a side-of-body shake condition are given in figure 39. Because the empennage properties were modified to match measured response, levels for section 48 (empennage), the bulkhead, and section 46 (passenger cabin sidewall) match closely. Acoustic levels show good agreement at low frequencies, but are overpredicted at higher frequencies, a trend seen with the low-frequency model as well. One possible explanation is the absence of interior trim panels in the models. In 1987 work, it was concluded from preliminary midfrequency model results that energy transfer through the trim (as compared to composite sidewall modes) was not important. In light of the most recent findings, this conclusion should be re-examined.

Predictions for flight conditions were again evaluated by comparing results using GVT measured transfer functions and SEA predicted transfer functions. Levels were estimated at fundamental and first harmonic blade-passage frequencies. Input power was determined by using measured exterior sound pressure levels and the GVT determined transfer functions. A power input was obtained by multiplying the measured exterior pressure by an effective excitation area to obtain an equivalent force input. This area was selected so that the average interior sound pressure level, predicted using the GVT transfer functions, was equal to the average interior level measured in flight. A prediction was then made using

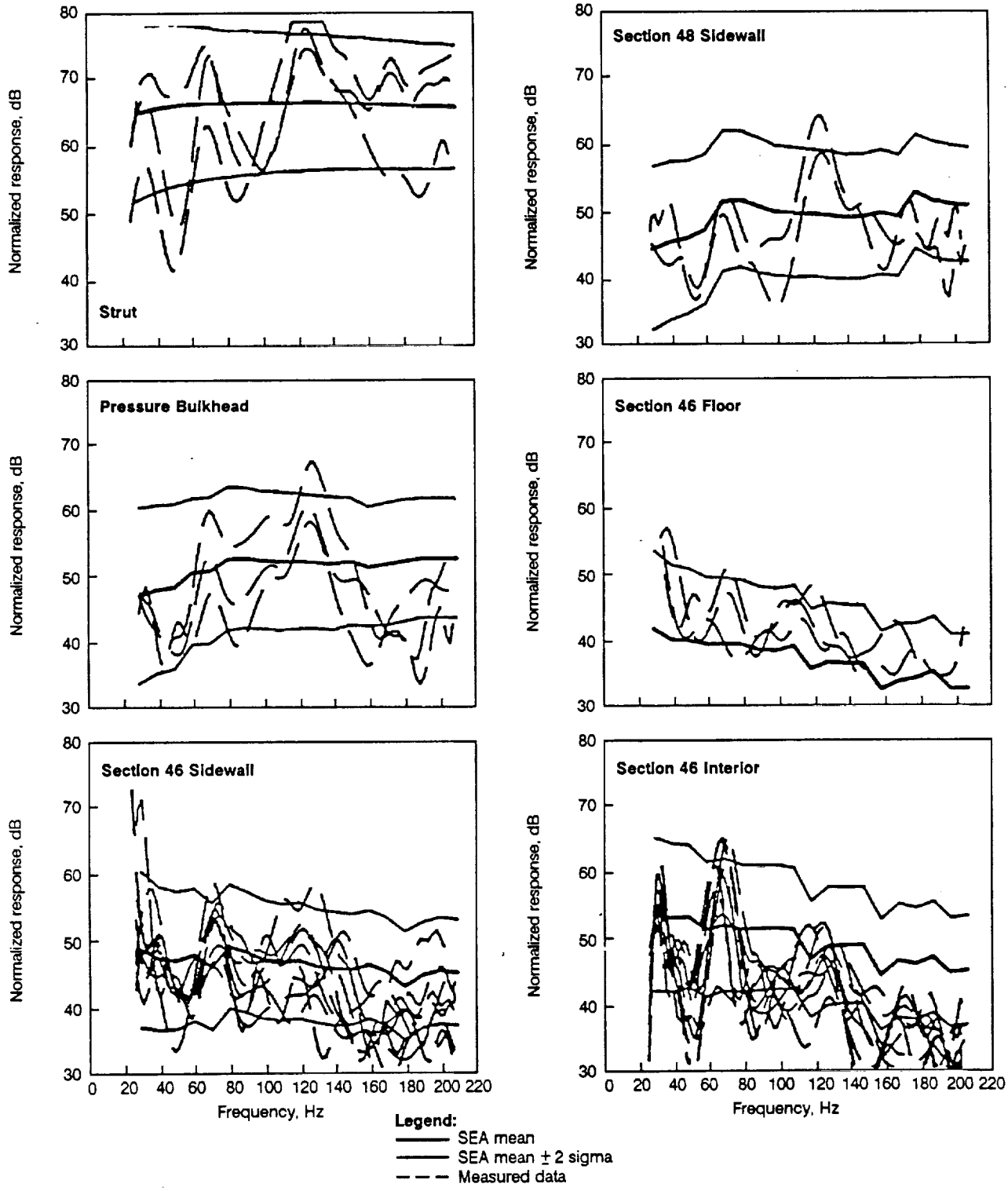

Figure 35. Response Predictions for the Low-Frequency Improved Model—Vertical Shake

U90196R1-40

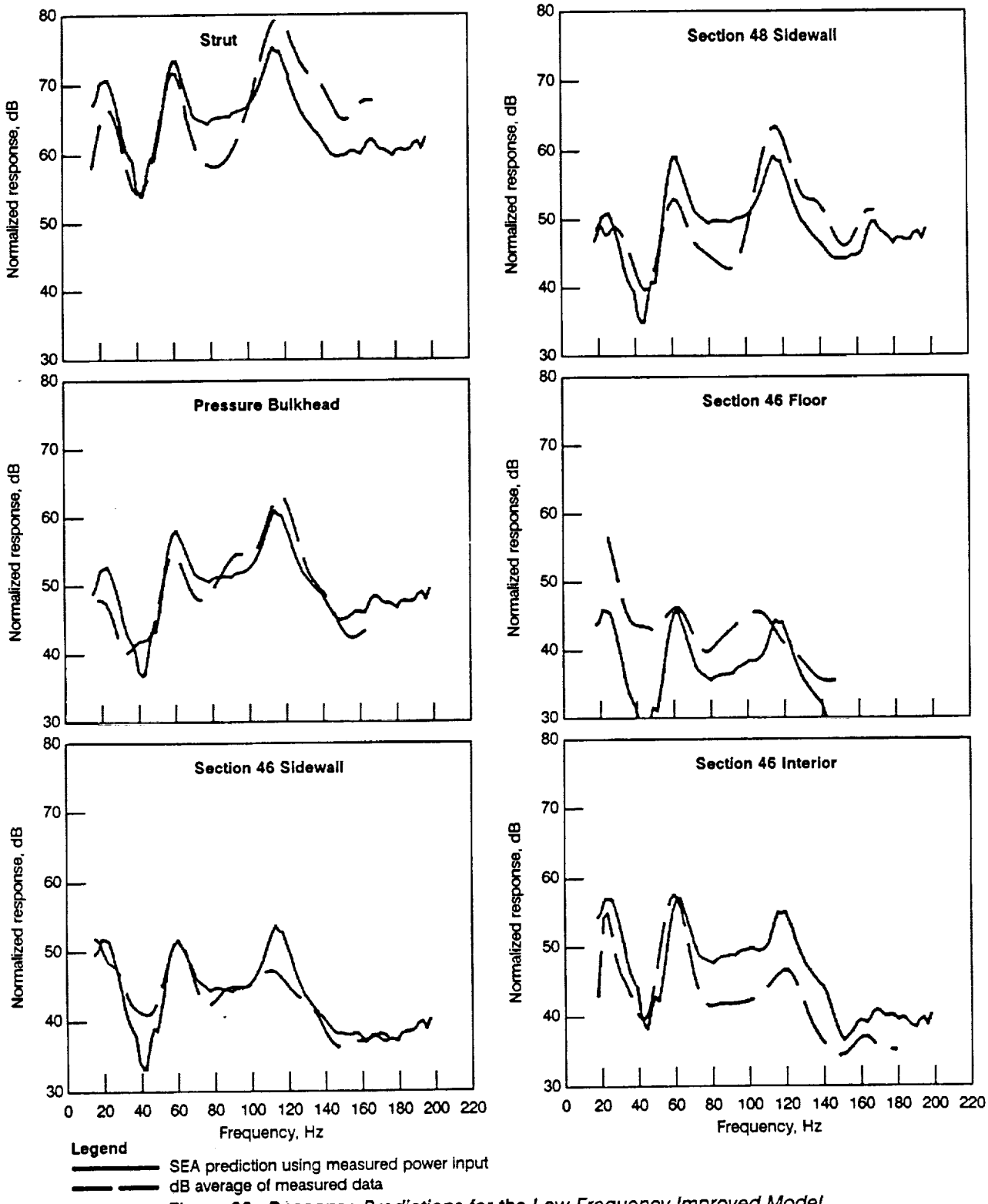

Figure 36. Response Predictions for the Low-Frequency Improved Model Using Measured Input Power Vertical Shake

9-U90196-41

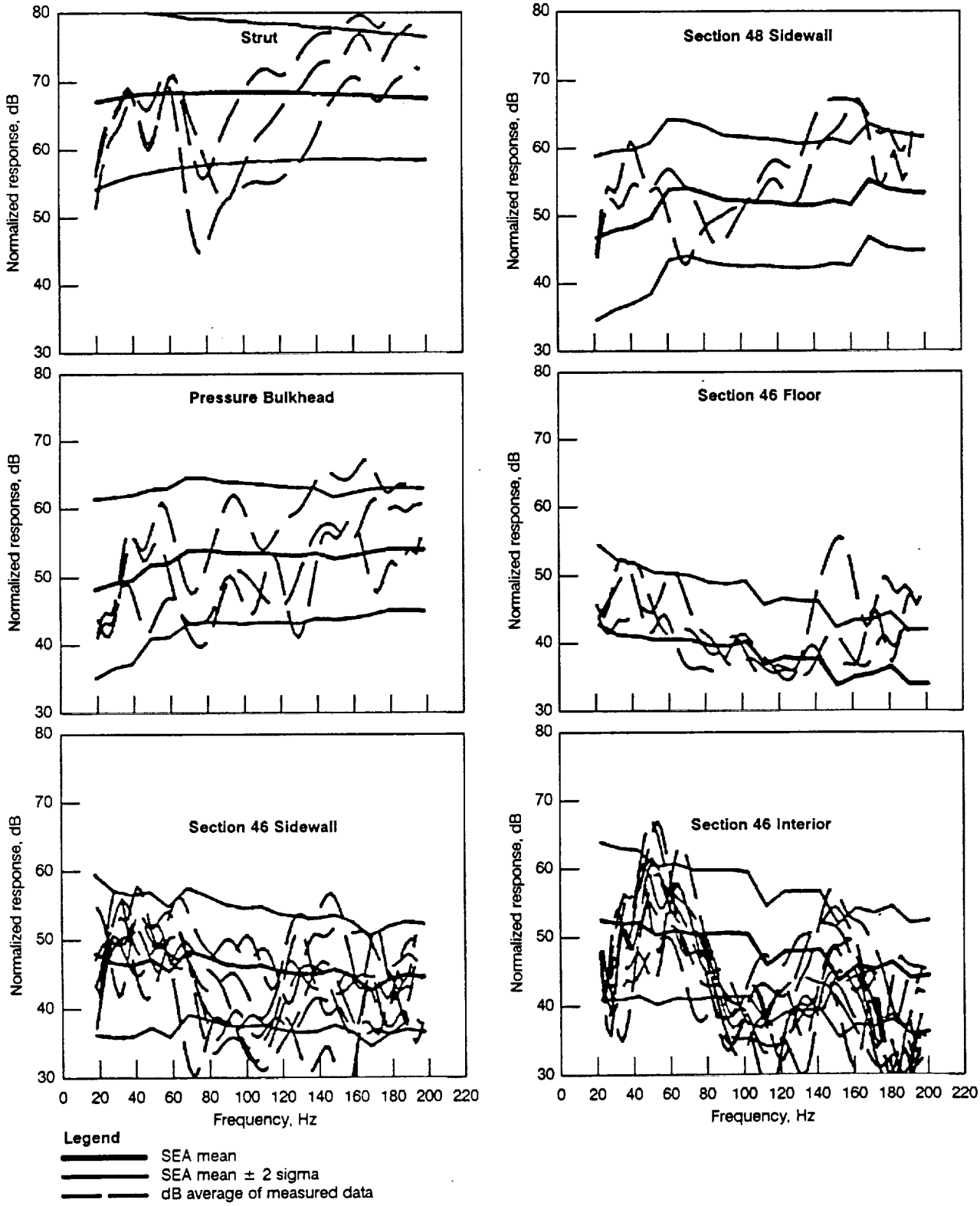

Figure 37. Response Predictions for the Low-Frequency Improved Model—Fore-Aft Shake

9-U90196-42

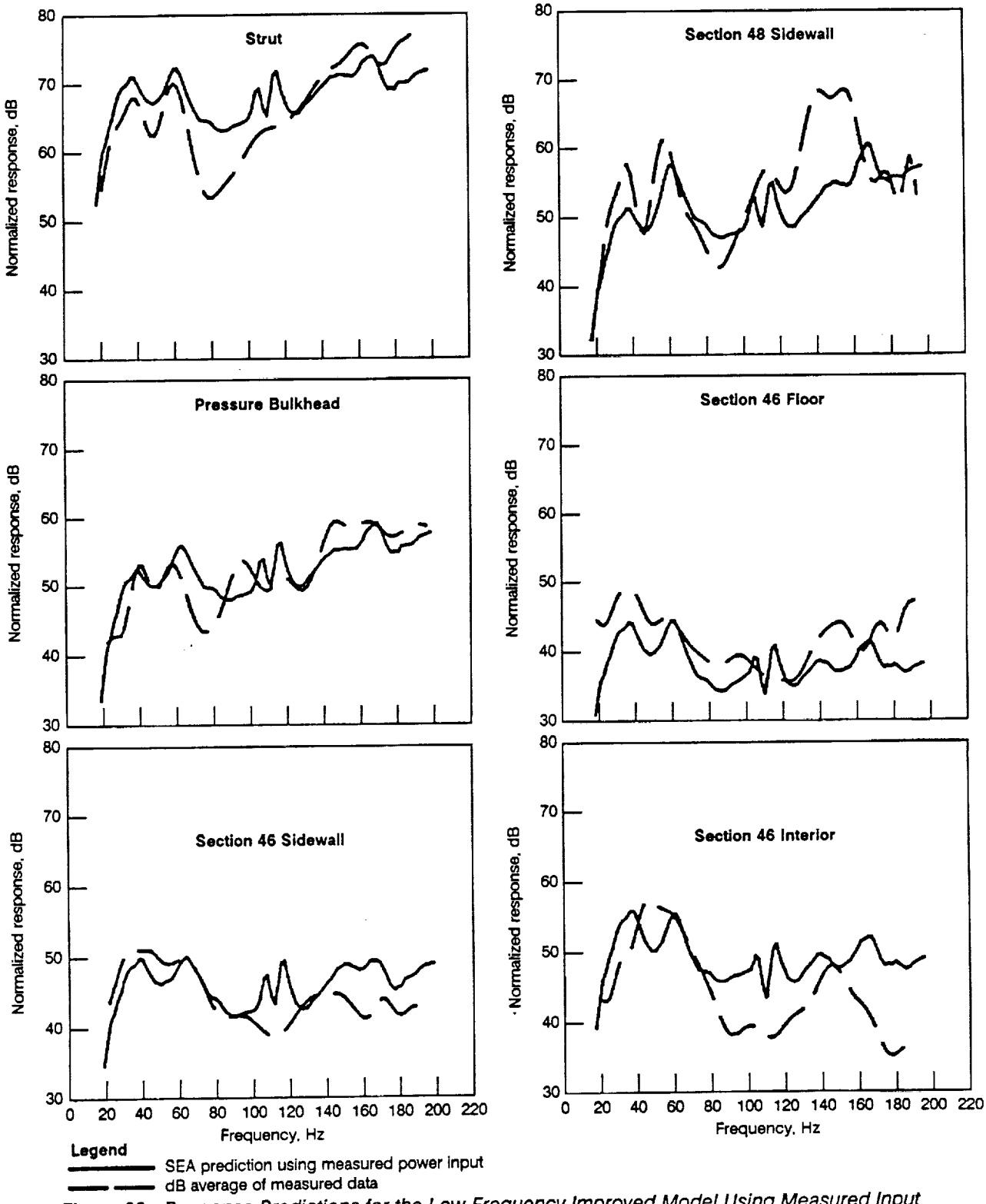

Figure 38. Response Predictions for the Low-Frequency Improved Model Using Measured Input Power Fore-Aft Shake

9-U90196-43

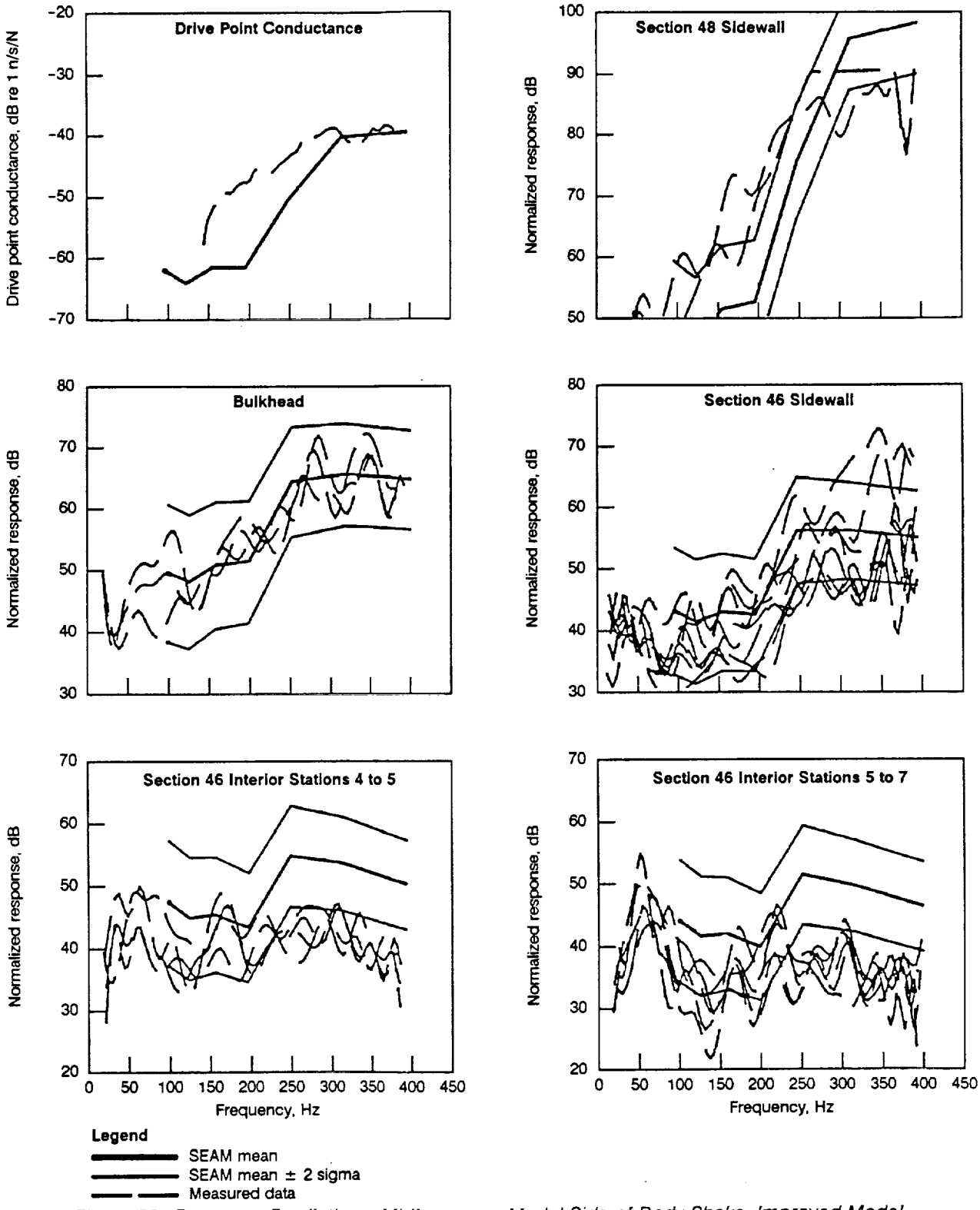

Figure 39. Response Predictions, Midfrequency Model Side-of-Body Shake, Improved Model

9-U90196R1-44

the same area but with the SEA transfer functions. With this procedure, SEA predictions were reasonable when compared to measured results at the blade-passage frequency, but high at the first harmonic (fig. 40). This is comparable to results obtained for GVT comparisons. One interesting result of this study is the small size (2400 in^2) of the empennage area used to convert measured pressure to power input. This result is very similar to conclusions from PAIN studies (sec. 4.11). That is, cabin propeller noise seems to be controlled by excitation of a small area by intense sound pressure levels opposite the fan blades. This result could be important to the designer in locating and optimizing acoustic treatments.

As with finite element modeling, SEA has not demonstrated an ability to predict absolute levels in the aircraft. However, as a result of these studies, a number of important conclusions were reached. First, the method can accurately predict energy flow within the structure as well as trends shown with changing frequency and excitation directions. Subsystems should be reviewed for modal density levels. Estimates for those subsystems with very low modal densities might be re-evaluated, perhaps by considering expanding the subsystem size or by considering the effects of neighboring subsystems. A procedure for validating modal density estimates using subsystem finite element models was developed.

Particular attention should be paid to the subsystem subjected to excitation forces. That is, the input power calculation has been shown to be critical and a more detailed understanding (than offered by SEA) of this subsystem may be required for low-frequency predictions. Again, selected use of finite element models to define or validate SEA parameters may be appropriate.

4.10 PAIN ANALYSIS RESULTS (FY 1987)

Predictions were made and compared with measured propeller-blade-passage frequency interior noise for three flight conditions. These included both cruise and holding conditions as shown in table 2. Engine power was set accordingly.

PAINUDF allows prediction of explicit empennage and passenger cabin structure modes. Structure response modes are based on a floor stiffened cylinder for the passenger cabin fuselage or stiffened plates for the empennage. In principle, power transfer can be calculated on a mode-by-mode basis. In this analysis, power transfer from the exterior pressure field to the empennage, from the empennage to the

	Blade-passage frequencies and harmonics			
	162	167	323	333
Measured transfer functions				
Aft cabin	+2	-7	+6	+3
Forward cabin	-5	-7	-1	-1
SEA transfer functions				
Aft cabin	+3	-6	+18	+16
Forward cabin	+1	-2	+15	+15

Figure 40. Measured Minus Predicted SPL Using Improved Midfrequency Model

9-U90196R1-45

passenger cabin fuselage, and from the passenger cabin fuselage to airspace was calculated using the structural modes. A power flow diagram for PAINUDF is shown in figure 41. The bulkhead junction between the empennage and fuselage influences the flow of energy between these elements. However, the bulkhead itself is incapable of transferring power (such as between the empennage and fuselage acoustic spaces).

For this effort, noise levels measured on the exterior of the empennage of the airplane were used in conjunction with estimated exterior noise phase behavior based on propeller systems having only one row of blades. Dummy phase data were required because the density of exterior test microphones was insufficient to produce accurate measurements. For the first two flight conditions (mach = 0.8 and 0.72), the two rotor speeds were sufficiently separated to extract data for the tone levels associated with the forward rotor only. For the holding condition (mach = 0.42), contributions from the forward and aft rotors could not be separated. Thus, predictions for each rotor were made using phase estimates for a forward downsweeping blade row and an aft upsweeping blade row.

Comparison of predicted and measured cabin noise levels is given in figure 42. For the cruise conditions, agreement between predicted and measured space average values was very good, within 1 dB. At the holding power condition, a large difference was noted that was attributed to the contribution of the aft rotor. Time and contract budget constraints did not allow further investigation of this difference. A

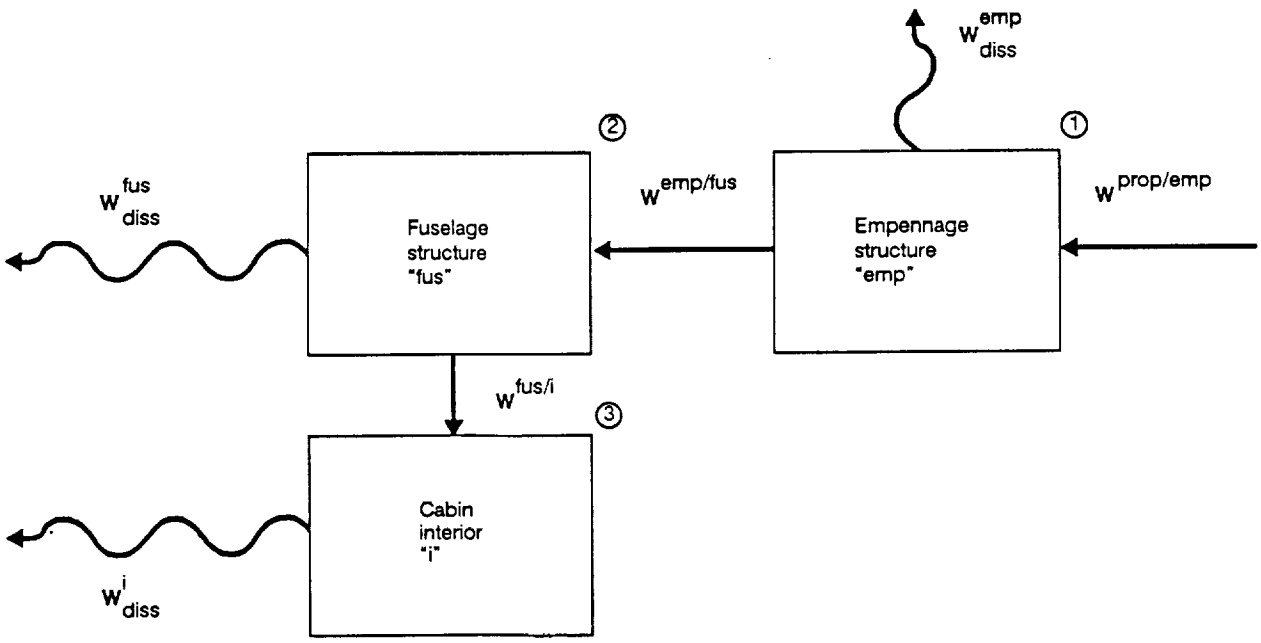

Figure 41. Power Flow Diagram for Elements of PAINUDF Model

9-U90196R1-46

check was made that showed no statistical difference (bias) between the measured and predicted results. The standard deviation was calculated to be 4.7 dB.

Flight condition	Rotor	BPF frequency, Hz	Predicted minus measured levels, dB
Mach = 0.80 at 35 000 ft	Forward	169	0.2
Mach = 0.72 at 35 000 ft	Forward	170	−0.3
Mach = 0.42 at 10 000 ft	Forward and aft	180	Forward 0.2 Aft 8.0] = 8.1 total

Figure 42. Measured Versus PAINUDF Predicted Levels

9-U90196R!-47

It was concluded that PAINUDF showed promise in providing models to predict propeller-blade-passage frequency interior noise for large commercial transports. Based on the FY 1987 results, a number of recommendations were made regarding further analytical studies and exploration of potential PAINUDF improvements. Description of these recommendations follows.

It was recommended that predictions for aft rotor noise levels for the holding condition be reviewed to determine why predicted levels for the aft rotor were so much higher than for the forward rotor.

Experience gained in using PAINUDF showed that flight measured exterior levels were on a much sparser grid than used by the program and not of sufficient quality to obtain phase relationships for program input. A fair amount of work involving interpolation of amplitude measurements and generation of dummy phase data from a simple propeller blade row engine model were required to generate program inputs. A study using the current 727 demonstrator airplane model was recommended to evaluate sensitivity to propeller signature amplitude and phase. This would help define input data requirements for future applications.

It was noted that the empennage representation in PAINUDF was for the rather unique 727 configuration. It was therefore recommended that a more general conical empennage section model be developed.

While predicted and measured space-averaged acoustic levels were within 1 dB, inspection of the data showed more than a 10-dB falloff from the back to the front of the compartment (fig. 43). The figure compares the individual measurement points and their relative location to the predicted and measured space average. Some estimate of peak levels and distribution would be useful to the designer for placement of acoustic treatments. Thus, a procedure for estimating noise gradients within an acoustic airspace was recommended.

4.11 PAIN ANALYSIS RESULTS (FY 1988)

Initial activity focused on understanding the anomalous prediction for the aft rotor contribution to the interior noise of the demonstrator airplane. It was felt that an evaluation of program coding was

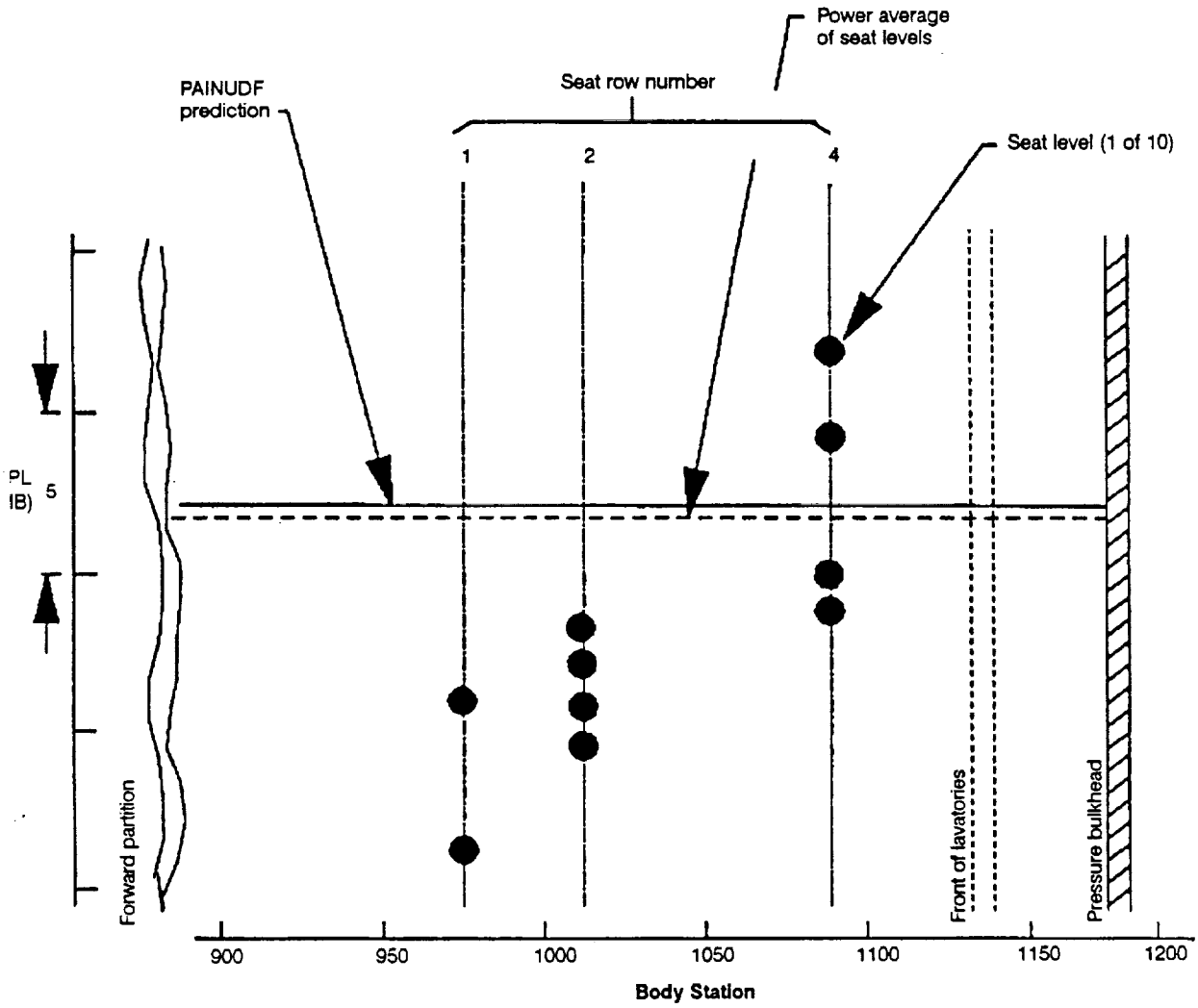

Figure 43. Average of Seat Measurements Versus PAINUDF Space Average Prediction

9-UB0196RI-4

warranted. As a result of this evaluation, two coding errors were discovered in the PAINUDF program and were corrected. The results of the code correction changed levels slightly, but did not significantly affect the large difference between forward and aft rotors.

From this point, the excitation field characteristics for forward (downsweeping) and aft (upsweeping) rotors were studied. The geometry for the open, curved panel model of the empennage and the relative position of the UDF engine is shown from the axial view in figure 44. Note that the line of normal incidence is nearer the center of the panel for blade upsweep than the downsweep. This means that in both cases, some energy from the excitation field cannot be represented, but for blade upsweep a greater portion of the excitation field is accounted for. Thus, it is reasonable to expect that the blade upsweep case would give the higher prediction for this particular geometry.

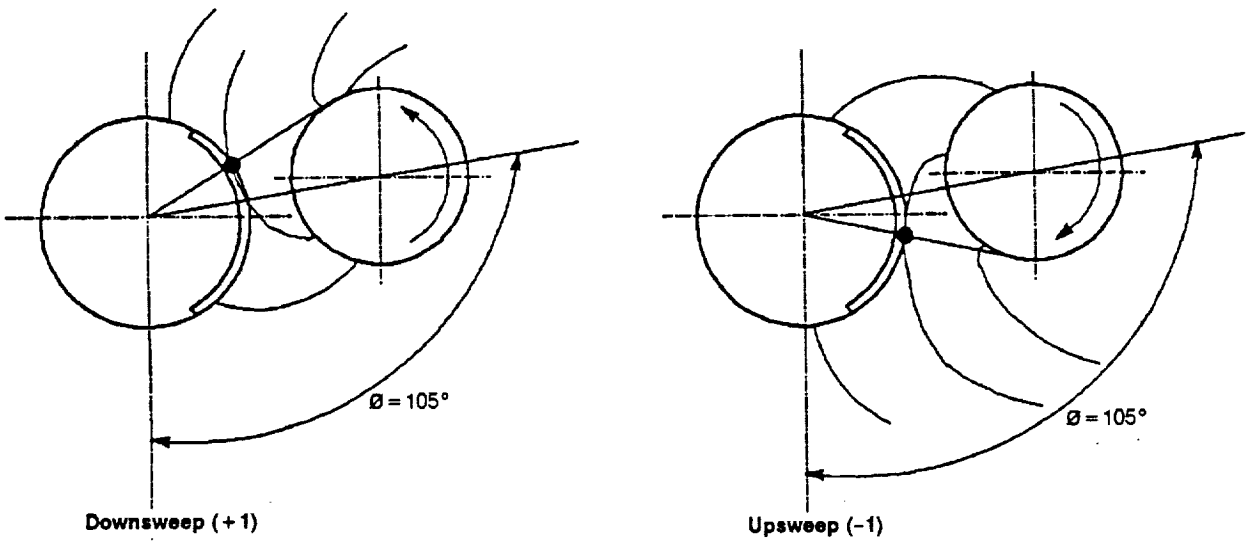

Figure 44. Propeller Wavefronts for Blade Downsweep (Forward Rotor) and Blade Upsweep (Aft Rotor) at Ø = 105°

9-U90196RI-49

To test this expectation, the axis of the propulsor was rotated downward so that the wavefronts for blade upsweep and downsweep strike the panel in an identical (mirror image) fashion (fig. 45). Predictions for this configuration show equal levels for blade upsweep and downsweep. However, predicted levels for this case were still 5 dB more than those measured on the airplane.

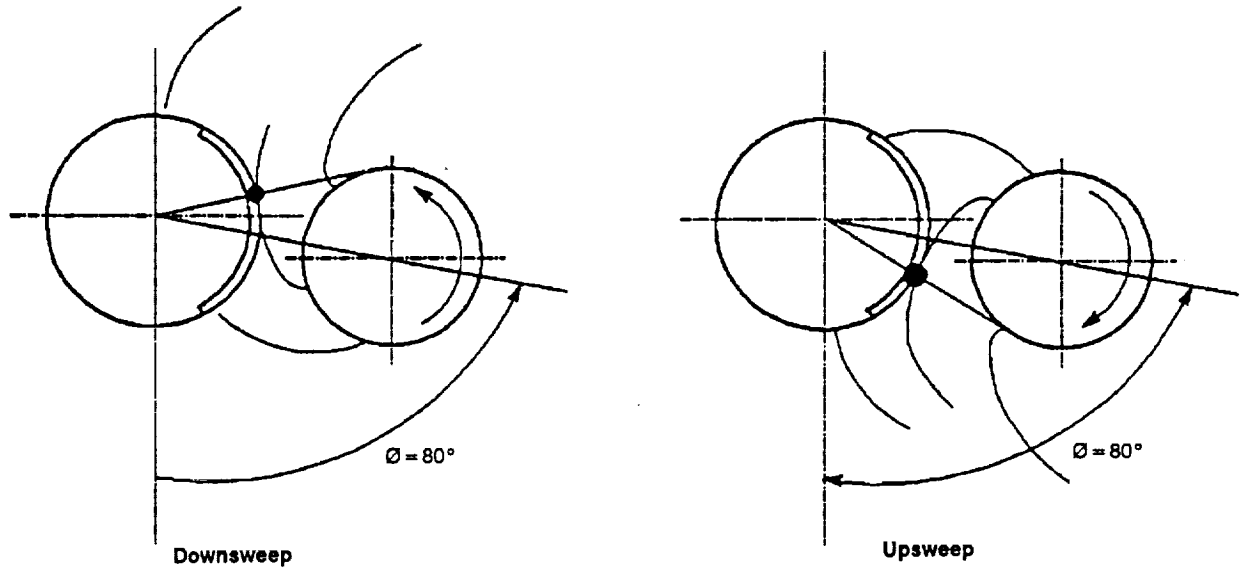

Figure 45. Propeller Wavefronts for Blade Downsweep (Forward Rotor) and Blade Upsweep (Aft Rotor) at Ø = 80°

9-U90196RI-50

Although predicted levels remain high, it was concluded that the model is working correctly. The original aft rotor prediction, thought to be anomalous, has been shown to be consistent with the forward rotor predictions and is associated with the position of the rotor with respect to the open panel boundaries of the empennage representation.

Based on the above results, it was decided that the empennage representation should be improved before further analysis. On the 727 demonstrator airplane, energy from the propeller blade rows is transmitted through the empennage sidewalls as well as the tail surface and bottom of the empennage, which are not represented by the open shell structure. A conical empennage section was modeled using local mass and stiffness properties similar to those of the curved open panels. Note that with the full conical section the entire excitation field can now be represented regardless of engine and strut angle or upsweep versus downsweep. Cabin interior noise levels were again estimated using the correct propulsor location. Results are shown in figure 46 and are compared to baseline results using the corrected code. Note that the differences between the aft and forward rotor are much smaller (but not zero because of the tapering geometry of the empennage versus blade row position). Also, the aft rotor prediction is now independent of the direction of rotation. Note also that the expected increase in level, due to the conical structure allowing full representation of the excitation field, is more than offset by the increased stiffness of the conical structure. That is, the stiffer (conical versus open panel) geometry results in a lower modal density and less efficient coupling with the exterior pressure field.

Because measured phase values are often difficult to obtain or estimate, it was desirable to determine the level of accuracy necessary for phase description. For a preliminary assessment, predictions using the model with the open panel empennage representation were made for constant phase, dummy phase, and rapidly varying phase. Predictions varied dramatically as seen in figure 47. The case of constant phase yields the highest interior levels and the case for rapidly varying phase yields the lowest

Flight condition	Rotor	Rotation	Predicted minus measured levels, dB	
			Open empennage	Conical empennage
Mach = 0.80 at 35 000 ft	Forward	Downsweep	1.1	-5.3
Mach = 0.72 at 35 000 ft	Forward	Downsweep	0.1	-5.9
Mach = 0.42 at 10 000 ft	Forward	Downsweep	2.1	-4.6
Mach = 0.42 at 10 000 ft	Aft	Upsweep	8.0	-2.8
Mach = 0.42 at 10 000 ft	Aft	Downsweep	-	-2.8

Figure 46. Measured and PAINUDF Predicted Levels for Open Panel and Conical Empennage Models

9-U90196RI-51

Flight condition	Rotor	Rotation	Predicted minus measured levels, dB		
			Dummy phase	Constant phase	Rapidly varying phase
Mach = 0.80 at 35 000 ft	Forward	Downsweep	1.1	8.9	-13.1
Mach = 0.72 at 35 000 ft	Forward	Downsweep	0.1	7.8	-23.2
Mach = 0.42 at 10 000 ft	Forward	Downsweep	2.1	10.0	-14.1
Mach = 0.42 at 10 000 ft	Aft	Upsweep	8.0	11.3	-6.6

Figure 47. Measured and PAINUDF Predicted Levels Phase Sensitivity Study

9-U90196RI-52

predictions. Although constant phase over the entire grid is unrealistic, it appears that significant energy flow from the propeller field to the empennage can be expected from regions where phase varies slowly and pressure levels are high.

It should be noted that the very stiff empennage structure representation results in low modal densities (long structural wavelengths) in the frequency range of interest. As a result, this particular model is very sensitive to phase variations. Further sensitivity studies to phase variation and receiving structure stiffness are presented in following sections.

It was felt that to improve 727 demonstrator airplane predictions an accurate estimation of the excitation field phase characteristics would be required. To this end, NASA supplied such data using Aircraft Noise Prediction Program (ANOPP) predictions for the test propeller engine configuration. The ANOPP predictions showed more rapidly varying phase than the dummy data, particularly forward of the propeller plane (fig. 48). A series of predictions were made using the 727 demonstrator airplane model with conical empennage, measured propeller excitation amplitudes, and either dummy or ANOPP phase data (fig. 49).

As expected, the prediction using the more rapidly varying ANOPP data is much lower than the prediction using dummy phase data (case 1 versus case 2). To study phase effects further, predictions using only

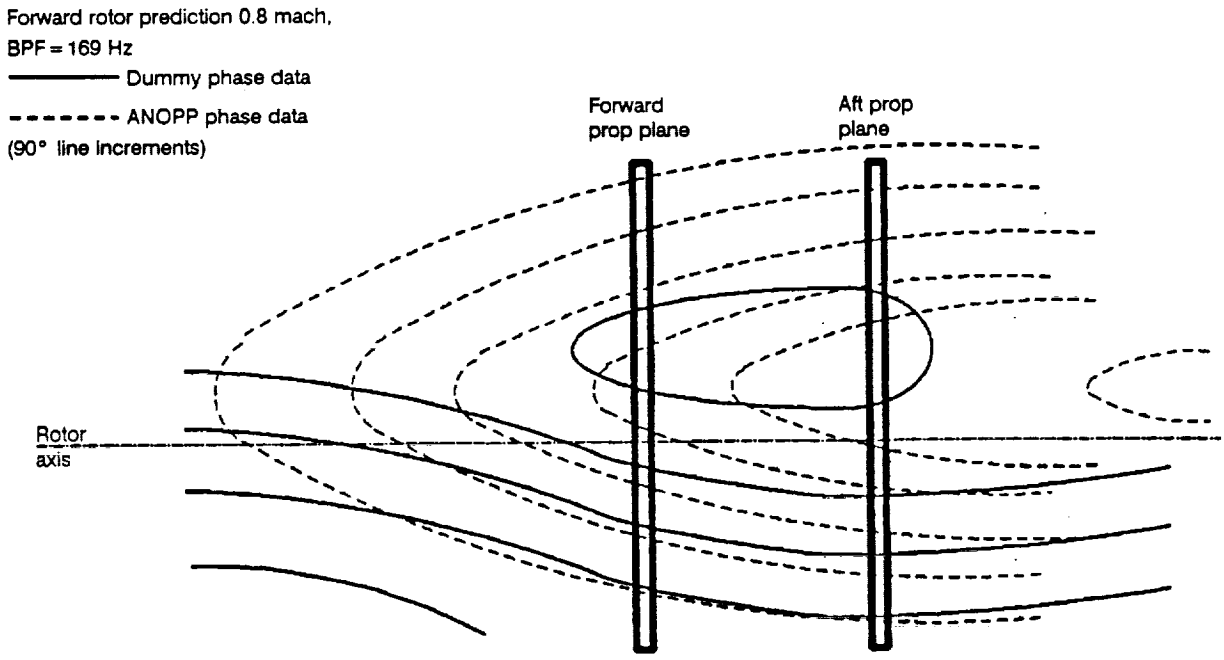

Figure 48. Comparison of Propeller Field Phase Contours ANOPP Phase Versus Dummy Phase

10-U90196R1-53

Case	Phase data	Grid size	Receiving structure	Predicted minus measured levels, dB
1	Dummy	Full	Empennage	-4.6
2	ANOPP	Full	Empennage	-22.9
3	Dummy	Rear-half	Empennage	-11.1
4	ANOPP	Rear-half	Empennage	-23.6
5	Dummy	Full	Fuselage	13.1
6	ANOPP	Full	Fuselage	10.2

Figure 49. Measured and PAINUDF Predicted Levels PAINUDF Sensitivity Study to Excitation Models (Mach = 0.80 at 35 000 ft)

10-U90196R1-54

the rear-half of the excitation grid were made. For the ANOPP phase data where phase changes rapidly in front of the propeller plane, nearly all the energy enters through the rear-half of the grid (case 4). For the dummy phase data the effect is not nearly so dominant (case 3).

Finally, the effect of modal density was studied. As noted earlier, very stiff structures, such as the empennage, will have low modal densities (long structural wavelengths), which will couple most efficiently with excitation fields of slowly varying phase. Predictions were made by subjecting the fuselage section directly to the excitation field. The fuselage is much less stiff than the empennage. Cases 5 and 6 of figure 49 now show much less sensitivity to phase than before. Levels are significantly higher because losses through the empennage structure are no longer accounted for.

Without additional test data to validate excitation field predictions it was felt that further attempts to improve the PAINUDF 727 demonstrator airplane model would not be useful. The above studies show that interior noise levels on propeller aircraft can be extremely sensitive to the excitation field phase and the receiving structure stiffness (or modal density). The analyst must be cognizant of the modal characteristics of the aircraft structure in the frequency range of interest and take pains to describe the excitation field in corresponding detail.

4.12 PAIN IMPROVEMENTS AND FEASIBILITY STUDIES

The second part of the 1988 effort focused on expanding capabilities of the PAIN program. As a first step, a five layer passenger cabin trim was incorporated. The original two layer model allowed an airgap or layer of insulation and a limp mass trim. The five layer model allows combinations of insulation, airgaps, and septa (with damping). An example of a five layer trim is given in figure 50.

A users manual was written and delivered to NASA that describes the aft propulsor version (PAINUDF) as well as the five layer cabin trim option.

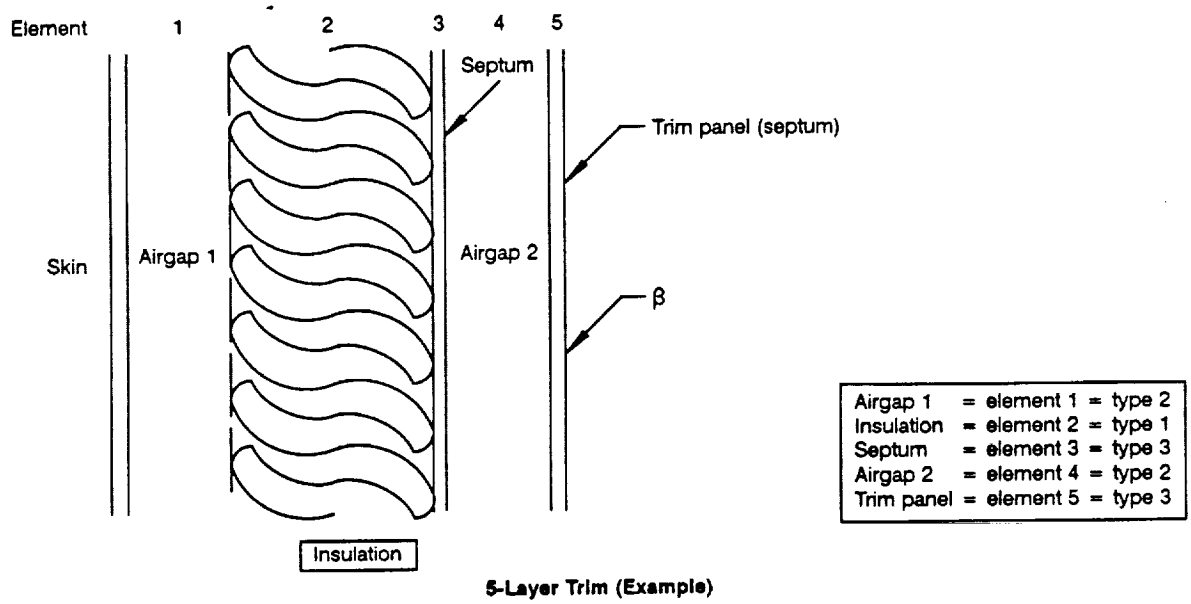

Figure 50. Example of Sidewall Layer Configurations

10-U90196R1-55

A number of potential features were studied that could further enhance the capability of the PAIN model. These features were bulkhead transmission and radiation, exterior pressure loading fore and aft of the pressure bulkhead, cabin noise caused by engine unbalance, and cabin noise gradient.

To add radiation by the bulkhead, the bulkhead must be included as a fourth element of the system. A fifth element, the acoustic cavity within the empennage must also be accounted for if transmission through the bulkhead is to be included. It was shown to be feasible to include the bulkhead as an independent element. It is also considered possible to include the bulkhead as part of the integral fuselage-bulkhead-empennage composite structure as was done in the original PAIN formulation for the fuselage and floor. Based on the expectation that low-frequency global modes will be important at propeller tone frequencies, the latter method was recommended.

Two methods for accounting for pressure loading fore and aft of the bulkhead were outlined. In the first method, it was pointed out that PAINUDF can currently run twice with separate pressure fields on the fuselage and empennage elements. The resulting interior space average sound pressure levels (SPL) can then be summed. In the second method, a power balance could be formulated on the three elements of the PAINUDF system (the empennage, fuselage, and cabin volume). Because it has been shown that the majority of power inflow occurs over small sidewall sections local to the propeller plane, no further work in this area was recommended. PAINUDF should be run twice for those cases when significant power inflow is expected through both the empennage and fuselage surfaces.

PAINUDF can be modified to predict cabin levels caused by engine unbalance in principle by simply including the strut as an element just as the bulkhead would be included in the first study. However, the difficulty in calculating the resulting modes of integral composite structure and the low modal density at

engine once-per-revolution frequencies make this enhancement of questionable value and therefore, it was not recommended.

The interior sound levels measured during flight varied significantly along the axis of the demonstrator airplane fuselage (fig. 43). Therefore, the feasibility was considered of accounting for the sound level gradient within the PAIN program. In order to account for the gradient, the power balance formulation presently used would be replaced by a general solution in which a cavity Green's function is defined with axial dependency. Space averages will then only be taken over the cross section.

5.0 CONCLUSIONS AND RECOMMENDATIONS

At the end of the first year's effort, it was concluded that each analysis procedure showed promise for use in predicting low-frequency noise associated with advanced propeller engine installations. It was noted, however, that variations between predicted and measured levels were large enough to remain cautious. The goal of the second year's effort was to explore modeling and analysis techniques to improve results. Assessment of the second year's results indicate that predictions of absolute levels, with accuracy typically required to make cabin noise guarantees, have not been demonstrated. However, the models have demonstrated the ability to predict trends and should be useful to a designer in assessing type and placement of suppression treatments. Thus, it is recommended to proceed by using the models to identify engine vibration and propeller noise transmission mechanisms and assess potential suppression concepts. Other conclusions are summarized in the following sections.

5.1 FINITE ELEMENT ANALYSIS

One of the initial objectives of the finite element modeling task was to demonstrate that loads analysis models could be modified for noise analysis at engine rotor frequencies. If possible, this would save a large amount of modeling effort. The 727 demonstrator airplane model was developed from such a loads model by adding mass elements for the structure and trim and a finite element representation of the cabin airspace. The general agreement with measured GVT levels and the ability to predict response sensitivity to different excitation directions indicate this objective has been met.

The 727 demonstrator airplane finite element model was found to be time consuming in terms of model checkout and turnaround of predicted results due to its large size. Studies were completed in which the model size was reduced by simplifying and then eliminating representation of wing, tail, and empennage structure. Results indicate that whole body and wing modes can contribute to transmission and radiation of engine rotor noise. Thus, some representation of all of the aircraft structure is required. Beam elements for structure not in the direct transmission path were found to be satisfactory. Inclusion of the baggage compartment airspace did not significantly affect results.

Studies with the model for flight predictions show that the phase relationship between multiple input forces can shift predicted levels by 20 dB or more. This result has been demonstrated independently on flight tests of conventional turbofan aircraft and suggests that engine response modes can couple effectively with strut modes to transmit vibration at engine rotor frequencies.

These results indicate that the analyst should have some understanding of potential engine and aircraft modes in order to properly model the structure and assess cabin noise. It is noteworthy that SEA results, described below, support these conclusions.

5.2 STATISTICAL ENERGY ANALYSIS

Studies have shown that the complex structure and low modal densities of the strut and empennage precluded accurate SEA predictions of input power and therefore, cabin noise levels. When measured input power from GVT tests was used, the models were shown to accurately predict power flow through the aircraft to the cabin. Procedures for estimating modal densities and input power using finite element analysis were developed and demonstrated. It now appears that development of selected small finite element models to determine input power coupled with SEA models to predict transfer functions to the passenger cabin forms a viable prediction procedure. In this way, a relatively small model can be developed that allows noise control engineers to evaluate and influence structural design before configurations are frozen. Final configuration details would be evaluated using finite element models.

Propeller tone vibration and noise levels in flight were overpredicted throughout the aircraft. This led to the conclusion that input power was being overestimated. This was confirmed by reducing the empennage excitation area used to convert measured pressure to force inputs so that measured empennage response was matched, resulting in good agreement at all other locations. Another conclusion from this exercise is that a significant portion of the propeller tone energy appears to enter through a relatively small portion of the empennage. Studies using PAIN confirm this conclusion and are described below.

Finally, it was noted during these studies that the low-frequency model provided relatively good predictions up to 200 Hz. This implies the more detailed subsystem representation in the midfrequency model may not be required for predictions at propeller-blade-passage frequencies. Further work in this area is recommended.

5.3 PAIN ANALYSIS

At the end of the first year's work, an apparent anomalous result regarding prediction of tone levels from the aft rotor was noted. These results were explored and found to be consistent with forward rotor predictions. This is a result of excitation field phase differences for forward (downsweep) and aft (upsweep) blade rows mapped over the open panel representation of the empennage. The open panel empennage was thus replaced by a conical representation.

Further studies with this model indicated that cabin levels were very sensitive to the excitation field phase and that by varying phase, the measured flight tone levels could be bracketed. Because test measurements were insufficient to describe excitation field phase (dummy values were used for all cases), further efforts to match predicted and measured levels were discontinued. As a result of these studies however, an important conclusion was reached. As with SEA results, it appears that most propeller tone energy enters the aircraft through a relatively small area of the empennage where the excitation field phase varies slowly. This is important because it implies that noise suppression treatments, which are inherently heavy and expensive, can be concentrated over small areas where power flow is the greatest.

The empennage is a stiff structure with low modal density (long structural wavelengths). When the softer fuselage structure was evaluated (by exposing it directly to the propeller noise field), it was found to be

less sensitive to phase of the excitation field. That is, the higher modal density of the fuselage allowed efficient excitation of several modes regardless of the propeller field phase. As with finite element analysis and SEA, this indicates that for low-frequency evaluation of aircraft structures, some knowledge of modal behavior is required.